Functions of inulosucrase and novel fructosyltransferase from the inulin-producing bacterium *Neobacillus drentensis* 57N

（イヌリン合成細菌 *Neobacillus drentensis* 57N 由来イヌロスクラーゼおよび新規フルクトシル転移酵素の機能に関する研究）

Hokkaido University　Graduate School of Agriculture

Division of Agriculture　Frontiers in Biosciences　Doctor course

Yusuke Kido

北海道大学　大学院農学院

農学専攻　生命フロンティアコース　博士後期課程

城戸　悠輔

CONTENTS

Abbreviations

1-FFT, 2,1-fructan:2,1-fructan 1-fructosyltransferase

1-SST, sucrose:sucrose 1-fructosyltransferase

6-SFT, sucrose:fructan 6-fructosyltransferase

ABC, ATP-binding cassette

BLAST, Basic Local Alignment Search Tool

BSA, bovine serum albumin

CFT, cycloinulooligosaccharide fructanotransferase

COSY, correlated spectroscopy

DDBJ, DNA Data Bank of Japan

DFA III, α-D-fructofuranose β-D-fructofuranose 1,2':2.3'-dianhydride

DP, degree of polymerization

E-Fru, D-fructosyl-enzyme intermediate

ESI-MS, Electrospray ionization-mass spectrometry

FOS, β-(2→1)-linked fructooligosaccharide

GC-MS, gas chromatography-mass spectrometry

GH, glycoside hydrolase family

H2BC, heteronuclear 2-bond correlation

HMBC, heteronuclear multiple bond correlation

HPAEC-PAD, high-performance anion exchange chromatography-pulsed amperometric detection

HPLC, high-performance liquid chromatography

HSQC, heteronuclear single quantum coherence

HSQC-TOCSY, HSQC-total correlation spectroscopy

IFT, inulin fructotransferase (DFA-III-forming)

IS, inulosucrase

NdIS, *Neobacillus drentensis* 57N IS

NMR, nuclear magnetic resonance

PMAA, partially methylated alditol acetate

PTS, sugar phosphotransferase system

RP-HPLC, reversed-phase HPLC

TLC, thin-layer chromatography

Chapter 1. General introduction

1.1. Inulin

Inulin, a type of polysaccharide found in chicory, burdock, onion, and roots of *Asteraceae* plants, etc., is a fructan composed of several tens of β-(2→1)-D-fructosyl residues, generally with a sucrose structure at the end (Pranznik and Beck 1985; Roberfroid 2005; Niness 1999). In a broader sense, β-(2→1)-fructans without the terminal D-glucosyl residue are also regarded as inulin. Inulin functions primarily as a storage polysaccharide and is used as energy source during dormancy and germination (Ritsema and Smeekens 2003). In addition to energy storage, inulin in plants has an important role in abiotic stress tolerance, such as drought, salinity, and cold (Ritsema and Smeekens 2003; Apolinário *et al.* 2014). As a molecular mechanism for enhanced tolerance to these stresses, the role of inulin in interacting with phospholipids in lipid bilayers to maintain proper membrane structure is noted (Demel *et al.* 1998; Vereyken *et al.* 2001).

Bacteria (some *Lactobacillales* and *Bacillales*) and archaea (Kirtel *et al.* 2019) also produce inulin-type polysaccharides. In *Lactobacillales*, inulin-type polysaccharide is a factor in biofilm formation. In *Lactobacillus reuteri* TMW1.106, deficiency of the ability of inulin-type polysaccharide synthesis reduces the fixation rate in the mouse gastrointestinal tract (Walter *et al.* 2008). Oral biofilm, formed by *Streptococcus mutans*, also contains inulin-type polysaccharides (Birkhed *et al.* 1979). On the other hand, the physiological significance of inulin in *Bacillales* is still unknown.

Inulin acts as a prebiotic. Inulin is not digested in humans' upper gastrointestinal tract and small intestines (Knudsen and Hessov 1995). This polysaccharide passes into the large bowel and stimulates the growth of *Bifidobacterium* spp. and *Lactobacillus* spp. while controlling other pathogenic bacteria, such as *Escherichia coli* and *Clostridia*, at low levels (Gibson *et al.* 1995). In addition, inulin functions as a gelation- and texture-adjusting agent. The use of inulin as a functional food ingredient has increased

in recent years (Morris and Morris 2012; Shoaib *et al.* 2016). This polysaccharide is also a superior starting material for the production of β-(2→1)-linked fructooligosaccharides (FOS; Singh and Singh 2010), including di-D-fructose-1,2':2,3'-dianhydride III (DFA III; Yokota *et al.* 1991). Inulin is produced industrially from the roots of chicory plants, which are rich in inulin (van Laere and van den Ende 2002). The production process includes cultivating the chicory, harvesting the roots, transportation to the plant, washing, peeling, cutting, drying, milling, sieving, and boiling the roots (Flores *et al.* 2016). Inulin is collected from the extract by ethanol precipitation (Zhu *et al.* 2016). The production of inulin from plant materials first requires the availability of sufficient raw materials, which requires adequate arable land area, a long cultivation period from spring to fall, and the management and use of fertilizers and other chemicals to control and prevent disease. Second, the inulin contained in the roots after harvesting tends to be decomposed during storage, and the roots themselves are susceptible to storage spoilage, so it is necessary to process the raw roots in as short a time as possible. Therefore, inulin production from plants requires large-scale machinery and equipment capable of quickly processing large quantities of roots. For these reasons, producing inulin from plants requires much labor and equipment, and the production cost is high. On the other hand, the bacterial inulin-type polysaccharides can be synthesized from sucrose by using inulosucrase (IS; EC 2.4.1.9), secreted by microorganisms, as described later. Currently, IS from *Bacillus* sp. 217C-11 is used for the industrial production of the inulin-type polysaccharide (Wada *et al.* 2005). The produced inulin-type polysaccharide has characteristics of lower DP and higher water solubility than plant inulin and is widely applied to food products.

1.2. Biosynthesis and metabolism of inulin

In plants, inulin is synthesized by the action of two enzymes: sucrose:sucrose 1-fructosyltransferase (1-SST; EC 2.4.1.99) and 2,1-fructan:2,1-fructan 1-fructosyltransferase (1-FFT; EC 2.4.1.100)

(Livingston *et al.* 2009). 1-SST transfers the D-fructosyl moiety of sucrose to another sucrose molecule to produce 1-kestose (Fruβ2-1Fruβ2-1αGlc) (Edelman and Jefford 1968). 1-FFT catalyzes the transfructosylation between β-(2→1)-fructan molecules to elongate β-(2→1)-D-fructosyl chains (Edelman and Jefford 1968; Vergauwen *et al.* 2003). Some plant species, such as wheat, barley, and plants of the *Rutaceae* family, contain fructans with both β-(2→1)- and β-(2→6)-linkages, which are called graminan-type fructans (van den Ende *et al.* 2000; Mancilla-Margalli and Lopez 2006). This type of fructan is often present in the aerial parts of plants, but is not used for industrial production due to its low content. The β-(2→6)-branching structure of graminan-type fructans is produced by sucrose:fructan 6-fructosyltransferase (6-SFT; EC 2.4.1.10) (Sprenger *et al.* 1995; Duchateau *et al.* 1995). 1-FFT transfers β-(2→1)-D-fructosyl unit to β-(2→6)-D-fructosyl residue, generated by 6-SFT, resulting in graminan-type fructans synthesis (Kawasaki and Yoshida 2005). According to the sequence-based CAZy classification of glycoside hydrolases (Drula *et al.* 2022), 1-FFT, 1-SST, and 6-SFT are classified into glycoside hydrolase family (GH) 32.

In contrast to plant inulin biosynthesis, microbial inulin is synthesized by a single enzyme, IS. This enzyme generally catalyzes transfructosylation from sucrose to sucrose and β-(2→1)-fructan (Ponstein and van Leeuwen 1993). IS has been found in several *Lactobacillales*, a few *Bacillales*, and an Archaeon. The structure of microbial β-(2→1)-fructans is diverse. *Bacillales* fructans are linear with a degree of polymerization (DP), 3–27 (Wada *et al.* 2003; Kralj *et al.* 2018; Yokoi *et al.* 2021). *Lactobacillales* fructans are highly β-(2→6)-branched, with much higher DPs ($1 \times 10^4 – 4 \times 10^5$) than *Bacillales* fructans (Rosell and Birkhed 1974; van Hijum *et al.* 2002; Anwar *et al.* 2008). It remains unknown how these branches are formed. Although little is known about archaeal fructans, they are insoluble in water when heated, indicating a higher DPs than Bacillales fructans (Ghauri *et al.* 2021a).

As inulin-degrading enzymes, extracellular inulinases have been identified in *Bacillaceae*,

Lactobacillales, and others (Keto *et al.* 1999; Pudjono *et al.* 1993). Inulinases include exo-inulinase (EC 3.2.1.80) and endo-inulinase (EC 3.2.1.7). Exo-inulinase releases D-fructose from the inulin terminus, and endo-inulinase randomly cleaves internal β-(2→1) bonds in the inulin molecule to produce inulooligosaccharides, including inulotriose and inulotetraose. These enzymes are both classified into GH32 in the CAZy database. *Geobacillus stearothermophilus* KP1289 and *Bifidobacterium adolescentis* G1 have intracellular exo-inulinases (Tsujimoto *et al.* 2003; Muramatsu *et al.* 1993). These bacteria are thought to digest inulin into short-chain inulooligosaccharides by the extracellular endo-inulinase. The oligosaccharides are then taken up intracellularly and broken down to D-fructose.

Bacillus circulans and *Paenibacillus polymyxa* secrete cycloinulooligosaccharide fructanotransferase (CFT; EC 2.4.1.-) extracellularly to produce cycloinulooligosaccharides from inulin (Kawamura *et al.* 1989; Nanjo *et al.* 2008). Cycloinulooligosaccharides comprise 6–8 β-(2→1)-D-fructosyl residues (Kawamura *et al.* 1989). Cycloinulooligosaccharides are opened by CFT itself or endo-inulinase (Kawamura and Uchiyama 1993). The metabolic mechanism of these cyclic oligosaccharides has not been fully understood yet.

An inulin fructotransferase (DFA-III-forming) (IFT; EC 4.2.2.18), which is secreted extracellularly by *Arthrobacter* sp. H65-7, converts inulin to α-D-fructofuranose β-D-fructofuranose 1,2':2.3'-dianhydride (DFA III; Yokota *et al.* 1991). DFA III is composed of two D-fructose units, which are linked by β-(2'→1) and α-(2→3') bonds. *Arthrobacter* sp. H65-7 also possesses intracellular DFA III hydrolase (EC 3.2.1.-) that specifically cleaves α-(2→3') bond of DFA III to produce inulobiose (Sakurai *et al.* 1997). DFA III is beneficial as a functional carbohydrate. In humans, DFA III has two types of mineral absorption-promoting effects: it acts on tight junctions in the small intestine to promote the absorption of minerals, and it solubilizes minerals by lowering pH through fermentation in the colon (Suzuki and Hara 2006; Minamida *et al.* 2006).

1.3. Structures and functions of GH68 enzymes

IS belongs to GH68, which contains sucrose-specific D-fructofuraoside-acting enzymes IS, levansucrase (EC 2.4.1.10), and β-fructofuranosidase (EC 3.2.1.26). Levansucrase synthesizes levan, β-(2→6)-fructan, from sucrose through β-(2→6)-transfructosylation (Gay *et al.* 1983). β-Fructofuranosidase mainly catalyzes the hydrolysis of non-reducing terminal β-D-fructofuranosidic linkage of β-D-fructofuranosides (Fujita *et al.* 1990). GH68 enzymes catalyze hydrolysis and transfructosylation using sucrose as a substrate, with net retention of the anomeric configuration of the substrate, through a double-displacement mechanism involving the formation of a covalently linked α-fructofuranosyl enzyme intermediate (Chambert *et al*. 1974; Chambert and Gonzy-Treboul 1976; Hernandez *et al.* 1995; Song and Jacques 1999). In GH68 enzymes, three-dimensional structures of six levansucrases, two ISs, and one β-fructofuranosidase have been determined (Table 1-1). The structures are similar to those of GH32 enzymes, and enzymes of GH32 and GH68 comprise clan GH-J (Lammens *et al.* 2009). The five-bladed β-propeller fold in the catalytic domain is common in the GH32 and GH68 enzymes. Most bacterial and archaeal GH68 ISs possess only the catalytic domain, but some enzymes have a short N-terminal domain in addition to the catalytic domain (Kralj *et al.* 2018; Frasch *et al*. 2017; Yokoi *et al.* 2021; Ghauri *et al.* 2021b). *Lactobacillales* GH68 ISs have additional domains at N- and C-termini (van Hijum *et al*. 2002; Olivares-Illana *et al*. 2002; Anwar *et al*. 2008). The C-terminal domain anchors the enzyme to the cell wall (Rathsam *et al.* 1993; van Hijum *et al.* 2002), whereas the function of the N-terminal domain is unknown (del Moral *et al.* 2008).

Each blade of the β-propeller fold consists of four antiparallel β-strands. In this thesis, the five blades are labeled 1-5, in order from the N-terminus, and the four β-strands forming each blade are named A-D, respectively, from the N-terminus. The residues that function as nucleophile, general acid/base catalyst, and transition-state stabilizer, are located on the β-strand 1A, 4A, and 3A, respectively (Meng and Fütterer

2003; Yanase *et al.* 2002; Song and Jacques 1999; Batista *et al.* 1999). In the complex structure of *B. subtilis* 168 levansucrase bound with sucrose (SacB; Fig. 1-1), the D-fructofuranosyl residue takes the envelope form with a more pronounced deformation amplitude between $^{3}T_{4}$ and E_{4}. Glu342 of this enzyme protonates the glycosidic oxygen of the substrate as the general acid/base catalyst, forming an oxonium ion with the envelope conformation E_{4} preferred (Seibel *et al.* 2006). From the mutagenesis and mechanistic studies of *Priestia megaterium* levansucrase, the reaction further proceeds through forming a covalent D-fructosyl-enzyme intermediate (E-Fru) and a nucleophilic attack of the acceptor substrate (Fig. 1-2; Homann *et al.* 2007). A similar reaction mechanism has been postulated in the case of IS (Charoenwongpaiboon *et al.* 2019a). The structures of the −1 to +2 subsites of the GH68 enzyme are similar even in IS, levansucrase, and β-fructofuranosidase. Thus, the product specificity of GH68 enzymes is thought to be provided not only by the +1 and +2 subsites but also by the other subsites (+3, +4, …, etc.) (Ozimek *et al.* 2006).

In *Limosilactobacillus reuteri* 121 IS, Asn543, Trp551, Asn555, and Asn561 are involved in the formation of +3 and further positive subsites, and Ala substitution of even one of these residues results in the production of only FOS up to DP 6 (Charoenwongpaiboon *et al.* 2019a). Trp551 and Asn555 are located in the α-helix in the loop connecting 4B and 4C, 4B-4C loop, which is unique to *Lactobacillales* ISs (Malik 2012; Anwar *et al.* 2008; Anwar *et al.* 2010). In addition to the residues mentioned above, Ala substitution of Arg483 in the α-helix between the 3B-3C loop of *L. reuteri* 121 IS has been shown to drastically reduce products above DP 10 from sucrose (Charoenwongpaiboon *et al.* 2019a). In *Lactobacillus johnsonii* NCC 533 IS (InuJ), the residues (Arg484, Asn544, Trp552, Asn556, and Asn562) corresponding to Arg483, Asn543, Trp551, Asn555, and Asn561 of *L. reuteri* 121 IS, respectively, are well conserved and are expected to interact with the long chain substrate similarly. These amino acid residues are not conserved at all in non-lactic acid bacterial and archaeal ISs (Fig. 1-3), which may have

different substrate recognition mechanisms (Frasch *et al.* 2017; Kralj *et al.* 2018; Yokoi *et al*. 2021; Ghauri *et al.* 2021b).

1.4. Purpose of this study

As described above, inulin is a carbohydrate with health functionality for humans and is also used as a starting material for production of functional oligosaccharides, and its industrial use, such as for DFA III producing, is expanding. Inulin is primarily extracted from plant roots. However, enzyme production from sucrose is attracting attention due to cost reduction and stable supply. Efficient and diversified production of inulin and related oligosaccharides requires not only useful ISs, but also a deep understanding of the mechanism of inulin synthesis by ISs. In this study, the aim was to elucidate the mechanism of inulin synthesis by IS and related enzyme produced by an inulin-synthesizing bacterium. In Chapter 2, a new inulin-synthesizing bacterium, *Neobacills drentensis* 57N, was isolated from the soil to establish an efficient inulin synthesis system for practical production from sucrose, and the inulosucrase of the bacterium, NdIS, was characterized. In Chapter 3, the substrate specificity of NdIS was analyzed kinetically to elucidate the molecular mechanisms for inulin production. In Chapter 4, the function of a functionally unknown sucrose-acting enzyme, NdFosA, found in *N. drentensis* 57N culture supernatant was analyzed, and revealed that NdFosA is a novel fructosyltransferase that introduces a β-(2→6)-branch to inulin. In Chapter 5, the usefulness of the products that were produced through the application of the results of this study was discussed. Furthermore, the metabolic mechanism of inulin is also discussed based on the related enzymes' gene structure and enzymatic functions.

Table 1-1. List of GH68 enzymes of known three-dimensional structure.

Enzyme	Origin	Reference	PDB entry
Levansucrase SacB	*Bacillus subtilis* 168	Meng and Fütterer 2003	1OYG
	Beijerinckia indica ATCC 9039	Tonozuka *et al.* 2020	6M0D
	Erwinia amylovora	Wuerges *et al.* 2015	4D47
	Erwinia tasmaniensis Et1/99	Polsinelli *et al.* 2020	6FRW
	Gluconacetobacter diazotrophicus SRT4	Martinez-Fleites *et al.* 2005	1W18
	P. megaterium DSM 319	Strube *et al.* 2011	3OM2
Inulosucrase InuHj	[*]*Halalkalicoccus jeotgali* B3T	Ghauri *et al.* 2021b	7BJ5
InuJ	[#]*Lactobacillus johnsonii* NCC 533	Pijning *et al.* 2011	2YFR
β-Fructofuranosidase	*Microbacterium saccharophilum* K-1	Tonozuka *et al.* 2012	3VSR

Enzymes from archaea and lactic acid bacteria are shown with asterisk and sharp, respectively. Others are from non-lactic acid bacteria.

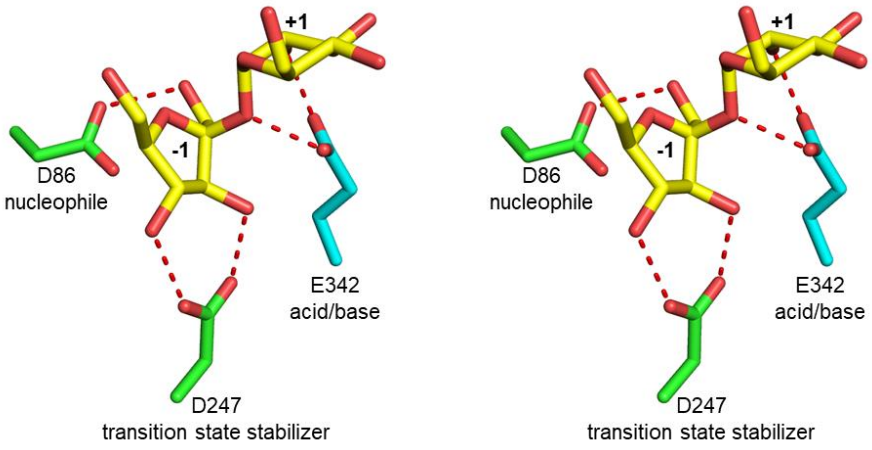

Fig. 1-1. Stereo view of three-dimensional structure of *Bacillus subtilis* 168 levansucrase.

The structure shown in green is *B. subtilis* 168 levansucrase E342A mutant lacking a general acid/base catalyst complex with sucrose (Meng and Fütterer 2003; PDB entry, 1PT2). Sucrose is in yellow. The nucleophile and transition state stabilizer are shown in green. Glu342, shown in cyan in the illustration, is that of the wild-type enzyme superimposed on 1PT2. Red dashed lines indicate the predicted hydrogen bonds between the residues and sucrose.

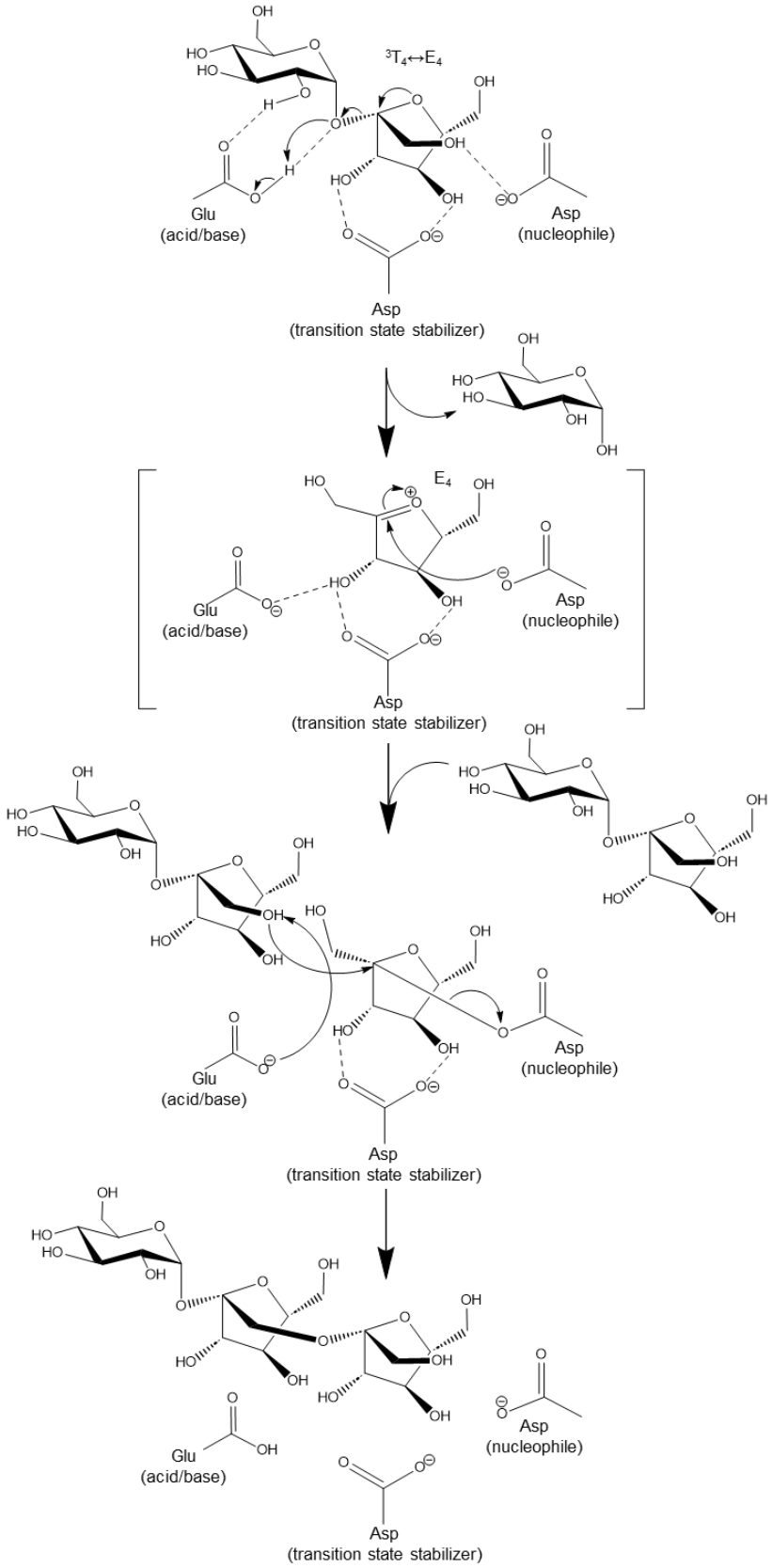

Fig. 1-2. Proposed reaction mechanism of inulosucrase (quoted from Homann *et al.* 2007 with some modification).

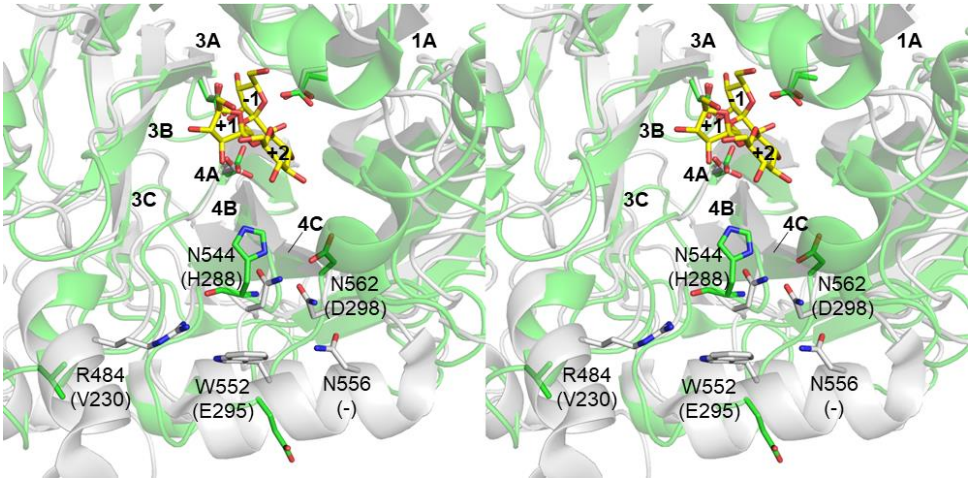

Fig. 1-3. Stereo view of InuJ (Pijning *et al.* 2011; PDB entry, 2YFT) and InuHj (Ghauri *et al.* 2021b; PDB entry, 7BJ4) in complex with 1-kestose (quoted from Charoenwongpaiboon *et al.* 2019a with some modification).

White and green cartoons indicate InuJ, IS from *L. johnsonii* NCC 533, and InuHj, IS from *H. jeotgali* B3T. 1-Kestose from 2YFT is shown in yellow. Subsites and strand numbers are shown in bold letters. The amino acid residues involved in forming long-chain products in InuJ and the corresponding residues of InuHj are indicated by un-parenthesized and parenthesized letters in the panel, respectively.

Chapter 2. Isolation of the inulin-producing strain *N. drentensis* 57N, sequence analysis of the *NdIS* and surrounding genes, and characterization of NdIS

2.1. Introduction

As described in Chapter 1, inulin is useful as a functional food stuff and starting material for fructooligosaccharides. Inulin is mainly produced by extraction from plant roots, but enzymatic synthesis of inulin using the microbial enzyme IS has attracted attention: enzymatic synthesis of inulin using IS from *Bacillus* sp. 217C-11 has been applied for commercial use. The inulin synthesized by this IS is widely used in the food industry because of its superior water solubility due to its lower DP compared to that of plant-derived inulin. The function of inulin as a prebiotic depends on its chain length. DP 2–8 FOSs are more proliferative against *Bifidobacterium longum* and *Bifidobacterium animalis* than long-chain inulin (Biedrzycka and Bielecka 2004). Using a human intestinal model, inulin with DP 3–60 induced the production of propionic acid and butyric acid, short-chain fatty acids with biological regulatory functions, by intestinal bacteria more than inulin with DP 2–20 (van de Wiele *et al.* 2007). Even in the direct effects of inulin on the immune system, not *via* the gut microbiota, different DPs have shown different results in their effects (Fransen *et al.* 2017). Therefore, the demand for various β-(2→1)-fructans is increasing. Regulation of product DP requires a useful IS and a deep understanding of the mechanism of inulin synthesis by the IS. In this chapter, *Neobacillus drentensis* 57N was isolated from soil as an inulin-producing bacterium, and the functions of its IS, NdIS, and the production of inulin-type polysaccharides were investigated using native and recombinant enzymes.

2.2. Materials and methods

2.2.1. Isolation of inulin-producing bacterium *N. drentensis* 57N

N. drentensis 57N was isolated from soil of grassy place in Hokkaido, Japan, on culture medium plates

containing 20 g/L sucrose (Fujifilm Wako Pure Chemical, Osaka, Japan), 5 g/L phytone peptone (Becton Dickinson, Franklin Lakes, NJ, USA), 10 g/L yeast extract (Nacalai Tesque, Kyoto, Japan), 5 g/L KH_2PO_4, and 15 g/L agar (Nacalai Tesque). The pH of the culture medium was adjusted with NaOH to pH 7.2. The plates were incubated at 35°C for 24 h. Single colonies were isolated and cultured in the same liquid medium without agar at 35°C with shaking for 48 h. Inulin-type-fructan-producing activity was evaluated as follows. The culture supernatant (20 μL) was mixed with 100 μL of 400 mM sucrose in 40 mM MES-NaOH buffer (pH 6.5), and incubated at 37°C for 20 h (sample 1; final sucrose concentration, 333 mM). A portion (40 μL) of sample 1 was mixed with 2 μL (0.4 U; 9.5 U/mL) of endo-inulinase from *Aspergillus niger* (Novozym 960; Novozymes, Bagsværd, Denmark) and incubated at 35°C for 24 h (sample 2). Here, 1 U of endo-inulinase was defined as the amount of enzyme that produced 1 μmol of reducing sugar from 4 g/L inulin at 37°C and pH 6.5 in 1 min. The amount of reducing sugars was determined colorimetrically by the dinitrosalicylic acid reagent using 0–5 mM D-glucose (Fujifilm Wako Purechemical) as a quantification standard (Miller 1959). The saccharides in samples 1 and 2 were analyzed by thin-layer chromatography (TLC). Sample 1 (20 μL) was subjected to digestion with recombinant levanase from *Bacillus* sp. (United States Biological, Salem, MA, USA) and dextranase from *Penicillium* sp. (Sigma Aldrich, St. Louis, MO, USA) under the same conditions as with endo-inulinase, but, at 0.5 U/mL in the reaction mixture.

2.2.2. TLC analysis

Samples containing 8.6 μg of saccharides were spotted onto a silica gel 60 plate (Merck, Darmstadt, Germany) and developed with the solvent, 2-propanol/1-butanol/water (2/2/1, v/v/v). Sugar spots were detected by spraying a detection reagent (H_2O/methanol/sulfuric acid [9/9/2, v/v/v]) and heating the plate at 105°C.

2.2.3. Identification of the bacterial strain

Chromosomal DNA extracted from lysed *N. drentensis* 57N using achromopeptidase (Fujifilm Wako Pure Chemical), was used as the PCR template to amplify the 16S rRNA gene. Tks Gflex DNA Polymerase (Takara Bio, Kusatsu, Japan) and a primer set of 9F (5´-GAGTTTGATCCTGGCTCAG-3´) and 1510R (5´-GGCTACCTTGTTACGA-3´) (Nakagawa and Kawasaki 2001) were used. A Bigdye Terminator v3.1 Cycle Sequencing Kit (Thermo Fisher Scientific, Waltham, MA, USA) and primers 9F, 515F (5´-GTGCCAGCAGCCGCGGT-3´), 1099F (5´-GCAACGAGCGCAACCC-3´), 536R (5´-GTATTACCGCGGCTGCTG-3´), 926R (5´-CCGTCAATTCCTTTGAGTTT-3´), and 1510R (Nakagawa and Kawasaki 2001) were used in the sequencing analysis. Sequencing was performed using an ABI Prism 3130xl Genetic Analyzer System (Applied Biosystems, Foster City, CA, USA) and Chromaspro version 2.1 (Technelysium, Tewantin, Australia). Sequence similarity searches and phylogenetic classifications were performed using ENKI (Techno Suruga Laboratory, Shizuoka, Japan), DB-BA (version 15.0; Techno Suruga Laboratory), GenBank, the DNA Data Bank of Japan (DDBJ), and the EMBL Nucleotide Sequence Database. *N. drentensis* 57N grown on LB medium (Lennox; Becton Dickinson) containing 20 g/L agar were used for subsequent tests. Morphological observations were performed using an optical microscope (BX50F4; Olympus, Tokyo, Japan). Feyber G Nissui (Nissui Seiyaku, Tokyo, Japan) was used for Gram staining. Carbohydrate utilization and enzyme activities were analyzed according to previously described methods (Barrow and Feltham 1993) using the API 20NE kit (bioMérieux, Lyon, France).

2.2.4. Production of NdIS in media containing various carbon sources

N. drentensis 57N was grown in 50 mL of medium in which the carbon source of the medium used to isolate the 57N strain was replaced with 20 g/L sucrose, D-glucose, or D-fructose with shaking at 130

rpm at 30°C for 24 h. From 1 mL of the culture aliquot, the supernatant and bacterial cells were separated by centrifugation at 8,000 × *g*. Bacterial cells were suspended in 200 μL of 10 mM MES-NaOH buffer (pH 6.5). Enzyme activity was measured using the standard activity assay method described in section 2.2.11.

2.2.5. Production and purification of IS from *N. drentensis* 57N

N. drentensis 57N was cultured in 400 mL of culture medium containing 20 g/L sucrose with shaking at 130 rpm at 30°C for 24 h. The supernatant was obtained by centrifugation at 12,000 × *g* at 4°C for 20 min. Ammonium sulfate was added to the supernatant up to 70% saturation, and the sample was kept at 4°C for 24 h with stirring. The precipitate was collected by centrifugation, dissolved in 50 mL of 10 mM sodium phosphate buffer (pH 7.0), and dialyzed against the same buffer. The samples were loaded onto a Toyopearl DEAE 650M column (2.5 cm i.d. × 20 cm; Tosoh, Tokyo, Japan) equilibrated with 10 mM sodium phosphate buffer (pH 7.0). The active fractions eluted in the non-adsorbed fraction were collected, and ammonium sulfate was added to bring the concentration to 80 mM. This sample was subjected to a Toyopearl Butyl 650M column (2.5 cm i.d. × 10 cm; Tosoh), equilibrated with 10 mM sodium phosphate buffer (pH 7.0) containing 80 mM ammonium sulfate. After washing the column with the same buffer, the adsorbed fractions were eluted by a linear gradient of 80-0 mM ammonium sulfate (total elution volume, 400 mL) and a further 10 mM sodium phosphate buffer (pH 7.0) without ammonium sulfate. Of the two active fractions eluted, the first fraction was collected and dialyzed against 10 mM phosphate buffer. Of the two active fractions eluted, the first fraction was collected as a purified enzyme and dialyzed against 10 mM phosphate buffer. The enzyme was stored at −80°C. The purity of each fraction was tested by SDS-PAGE. Active fractions from the first major high-purity peak were collected. The purity of the fractions was determined using SDS-PAGE (Laemmli 1970). The collected sample was

dialyzed against 10 mM sodium phosphate buffer (pH 7.0) and stored at −80°C.

2.2.6. Sequence analysis of *NdIS* and neighboring genes

Purified NdIS was transferred onto a polyvinylidene difluoride membrane (Immobilon-PSQ; Merck Millipore, Burlington, MA, USA) using a semi-dry electroblotting apparatus (Bio-Rad, Hercules, CA, USA). The protein band on the membrane was detected using Coomassie Brilliant Blue R-250 (Fujifilm Wako Pure Chemical). The band was then cut off and subjected to N-terminal amino acid sequence analysis using Protein Sequencer Procise 492HT (Perkin Elmer; Waltham, MA, USA). The lysyl endopeptidase digestion to determine the internal amino acid sequence was performed as follows. NdIS (70 μg) was dried *in vacuo* and dissolved in 75 μL of 0.25 M Tris-HCl buffer (pH 8.9) containing 10 mM EDTA, along with 24 mg urea. One microliter of 1.17 mg/mL lysyl endopeptidase (Fujifilm Wako Pure Chemical) was added and incubated at 37°C for 20 h. The mixture of peptidase digestion was separated using reversed-phase high-performance liquid chromatography (RP-HPLC) to obtain peptides. The conditions for RP-HPLC were as follows: sample injection volume, 50 μL; column, Capcell Pak C18 UG120 (4.6 mm i.d. × 150 mm; Shiseido, Tokyo, Japan); column temperature, room temperature; elution, linear gradient of 0–80% acetonitrile in 0.1% trifluoroacetic acid in 100 min; flow rate, 1 mL/min; and detection, A_{280}. Each peak isolated, was dried *in vacuo*, dissolved in 50 μL of 80% acetonitrile containing 0.1% trifluoroacetic acid, and subjected to Protein Sequencer Procise 492HT.

PCR was performed using the following degenerate primers designed based on the amino-acid sequences of peptides 1 and 2 (Fig. 2-6a): sense primer, 5´-AAYTGGGAYAAYAAYGGNTGGGA-3´ (Y: T or C; N: A, T, C, or G); antisense primer, 5´-GTNGGNGCRAANGTNCCNCCRAA-3´ (R: A or G). KOD FX (Toyobo, Osaka, Japan) was used as the DNA polymerase, and the chromosomal DNA of *N. drentensis* 57N was used as a template. The amplified DNA fragment (737 bp) was cloned into

pBluescript II SK (Stratagene, La Jolla, CA, USA) and sequenced using universal primers (T7 promoter and T3 promoter). The LA PCR *in vitro* Cloning kit (Takara Bio) was used to amplify the 5′ and 3′ flanking regions of the obtained DNA fragments. First, chromosomal DNA was digested with *Eco*RI or *Pst*I, and the corresponding cassettes were linked by ligation reaction. For amplification of the 5′ flanking region, the first PCR was performed using a primer that binds specifically to the cassette, Primer C1, and an antisense primer (5′-CAGATGAACCCCGTTTTTATCCG-3′) that binds specifically to the known region of the *NdIS* gene. Next, using a portion of the reaction solution of the first PCR as a template, a second PCR, nested PCR, was performed using the inner cassette primer (Primer C2) and the antisense primer of the gene-specific primer (5′-CAAAGGTTGTTTTCGCAATCCGC-3′). For amplification of the 3' flanking region, PCR was first performed using C1 and sense primer, 5′-CTTCCAGACCAGCAGGTAATCAGC-3′, followed by nested PCR using C2 and sense primer, 5′-AACGAGCCGAAAGATGAGAACG-3′. The cloning of DNA fragments and nucleotide sequence analyses were performed as described above. The DNA sequence of *NdIS*-gene was deposited to DDBJ with accession number LC767464. Further downstream DNA sequence was determined by the same method described above. *Hin*dIII or *Eco*RI digests of the genomic DNA with cassette DNA attachment as templates. The primers used were as follows: sense primers for *Hin*dIII digest (5′-GAATGTCGTCGGGTTTGCCC-3′ for first PCR and 5′-TTAGGCAACATGTCAATTGG-3′ for second PCR) and *Eco*RI digest (5′-GGATCCAAAGACTGGGGAAG-3′ for first PCR and 5′-TTTGAAGCGAACTCCGCAGG-3′ for second PCR), antisense primers used were universal, containing the cassette DNA sequence.

2.2.7. Multiple sequence alignment

The deduced amino acid sequence of NdIS was aligned with characterized GH68 enzymes using

ClustalW 2.1 (Thompson *et al.* 1994) and depicted with ESPript 3.0 (Robert and Gouet 2014). The ISs used and their GenBank accession numbers were as follows: *H. jeotgali* B3T IS (InuHj), ADJ14334.1; *Salipaludibacillus agaradhaerens* WDG185 IS (InuO), ATN45518.1; *Alkalihalobacillus krulwichiae* JCM11691 IS (InuBK), ARK30072.1; *Streptomyces viridochromogenes* DSM 40736 IS (HugO), EFL36273.1; *L. johnsonii* NCC 533 IS (InuJ), AAS08734.1; *Lactobacillus gasseri* DSM20604 IS, ACZ67286.1; *L. reuteri* 121 IS, OJI11288.1; *L. reuteri* TMW 1.106 IS, CAL25302.1; *Lactobacillus jensenii* JV-V16 IS, EFH30007.1; *S. mutans* GS-5 IS, AAA88584.1; *Weissella confusa* MBFCNC-2 (1) IS, ADB27748.1; *Leuconostoc citreum* CW28 IS, AAO25086.1; *Zymomonas mobilis* ATCC29191 β-fructofuranosidase (FF*Zm*), AFN56767.1; and *Z. mobilis* ATCC29191 levansucrase (LS*Zm*), AFN56768.1. The crystal structure of InuHj (PDB entry, 7BJ5) was used for the secondary structure representation.

2.2.8. Preparation of recombinant NdIS

The *NdIS* gene was amplified from the genomic DNA of *N. drentensis* 57N by PCR using Primestar Max DNA polymerase (Takara Bio) and the following primers: 5′-GGAGATATACATATGGCGGAAATCAGTTCAGAT-3′ (sense) and 5′-GTGGTGGTGGTGGTGGCGATTTGCCCCAAATGG-3′ (antisense). DNA fragment amplified was cloned into a pET-22b vector (Novagen, Darmstadt, Germany), which was double digested with *Nde*I and *Xho*I, using In-Fusion HD Cloning Kit (Takara Bio), and the inserted DNA fragment and conjunctive regions were sequenced. The deduced amino-acid sequence of the recombinant NdIS was identical to Ala33-Arg443 of the NdIS sequence (GenBank accession number, BEH79729.1) with Met and His_6 at the N- and C-termini, respectively. A transformant of *E. coli* BL21 (DE3) harboring the expression plasmid was cultured in 500 mL of LB medium containing 100 μg/mL ampicillin at 37°C until the $O.D._{600}$

reached 0.5. Isopropyl β-D-1-thiogalactopyranoside (Fujifilm Wako Pure Chemical) was added to a concentration of 0.1 mM, and the incubation was continued at 18°C for 18 h with vigorous shaking. The *E. coli* cells were harvested by centrifugation (5,000 × *g*, 4°C, 10 min), suspended in 10 mL of 10 mM sodium phosphate buffer (pH 7.5), and disrupted by sonication using a Sonifier 450 instrument (Branson; Danbury, CT, USA). The supernatant, obtained by centrifugation (12,000 × *g*, 4°C, 10 min), was loaded onto a Ni^{2+}-immobilized Chelating Sepharose Fast Flow column (2.5 cm i.d. × 6 cm; GE Healthcare, Uppsala, Sweden), which was pre-equilibrated with 10 mM sodium phosphate buffer (pH 7.5). After thoroughly washing the column with a buffer containing 50 mM imidazole, the adsorbed protein was eluted using a linear gradient of imidazole (50–300 mM, total elution volume, 400 mL). Fractions containing highly purified enzymes were collected and dialyzed against 10 mM sodium phosphate buffer (pH 7.0). The purified enzyme was stored at −80°C.

2.2.9. Protein assay

The protein concentrations of the chromatographic fractions were determined by the UV method (A_{280}) (Mach *et al.* 1995). The molar concentration of the purified enzyme was calculated based on the molar quantities of each amino acid measured using a JLC-500/V (JEOL, Tokyo, Japan) after complete acid hydrolysis of the enzyme (6 M HCl, 110°C, 24 h) (Moore and Stein, 1948).

2.2.10. Blue native PAGE

The molecular mass of NdIS under non-denaturing conditions was determined by blue native PAGE (Schägger *et al.* 1994). Analytical samples were prepared using a Native PAGE Sample Prep Kit (Life Technologies, Carlsbad, CA, USA). Novex Native PAGE 4–16% Bis-Tris Gels (Life Technologies) were used, and electrophoresis was performed at a constant voltage of 150 V for 115 min on ice. The Native

Mark Unstained Standard (Life Technologies) was used as the molecular size standard.

2.2.11. Standard enzyme activity assay of NdIS

A reaction mixture (100 μL), consisting of 80 mM sucrose, 40 mM MES-NaOH buffer (pH 6.5), 0.2 g/L bovine serum albumin (BSA; Fujifilm Wako Pure Chemical), and an appropriate concentration of enzyme, was incubated at 37°C for 10 min. The reaction was terminated by adding 20 μL of 0.5 M NaOH. The sample for 0-min reaction was prepared by pre-mixing the enzyme solution with 20 μL of 0.5 M NaOH and adding the other reaction mixtures. Liberated D-glucose was measured using an F-kit, D-glucose/D-fructose (Roche Diagnostics, Basel, Switzerland). One unit of IS activity was defined as the amount of enzyme yielding a D-glucose-releasing rate of 1 μmol/min under these conditions.

2.2.12. Effects of pH, temperature, and metal ions on the activity and stability of NdIS

The optimum pH and temperature of the enzyme reaction were determined by modifying the buffer solution and reaction temperature in the standard enzyme activity assay. In all reactions, the enzyme concentrations were 6.48 nM for native NdIS and 10.1 nM for recombinant NdIS. For the optimal pH evaluation, a 40 mM Britton-Robinson buffer (pH 3.0–12.0; a mixture of 40 mM acetic acid, 40 mM phosphoric acid, and 40 mM glycine, to which 200 mM NaOH was added to adjust the pH) was used as the reaction buffer. For the optimal temperature evaluation, the reaction temperature was set between 30°C and 60°C for native NdIS, 30°C and 65°C for recombinant NdIS. For pH stability measurements, 3.24 μM of native NdIS and 5.04 μM of recombinant NdIS were kept in 80 mM Britton-Robinson buffer (pH 4.1–11.0) at 4°C for 24 h, diluted 100-fold with 10 mM MES-NaOH buffer containing 1 g/L BSA, and then the residual activity was determined. To assess temperature stability, 32.4 nM of native NdIS and 50.4 nM of recombinant NdIS were kept in 10 mM MES-NaOH buffer (pH 6.5) containing 1 g/L

BSA at 30–65°C for 15 min. In native NdIS, the effects of metal ions on activity were evaluated in the presence of 10 mM LiCl, NaCl, KCl, NH_4Cl, $MgCl_2$, $CaCl_2$, $CoCl_2$, $NiCl_2$, and EDTA under standard conditions as in section 2.2.11. For recombinant NdIS, optimal temperature in the presence of 10 mM $CaCl_2$ was evaluated. Other conditions were same as in the absence of $CaCl_2$. To assess temperature stability in the presence of 10 mM $CaCl_2$, 50.4 nM of recombinant NdIS was kept in 10 mM MES-NaOH buffer (pH 6.5) containing 1 g/L BSA and 10 mM $CaCl_2$ at 30–65°C for 15 min. The activity of recombinant NdIS in the presence of 10 mM EDTA was measured under standard conditions as in section 2.2.11.

2.2.13. Kinetic parameters of the reaction of NdIS with sucrose

D-Glucose and D-fructose were quantified using an F-kit to determine NdIS-catalyzed D-glucose and D-fructose release rates from various concentrations of sucrose (1, 2.5, 5, 10, 25, 50, 100, 200, 400, and 800 mM). The amount of enzyme used in this study was 10.1 nM, and conditions other than substrate concentration followed the standard activity assay. The D-glucose release rate was defined as the aglycon release rate (v_{ag}) and the D-fructose release rate as the hydrolysis rate (v_h), and the transglycosylation rate, v_{tg}, was calculated by subtracting v_h from v_{ag}. Each rate obtained was regressed nonlinearly using CurveExpert 1.4 (Hyams 2010) to the following rate equations derived from the reaction scheme shown in Fig. 2-1 (Bruker *et al.* 1999; Kawai *et al.* 2004; Kobayashi *et al.* 2011).

Eq. 2-1, $v_{ag}/[E]_0 = (k_{cat2}[S]^2 + k_{cat1}K_{m2}[S])/([S]^2 + K_{m2}[S] + K_{m1}K_{m2})$

Eq. 2-2, $v_h/[E]_0 = k_{cat1}K_{m2}[S]/([S]^2 + K_{m2}[S] + K_{m1}K_{m2})$

Eq. 2-3, $v_{tg}/[E]_0 = k_{cat2}[S]^2/([S]^2 + K_{m2}[S] + K_{m1}K_{m2})$

The four kinetic parameters were expressed according to the rate constants shown in Fig. 2-1.

$K_{m1} = k_3(k_{-1} + k_2)(k_{-4} + k_5)/\{k_4k_5(k_{-1} + k_2) + k_1(k_{-4} + k_5)(k_2 + k_3)\}$

$K_{m2} = \{k_4k_5(k_{-1} + k_2) + k_1(k_{-4} + k_5)(k_2 + k_3)\}/k_1k_4(k_2 + k_5)$

$k_{cat1} = k_1k_2k_3(k_{-4} + k_5)/\{k_4k_5(k_{-1} + k_2) + k_1(k_{-4} + k_5)(k_2 + k_3)\}$

$k_{cat2} = k_2k_5/(k_2 + k_5)$

The transglycosylation ratio r_{tg} was defined as follows:

Eq. 2-4, $r_{tg} = v_{tg}/v_{ag} \times 100 = [S]/(K_{TG} + [S])$

K_{TG} (= $k_{cat1}K_{m2}/k_{cat2}$) is the substrate concentration providing a 50% transglycosylation ratio.

2.2.14. Analysis of transglycosylation at the initial reaction of recombinant NdIS

The reaction (1 mL) was done according to the standard activity assay, but concentrations of sucrose and recombinant NdIS were set to 800 mM and 50.4 nM, respectively. At each time point, 100 µL of the reaction solution was sampled and mixed with 20 µL of 0.5 M NaOH to stop the reaction. The sample for 0-min reaction was prepared by pre-mixing the enzyme solution with 20 µL of 0.5 M NaOH and adding the other reaction mixtures. The samples were diluted 10-fold with water and analyzed using high-performance anion-exchange chromatography-pulsed amperometric detection (HPAEC-PAD) in section 2.2.18.

2.2.15. Preparation of polysaccharides synthesized from sucrose by recombinant NdIS

A reaction mixture (10 mL) consisting of 400 mM sucrose, 40 mM MES-NaOH buffer (pH 6.5), and 504 nM recombinant NdIS was incubated at 37°C for 20 h. Two volumes of ethanol (−20°C) were added to the reaction mixture to precipitate the polysaccharide produced. After overnight incubation at 4°C, the precipitate was collected by centrifugation at 4°C at 12,000 × *g* for 5 min, washed thoroughly with 50% ethanol, and lyophilized. TLC analysis was performed in section 2.2.2 and HPAEC-PAD analysis was performed in section 2.2.18.

To determine the effects of sucrose concentration on polysaccharide production, 20, 50, 100, 200, 400, 800, 1,600 mM sucrose and recombinant NdIS (1.26 nM per 1 mM sucrose) were used. Reaction conditions other than sucrose and enzyme concentration were the same as above. The samples were appropriately diluted with water and analyzed using HPAEC-PAD and HPLC, as described in section 2.2.18 and 2.2.17, respectively.

2.2.16. ^{13}C-nuclear magnetic resonance (NMR) analysis of the polysaccharide products of NdIS

Recombinant NdIS-producing polysaccharides lyophilized, inulin from chicory (Raftiline HP; Beneo-Orafti SA, Tienen, Belgium), and levan from *Z. mobilis* (Sigma Aldrich) were dissolved in 99.9% D_2O (Sigma Aldrich) at approximately 10 g/L. ^{13}C-NMR was performed at 27°C using a Bruker Advance Neo instrument (126 MHz; Bruker, Billerica, MA, USA).

2.2.17. Evaluation of the average DP of the polysaccharide products of NdIS

The average number of D-fructosyl residues transferred from sucrose was calculated from the ratio of the sucrose concentrations used as the donor and acceptor, and the average DPs of the inulin-type polysaccharides were calculated using the following equation:

$$\text{Average DP} = 2 + ([\text{Glc}] - [\text{Fru}])/([\text{Suc}]_0 - [\text{Suc}] - [\text{Glc}]),$$

where [Suc], [Glc], and [Fru] are the molar concentrations of sucrose, D-glucose, and D-fructose, respectively, measured in the reaction mixtures and $[\text{Suc}]_0$ denotes the initial sucrose concentration. The transglycosylation ratio was calculated from the following equation:

$$\text{Transglycosylation ratio} = ([\text{Glc}] - [\text{Fru}])/[\text{Glc}] \times 100,$$

the concentrations of sucrose, D-glucose, and D-fructose in the reaction mixtures of recombinant NdIS and 20–1,600 mM sucrose described in section 2.2.15 were measured using HPLC. The HPLC conditions

were as follows: Sugar KS-801 column (8.0 mm i.d. × 300 mm; Shodex, Tokyo, Japan) at 60°C and 50 μM NaOH as the eluent at a flow rate of 1.0 mL/min. The refractive index was monitored and 5 g/L sucrose, D-glucose, and D-fructose solutions were used as quantification standards.

2.2.18. HPAEC-PAD analysis

Transglycosylates produced in the early stage of the reaction were analyzed using a Dionex ICS-3000 equipped with CarboPac PA1 (4 mm i.d. × 250 mm; Thermo Fisher Scientific) under the following conditions: sample injection, 5 μL; column temperature, room temperature; flow rate, 1 mL/min; detection, pulsed amperometry; and mobile phase, 150 mM NaOH containing sodium acetate (25 mM, 0–1 min; 25–50 mM, 1–2 min; 50–200 mM, 2–20 min). D-Glucose, D-fructose, sucrose, FOSs (1-kestose, nystose, and fructosylnystose; Fujifilm Wako Pure Chemical), and inulin from chicory (40–200 μM, 5 μL) were used as standards. For the analysis of polysaccharide DP, elution was performed using a linear gradient of 0–600 mM sodium acetate in 100 mM NaOH as the mobile phase for 60 min.

2.2.19. Prediction of the three-dimensional structure of NdIS

The three-dimensional structure of NdIS was predicted by ColabFold using the default parameters (Mirdita *et al.* 2022) and displayed using PyMOL version 2.5.0 (Schrödinger, New York, NY, USA). The three-dimensional structural model of NdIS was compared with the crystal structures of IS from *H. jeotgali* B3T (InuHj) in complex with 1-kestose and sucrose (Ghauri *et al.* 2021b; PDB entry, 7BJ4 and 7BJC, respectively) and IS from *L. johnsonii* NCC 533 (InuJ) in complex with 1-kestose (Pijning *et al.* 2011; PDB entry, 2YFT).

2.3. Results

2.3.1. Inulin-type polysaccharide synthesizing bacterium

Strain 57N, isolated from soil, exhibited a cream-colored, round-shaped colony morphology on a sucrose-containing agar-based medium. In the liquid fermentation supernatant of strain 57N, activity to produce inulin-type polysaccharides from sucrose was observed (Fig. 2-2a). TLC analysis of the reaction mixture detected polysaccharides that did not migrate from the TLC origin, in addition to residual sucrose. This polysaccharide was broken down to D-fructose by an endo-inulinase, as with authentic inulin (Fig. 2-2a), but not by levanase and dextranase (data not shown). HPAEC-PAD analysis showed that fructan chain was elongated in the reaction using the culture supernatant of strain 57N (Fig. 2-2b). Most of the peaks of the linear inulin was accompanied with smaller peaks, eluted just after the peaks of linear inulin.

The partial 16S rRNA gene sequence of strain 57N was 99.6% identical to the 16S rRNA gene sequence of *N. drentensis* LMG21831 (Heyrman *et al.* 2004; GenBank accession number, AJ542506.1). Physiological tests revealed that strain 57N is a non-motile Gram-positive rod (1.0–1.2 × 2.5–4.0 μm) that grows below 50°C under aerobic and anaerobic conditions. This strain was capable of spore formation. Carbohydrate utilization and enzymatic activity were almost consistent with those of *N. drentensis* strains (Table 2-1; Heyrman *et al*. 2004). Therefore, strain 57N was identified as *N. drentensis* and named *N. drentensis* 57N.

2.3.2. Purification and basic properties of native NdIS

The growth of *N. drentensis* 57N and its enzyme production were tested in a shake flask culture with liquid media containing sucrose, D-glucose, and D-fructose as carbon sources. It grew well in all media (data not shown), but IS activity, as indexed by the release of D-glucose when sucrose was used as a substrate, was detected only in cultures grown in a medium containing sucrose. No detectable activity (<

0.076 U/mL culture) was observed in culture supernatants of other carbon sources or cell suspensions.

NdIS was purified to homogeneity from 400 mL of the culture supernatant of *N. drentensis* 57N by ammonium sulfate precipitation and two column chromatographies, with a 22% yield of activity (276 U, 7.2 mg). In the hydrophobic column chromatography, two sucrase activity peaks were observed in the adsorbed fractions (Fig. 2-3). NdIS was obtained from the first active peak. The enzyme in another active peak is described in Chapter 4. The IS purified from the culture supernatant of *N. drentesis* 57N is referred to as native NdIS in this dissertation. Native NdIS showed a single protein band of 44 kDa on SDS-PAGE and 174 kDa on blue native-PAGE (Fig. 2-4). This indicated that NdIS is a homotetrameric protein. From 400 mL of culture, 7.2 mg of enzyme with specific activity of 38.3 U/mg was obtained. NdIS exhibited the highest activity at pH 6.1 and 45°C (Fig. 2-5a and b). More than 90% of its original activity was retained after incubation in a pH range of 5.1–7.5 at 4°C for 24 h and at 45°C or lower temperature at pH 6.5 for 15 min (Fig. 2-5a and c). The NdIS activity decreased to 51% and 35% in the presence of 10 mM $CoCl_2$ and $NiCl_2$, respectively, and increased to 112% in the presence of 10 mM $CaCl_2$. The monovalent cations tested and EDTA had no effect on NdIS activity (Table 2-2).

The reaction product from sucrose by a purified enzyme was analyzed. This enzyme produced an inulin-type polysaccharide detected as a non-migratory spot on TLC and almost entirely degraded by endo-inulinase (Fig. 2-2a). In the HPAEC analysis of native NdIS reaction products, saccharides up to an approximate DP of 42 were detected at the same retention times as authentic inulin (Fig. 2-2b). The small peaks, detected in the analysis of the product prepared using the culture supernatant of *N. drentensis* 57N were not observed. Polysaccharides were recovered from the reaction mixture *via* ethanol precipitation. The ^{13}C-NMR spectrum was in good agreement with that of authentic inulin, but not with that of levan (Fig. 2-2c). These results indicated that the NdIS product was an inulin-type β-(2→1)-fructan.

2.3.3. Sequence analysis of NdIS

Partial amino acid sequences of NdIS derived from its N-terminus and five peptides from lysyl-endopeptidase digests were determined (Fig. 2-6a, underlined). PCR obtained five DNA fragments; sequence analysis of the DNA fragments determined a DNA sequence of 6,883 bp in total length, including the 1,332 nt-long *NdIS* gene (Fig. 2-6b). The *NdIS* gene encoded a protein comprising 443 amino acids. Partial amino acid sequences determined by Edman degradation were all included in the putative amino acid sequence encoded by this gene (Fig. 2-6a). The N-terminal sequence of purified NdIS was identical to that of Ala33–Trp43 in the deduced sequence. The SignalP-5.0 program (Armenteros *et al.* 2019) suggested that the N-terminal Met1–Ala32 is a signal peptide. Taken together, the 32-residue-long N-terminal region was regarded as the secretion signal sequence, and the mature NdIS was composed of 411 residues. The calculated molecular mass of the mature NdIS (45.9 kDa) matched well with the mass (44 kDa) measured by SDS-PAGE (Fig. 2-4). A sequence similarity search using the Basic Local Alignment Search Tool (BLAST) program (Altschul *et al.* 1990) indicated that NdIS was 99.8% identical to a putative GH68 fructosyltransferase from *Bacillus* sp. AFS031507 (NCBI accession number, WP_098930566.1). According to protein sequence alignment by ClustalW 2.1, NdIS also showed high sequence identity with the following characterized GH68 IS enzymes: 68% identity with *S. agaradhaerens* InuO, 66% with *A. krulwichiae* InuBK, and 37% with *S. viridochromogenes* HugO. The sequence similarity of NdIS to two known ternary structure IS enzymes was not high. The overall NdIS sequence showed 33% identity with InuHj from the archaeon *H. jeotgali* B3T and 14% identity with the catalytic domain of InuJ (Ala180–Gln707) from *L. johnsonii*. The High similarity to *Bacillales* ISs indicated that NdIS is a member of GH68. No extra domains, such as the N-terminal variable domain or the C-terminal cell-wall-anchoring domain of ISs from *L. johnsonii* and other *Lactobacillales*, were found in the NdIS sequence, indicating that NdIS is composed solely of a catalytic domain. NdIS, characterized

ISs, and two non-IS enzymes (β-fructofuranosidase and levansucrase from *Z. mobilis* ATCC29191, FF*Zm*, and LS*Zm*, respectively) were aligned, and its partial amino acid sequence alignments of the GH68 enzymes, including the catalytic center and amino acid residues involved in substrate binding, are shown in Fig. 2-7. This alignment suggests that the three possible catalytic residues acting as nucleophile, general acid/base, and transition-state stabilizer of NdIS are Asp77, Glu317, and Asp233, respectively. In addition, most of the other residues involved in the formation of subsites −1 to +2 of the archaeal IS InuHj are conserved in NdIS (His112, Ala148, Arg232, His335, and Asn398). Glu266 of InuHj, hydrogen-bonded to the D-glucosyl moiety of sucrose and inner D-fructofuranosyl moiety of 1-kestose in subsite +1, was not conserved, but corresponded to Gln315 in NdIS. His112 of NdIS corresponds to His79 of FF*Zm* and Asn84 of LS*Zm*. A mutagenesis experiment suggested that the His residue in this position is crucial for the β-(2→1)-linked substrate preference (Okuyama *et al.* 2021). The residues comprising subsites −1 to +2 in NdIS (His112, Ala148, Arg232, His335, and Asn398) were more similar to ISs from non-lactic acid bacteria and even to FF*Zm* and LS*Zm* than to *Lactobacillales* ISs. The residues constituting the Ca^{2+}-binding site 1 of *L. johnsonii* InuJ, Asp419, Gln450, Trp487, Asn489, and Asp521, were not conserved in the NdIS sequence, except for the Asn489 equivalent (Asn284 of NdIS; Table 2-3). The residues involved in the Ca^{2+}-binding site 2 were not conserved in NdIS.

The determined 6,883-nt-long DNA sequence contained four other open reading frames, *NdGH32A* (partial), *NdGH68B*, *NdGH68C*, and *NdPTS* (partial), neighboring the NdIS-coding gene (*NdGH68A*) (Fig. 2-6b). A DNA sequence with 96.4% identity was found in the correspoinding region of the *Bacillus* sp. AFS031507 genome (Fig. 2-6c). The amino acid sequences of NdGH32A (partial), NdGH68B, NdGH68C, and NdPTS corresponded to the C-terminal region (Asp362–Asp798) of the putative GH32 protein of the *Bacillus* strain (NCBI accession number, WP_098930310.1) with 88.6% identity, the putative GH68 protein (WP_098930308.1) with 98.7% identity, the putative GH68 protein

(WP_098930306.1) with 96.9% identity, and the N-terminal region (Met1–Tyr292) of the putative sugar phosphotransferase system (PTS) transporter (WP_098930304.1) with 95.9% identity, respectively. The *Bacillus* putative GH32 protein is similar to GH32, CFTs from *B. circulans* (Kanai *et al.* 1997; Genbank accession number, BAA24360.1), *Paenibacillus macerans* (Kim and Choi 2001; Genbank accession number, AAG47946.1) and endo-inulinase from *Pseudomonas mucidolens* (direct submission; Genbank accession number, AAF24999.1), with approximately 40% sequence identity. NdGH68B protein shows a high sequence identity of 66% with *S. agaradhaerens* WDG185 FosA, 31–40% identity with GH68 ISs from *H. jeotgali* B3T (InuHj), *S. agaradherens* WDG185 (InuO) and levansucrases from *E. amylovora* (Sebaihia *et al.* 2010; Genbank accession number, CBJ48143.1), *B. indica* ATCC 9039 (Tamas *et al.* 2010; Genbank accession number, ACB95643.1). Thus, NdGH68B was named NdFosA. NdGH68C protein shows 41% identity with InuHj and GH68 levansucrase from *Clostridium acetobutylicum* (Mo *et al.* 2015; Genbank accession number, KHD38064.1).

2.3.4. Production of the recombinant NdIS in *E. coli*

Recombinant NdIS with a C-terminal His_6 tag was produced in *E. coli* BL21 (DE3) transformants and purified by Ni^{2+}-immobilized affinity column chromatography to homogeneity by SDS-PAGE (Fig. 2-4a). Recombinant NdIS showed a slightly higher molecular mass than naive NdIS as expected with the addition of the C-terminal His_6 tag. A total of 8.4 mg of recombinant NdIS was obtained from 500 mL of shake-flask culture cells. Its specific activity (34.1 U/mg) was almost identical to that of the native enzyme (38.3 U/mg). The effects of pH and temperature on the activity and stability were almost identical to those of the native enzyme. The NdIS was most active at pH 6.1 and stable in a pH range of 5.1–8.1 (Fig. 2-8a). Its optimum temperature for activity was 40°C, but 45°C in the presence of 10 mM $CaCl_2$ (Fig. 2-8b). The temperature stability range at ≤ 40°C was not significantly changed by the addition of 10 mM $CaCl_2$

(Fig. 2-8c). The activity, measured at 37°C, in the presence of 10 mM EDTA was 99.0 ± 0.3% of that in the absence of EDTA, indicating that EDTA does not directly affect catalytic activity. Recombinant NdIS produced inulin from 400 mM sucrose, with a chain length distribution similar to that produced by the native enzyme (Fig. 2-2b).

2.3.5. Kinetic analysis of the reaction with sucrose of NdIS

The initial reaction rates for aglycone release, hydrolysis, and transglycosylation were determined at various sucrose concentrations by colorimetric quantifying released D-glucose and D-fructose. The aglycone release and hydrolysis rates were almost identical up to 20 mM sucrose (Fig. 2-9a and b), indicating that the enzyme mostly catalyzed hydrolysis at sucrose concentrations up to 20 mM (Fig. 2-9c). The reaction rate for transglycosylation increased with increasing substrate concentration. The three reaction rates followed the rate equations (Eq. 2-1 to 2-3) from the reaction scheme shown in Fig. 2-1 (Fig. 2-9a) well. The kinetic parameters determined were as follows: k_{cat1}, 22.6 ± 0.4 s^{-1}; k_{cat2}, 60.2 ± 0.4 s^{-1}; K_{m1}, 0.510 ± 0.06 mM; and K_{m2}, 918 ± 67 mM. The r_{tg} values determined at various sucrose concentrations followed Eq. 2-4. The transglycosylation parameter K_{TG}, the substrate concentration that provides the same rates of hydrolysis and transglycosylation, was 344 ± 19 mM (Fig. 2-9b).

2.3.6. Analysis of transglycosylates in the initial reaction

The kinetic analysis in the previous section was based on the D-glucose and D-fructose release rates. This assumption does not take into account the possibility that reactions in which the transglycosylation product becomes an acceptor early in the reaction and the initial rate is not accurately estimated may occur. It also does not account for the possibility that NdIS forms bonds other than the β-(2→1)-linkage, such as the unexpected formation of the β-(2→1)-bond by levansucrase, an enzyme that typically forms the β-

(2→6) bond (Crittenden and Doelle 1993; Euzenat *et al.* 1997). Therefore, the reaction products in the initial reaction stage were analyzed using HPAEC. NdIS concentration (50.4 nM) was almost 5 times higher than that used in the rate measurement in the previous section, and 800 mM sucrose was used as substrate. Products were detected with HPAEC-PAD (Fig. 2-10). 1-Kestose and D-glucose were detected as the major products, whereas D-fructose was detected as a minor product. No other trisaccharides were detected. In the 5-min reaction, the concentration of D-glucose (511 μM) was almost equal to the sum of the concentrations of D-fructose (125 μM) and 1-kestose (404 μM). The ratio of 1-kestose production to D-glucose production was 404 μM/511 μM × 100 = 79%. These results indicated that, at 800 mM sucrose, transglycosylation was predominant, the transglycosylation acceptor was limited to sucrose, and no obvious transglycosylation was observed with 1-kestose as acceptor. NdIS catalyzed β-(2→1)-specific transfructosylation with sucrose even at the early stage of the reaction. The ratio of 1-kestose/sucrose concentrations (404 μM/800 mM) in the 5-min reaction is higher than the calculated 1-kestose/sucrose concentrations in the rate measurement in the previous section (156 μM/800 mM). Even at higher 1-kestose/sucrose ratios, no transglycosylation with 1-kestose acceptor was observed, suggesting that all transglycosylation rates determined in the previous section occurred only with sucrose at all concentrations.

2.3.7. Effect of sucrose concentration on the chain-length distribution of inulin-type polysaccharides

The recombinant NdIS produced inulin after 20 h of reaction with sucrose ranging from 20 to 1,600 mM. HPAEC-PAD analysis revealed that at the beginning of the reaction with 20 mM sucrose, hydrolysis was predominant, but when the reaction time was extended to 20 h, inulin were formed (Fig. 2-11a). An insoluble product was observed in the reaction with 1,600 mM sucrose (Fig. 2-11b). The insoluble product dissolved rapidly upon heating to 100°C. The DPs of the most abundant polysaccharides from 20, 50, 100,

200, 400, 800, and 1,600 mM sucrose were 16, 21, 22, 22, 22, 22, and 18, and the maximum DPs were 32, 39, 42, 42, 42, and 32, respectively. From the concentrations of sucrose, D-fructose, and D-glucose in the reaction mixture, the ratios of sucrose consumed as donors and acceptors in the D-fructosyl transfer reaction were calculated. The average DP of inulin-type polysaccharides produced from 20, 50, 100, 200, 400, 800, and 1,600 mM sucrose were 7.2, 12.1, 14.9, 16.5, 18.0, 18.2, and 14.3, respectively. The transglycosylation ratio in the reactions with 20, 50, 100, 200, 400, 800, and 1,600 mM sucrose were 34, 63, 77, 86, 92, 96, and 98%, respectively, and increased with increasing sucrose concentration.

2.4. Discussion

IS is a promising enzyme for mass production of inulin via successive β-(2→1)-transfructosylation from sucrose to acceptors. In this chapter, the soil bacterium *N. drentensis* 57N was isolated as an IS-producing bacterium, and its enzymatic characteristics and amino acid sequences were investigated.

N. drentensis 57N secreted IS extracellularly when cultured with sucrose as a carbon source but not with D-glucose and D-fructose as the carbon source. No IS activity was detected in cell suspensions grown on any of the carbon sources tested. This indicates that *N. drentensis* 57N possesses no cell-associated IS, whereas the GH68 levansucrase from *Streptococcus salivarius* and IS from *S. mutans* GS-5 are produced in cell-associated forms (Milward and Jacques 1990; Rozen *et al*. 2004). *S. salivarius* levansucrase is known to vary in its localization depending on the carbon source in the medium, being produced as a cell wall-bound form in cultures with D-glucose as the carbon source and being released into the medium when sucrose is the carbon source (Milward and Jacques 1990). Sucrose induced NdIS production, but D-glucose and D-fructose did not. In other words, in *N. drentensis* 57N, the carbon source in the medium regulated IS production but not its localization. The suppression of IS production by the monosaccharides is likely to be catabolite repression. Cell-associated GH68 enzymes such as *Lactobacillales* ISs have a

cell-wall-anchoring C-terminal domain containing a PXX-repeat region, an LPXTG cell-wall-anchoring motif, and a hydrophobic stretch region (Rathsam *et al.* 1993; van Hijum *et al.* 2002), but NdIS has no such additional domain. This was consistent with the finding that NdIS activity was detected only in the culture supernatant.

The *NdIS*-neighboring genes and the corresponding gene cluster in *Bacillus* sp. AFS031507 suggest that extracellularly produced β-(2→1)-fructan is assimilated by *N. drentensis* 57N as a carbon source, whereas the fructan contributes to bacterial aggregation in *L. reuteri* TMW1.106 and *S. mutans* GS-5 (Walter *et al*. 2008; Rozen *et al.* 2004). Upstream of the *NdIS* gene, a putative CFT/endo-inulinase, NdGH32A, was encoded, and downstream of the *NdIS* gene, a putative IS/levansucrase, NdFosA and a putative levansucrase, NdGH68C, were encoded (Fig. 2-6b). The genome of *Bacillus* sp. AFS031507, which has these homologous genes with high sequence identity, encoded a putative extracellular GH32 enzyme composed of two GH32 catalytic domains (COE25_RS31310), another intracellular CFT (COE_RS01290), and putative ATP-binding cassette (ABC) transporter components (COE25_RS01305, _RS01310, and _RS01315) further upstream (Fig. 2-6c). The metabolic pathways based on these possible activities will be discussed in detail in Chapter 5.

The structure of the active center of NdIS is discussed. To date, the crystal structures of two enzyme have been determined as complex with 1-kestose (archaeal InuHj and *L. johnsonii* InuJ, PDB entry, 7BJ4 and 2YFT, respectively; Ghauri *et al.* 2021b; Pijning *et al.* 2011), and they show two significant differences in 1-kestose binding (Fig. 2-12). His82 in the α-helix in the loop connecting 1B and 1C in InuHj is located near the three sugar moieties of 1-kestose, indicating that it plays an essential role in binding to this sugar. On the other hand, in *L. johnsonii* InuJ, the corresponding loop is short and the helix is absent, and the residue corresponding to His82 is absent. Instead, Arg623, located in the loop connecting 5B and 5C, is spatially close to His82. This amino acid side chain interacts with Fru O-6 *via*

water molecules (Pijning *et al.* 2011). The D-glucosyl moiety of 1-kestose binds differently to the +2 subsite, with the different binding residues (Fig. 2-12): Arg81, His82, His286 and Asn351 in InuHj and Arg542 and Arg545 in InuJ. NdIS shared almost all InuHj substrate-binding residues including the two His residues, although the whole sequence identity was only 33%. His112 and His335 of NdIS are equivalent to His82 and His286 of InuHj, respectively. This suggested that NdIS accommodates 1-kestose in a manner similar to InuHj (Fig. 2-12). The difference is Gln315 of NdIS at the position of Glu266 in InuHj, which interacts with the D-fructosyl moiety of 1-kestose in the +1 subsite. At this position, Glu is shared by *Lactobacillales* ISs and Gln by other ISs (Fig. 2-7). This Glu residue is presumed to be involved in the formation of inulin-like polymers with tens of thousands of DP (Ghauri *et al.* 2021b), consistent with the fact that NdIS does not produce this polymer.

NdIS did not lose catalytic activity with the addition of EDTA, suggesting that metal ions, including Ca^{2+}, are not essential for its activity and stability. Its effect was limited to increasing activity by 12% (Table 2-2) and the optimum temperature by 5°C (Fig. 2-8b and c). The addition of Ca^{2+} did not improve thermal stability. Taken together, Ca^{2+} may have the effect of stabilizing the complex structure during the reaction process or inhibiting reversible thermal denaturation. The effects of Ca^{2+} have been observed in many *Lactobacillales* ISs, including InuJ (Anwar *et al.* 2008; Ozimek *et al.* 2005), but not in ISs from non-lactic-acid bacteria or archaea, including InuHj (Kralj *et al.* 2018; Frasch *et al.* 2017; Yokoi *et al.* 2021; Ghauri et al. 2021a). Most of the Ca^{2+}-binding residues found in the InuJ structure are not conserved in the NdIS or in Ca^{2+}-independent ISs, including InuHj (Table 2-3). This may explain the limited effect of Ca^{2+} on the NdIS. In InuHj, it is suggested that a disulfide bridge (Cys226–Cys262) in InuHj partially compensates for the interactions *via* Ca^{2+} ions (Ghauri *et al.* 2021a), but NdIS and other Ca^{2+}-independent ISs, except the *Streptomyces* enzyme HugO, have no Cys residues in the corresponding positions.

No study has so far demonstrated a reaction scheme for IS. This chapter shows that NdIS follows the reaction scheme of retaining glycosidase by kinetic analysis of the reaction rate using sucrose as a substrate. NdIS mostly catalyzed hydrolysis at low concentrations of sucrose (≤ 20 mM), but the transglycosylation ratio increased with increasing sucrose concentration, and the K_{TG} was 344 mM (Fig. 2-9). The K_{TG} value indicated that sucrose is an unfavorable acceptor substrate for NdIS. Although no obvious transglycosylation was detected in the initial reaction at low substrate concentrations (Fig. 2-9), inulin-type polysaccharides were produced as the reaction progressed (Fig. 2-11). This suggests that sucrose serves predominantly as a donor substrate rather than an acceptor substrate, and the oligosaccharides formed slightly by transfructosylation act as superior acceptors. It was implied that transglycosylation products formed early in the reaction are act as preferential acceptors, and the molar concentration of transglycosylation products is kept low, resulting in the formation of long-chain fructans with DP 42 or higher at 100 to 800 mM sucrose. This chain-length is higher than that of inulin-type polysaccharide (≤ DP 27) synthesized from 100 to 800 mM sucrose by other *Bacillales* ISs, *Bacillus* sp. 217C-11 IS, InuO, and InuBK (Wada *et al.* 2003; Kralj *et al.* 2018; Yokoi *et al.* 2021). Multiple sequence alignment showed that the residues predicted to form the 1-kestose binding site were identical in NdIS and other *Bacillales* ISs (Fig. 2-7). The structure of the ≥ +3 subsite and the differences in amino acid residues near the subsite may have changed the orientation, affecting substrate specificity, and changing the chain length of the product. To determine the mechanism of synthesis of inulin-type polysaccharides, it is necessary to analyze their preference for acceptor substrates, which is discussed in Chapter 3.

Table 2-1. Comparison of the characteristics of strain 57N and *N. drentensis* strains.

Characteristic	*N. drentensis* strains	Strain 57N
Gram stain	+	+
Spore shape	E/C	E
Spore position	Pc	Pc
Growth at 50°C	+	−
Anaerobic growth	+	+
Hydrolysis of:		
Casein	−	−
Gelatin	−	−
2-Nitrophenyl-β-D-galactopyranoside	+	+
Urease	−	−
Nitrate reduction to N_2	V	−
Acid production from:		
Amygdalin	V	+
D-Cellobiose	−	+
l-Fucose	−	−
β-Gentiobiose	−	+
Glycerol	−	−
Glycogen	−	+
Lactose	+	+
D-Mannitol	−	−
D-Melibiose	+	+
D-Melezitose	V	+
Methyl α-D-glucoside	V	+
Raffinose	V	+
Ribose	V	−
Salicin	+	+
Starch	V	+
Sucrose	V	+
D-Turanose	V	+

V, results vary between strains; E, ellipsoidal; C, circular; Pc, Paracentral
Characteristics of *N. drentensis* strains are from Heyrman *et al.* 2004.

Table 2-2. Effects of 10 mM metal ions and EDTA on NdIS activity.

10 mM additive	Activity (%)[a]
LiCl	103 ± 3
NaCl	100 ± 3
KCl	99 ± 2
NH_4Cl	100 ± 3
$MgCl_2$	102 ± 1
$CaCl_2$	112 ± 1
$CoCl_2$	51 ± 1
$NiCl_2$	35 ± 2
EDTA	99 ± 1

[a] Relative to activity in the absence of the metal ions.

Table 2-3. Comparison of amino acid residues of the Ca^{2+}-binding site 1 of *L. johnsonii* NCC 533 InuJ with corresponding residues of *H. jeotgali* B3T InuHj and NdIS.

Ca^{2+}-binding residues	Corresponding residues	
of InuJ	InuHj	NdIS
Asp419	Met191	Ile227
Gln450	Ile219	Arg257
Trp487	Glu233	Leu282
Asn489	Asn235	Asn284
Asp521	Gln265	His314

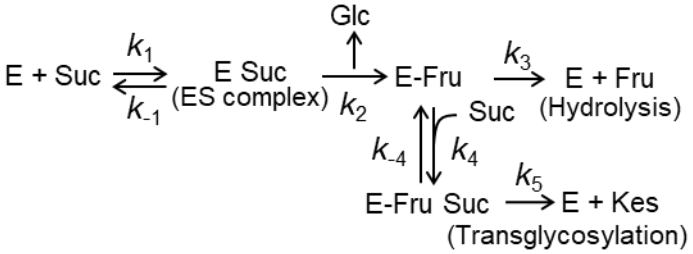

Fig. 2-1. Kinetic scheme of NdIS reaction on sucrose.

E, enzyme; Suc, sucrose; Kes, 1-kestose; E-Fru, D-fructosyl-enzyme intermediate.

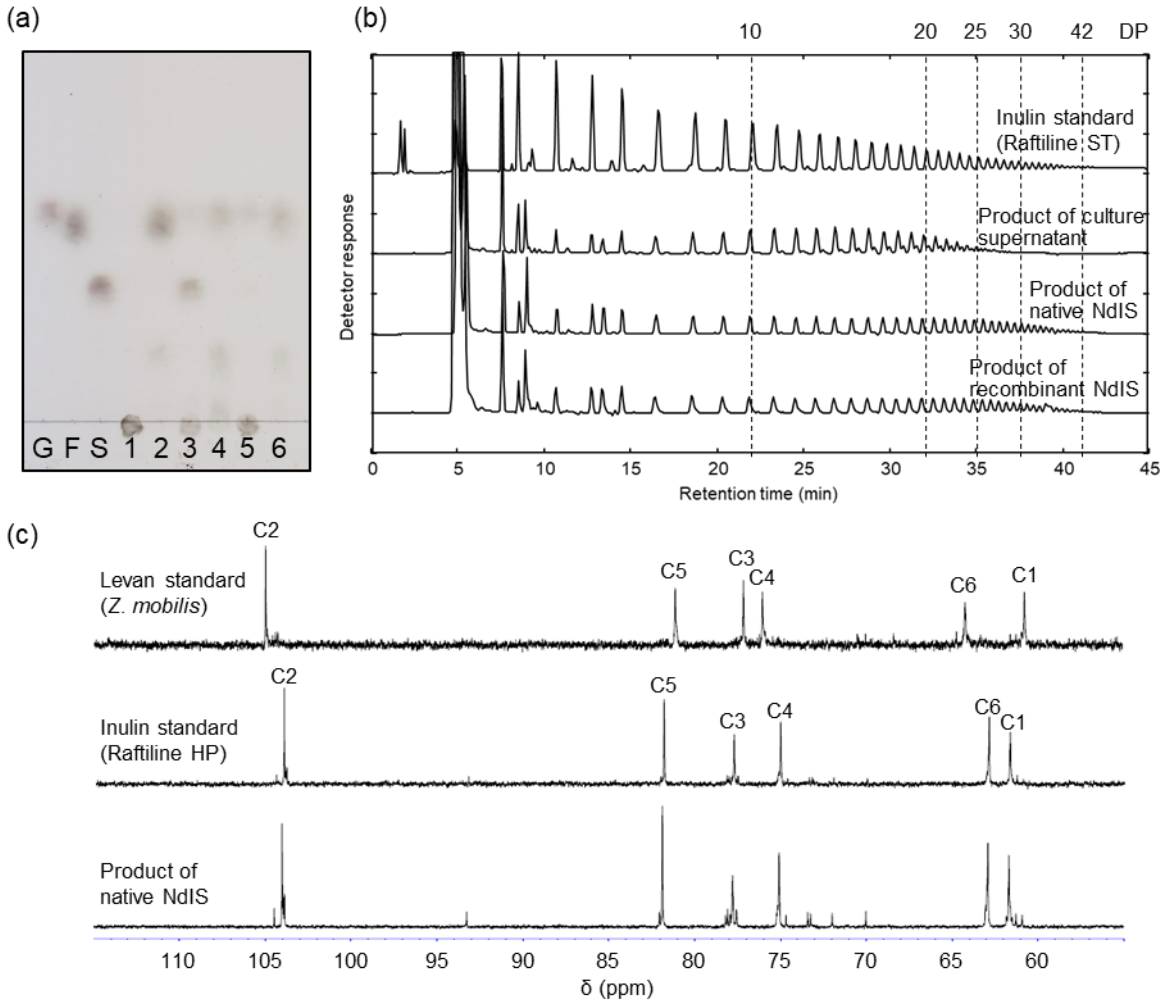

Fig. 2-2. Structural analysis of polysaccharide produced by NdIS.

(a) TLC analysis of reaction products from 333 mM sucrose using culture supernatant of *N. drentensis* 57N (lane 3) and by purified native NdIS (lane 5), and their digests by endo-inulinase (lanes 4, 6, respectively). Lanes 1, 2, inulin standard (Raftiline HP) and its digest by endo-inulinase, respectively. Lanes G, F, and S, D-glucose, D-fructose, and sucrose standards, respectively. (b) HPAEC-PAD analysis of the reaction products from 400 mM sucrose by culture supernatant of *N. drentensis* 57N, native and recombinant NdIS. DP of the reaction products are shown at the top of the figure. (c) ^{13}C-Nuclear magnetic resonance spectra of levan standard, inulin standard, and product of purified native NdIS from 400 mM sucrose.

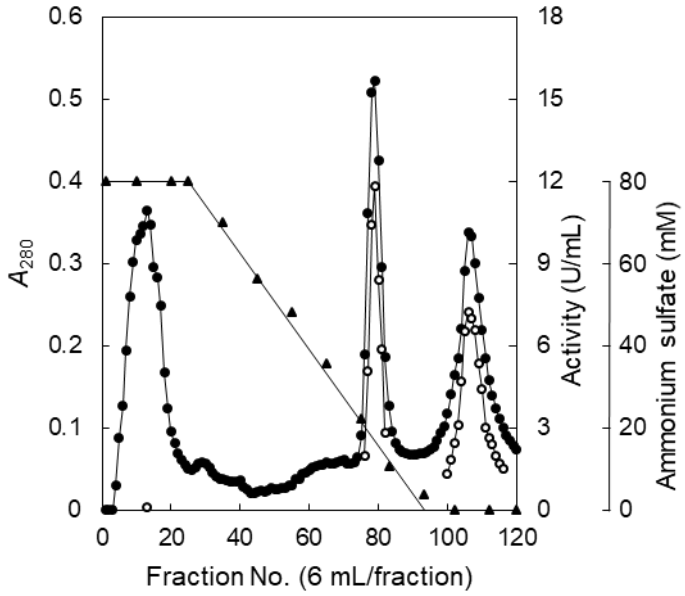

Fig. 2-3. Elution profiles of hydrophobic column chromatography of native NdIS.

A Toyopearl Butyl 650M column was used. Filled circle, A_{280}; open circle, D-glucose-releasing activity; filled triangle, ammonium sulfate concentration.

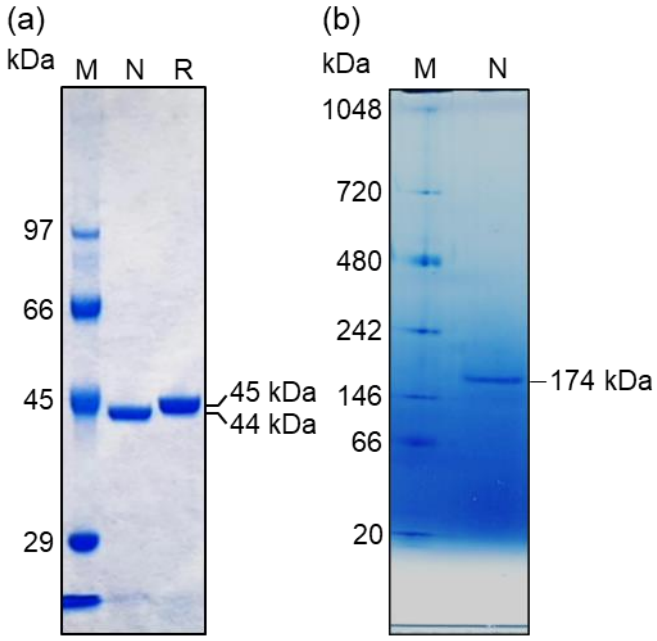

Fig. 2-4. Electrophoretic analyses of native and recombinant NdIS.

(a) SDS-PAGE. (b) Blue native PAGE. Lane N, native NdIS (1 μg); lane R, recombinant NdIS (1 μg); lane M, size markers. The molecular masses of the standards are shown on the left.

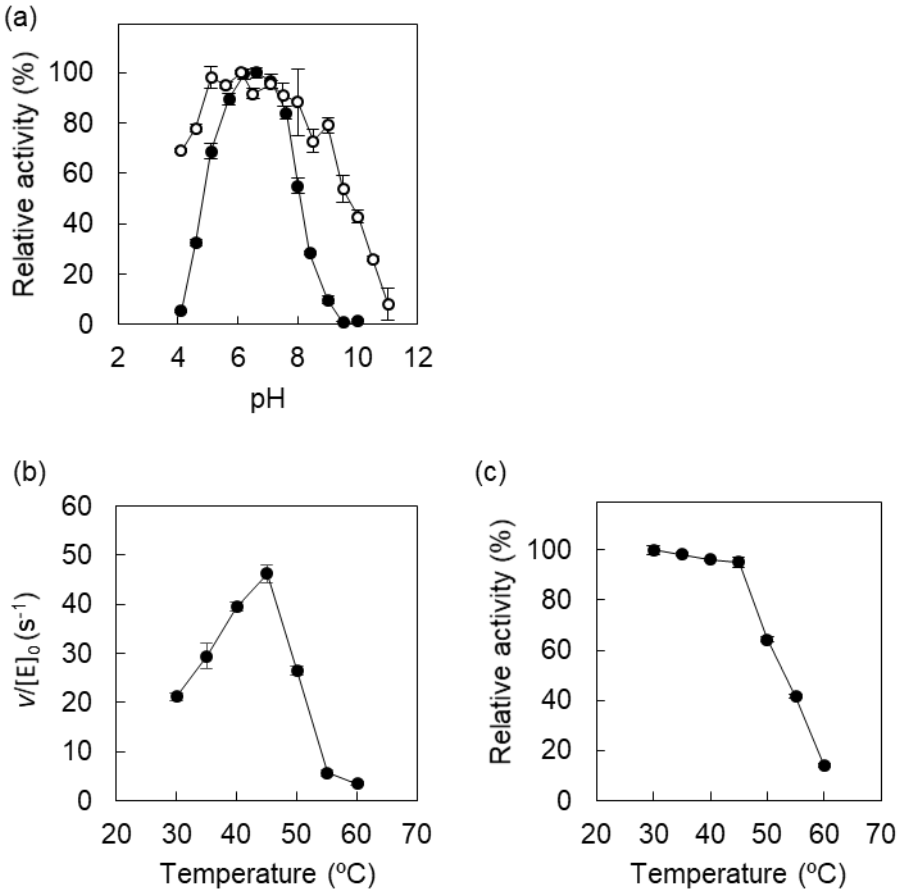

Fig. 2-5. Effects of pH and temperature on activity and stability of native NdIS.

(a) Effects of pH on activity at 37°C (filled circle) and remaining activity after incubation at 4°C for 24 hours (open circle). (b) D-Glucose releasing velocity measured at the indicated temperatures at pH 6.5 in a 10-min reaction. (c) Residual activity after incubation at the indicated temperatures at pH 6.5 for 15 min. The results are presented as the means of triplicate experiments with standard deviations.

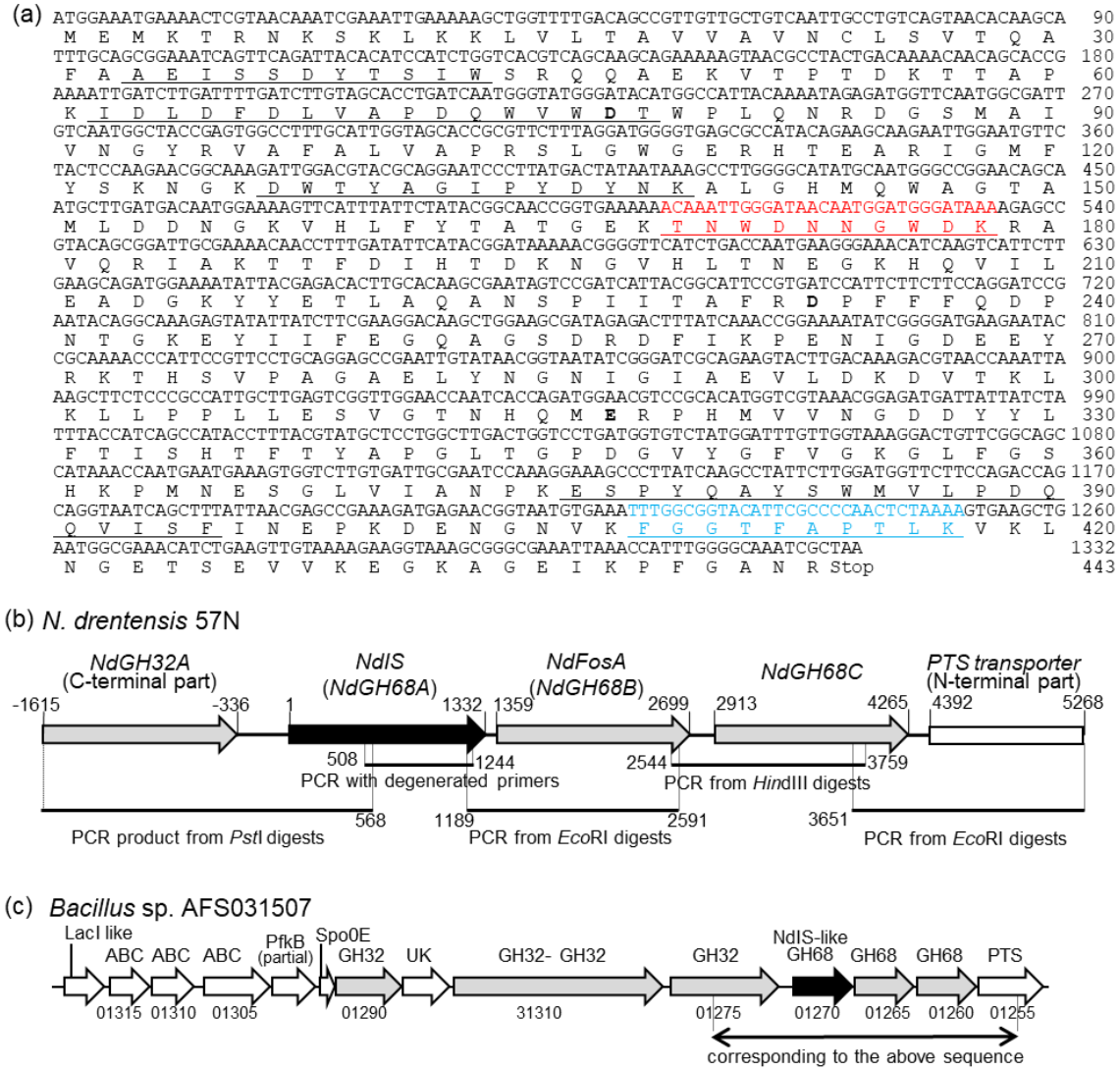

Fig. 2-6. Sequence analysis of the *NdIS* gene.

(a) Nucleotide sequence of the *NdIS* gene and its deduced amino-acid sequence. Amino-acid sequences determined by Edman degradation are underlined. The catalytic residues are in bold. Red and blue letters indicate the sequences of peptides 1 and 2, respectively. (b) PCR-amplified DNA fragments and the partial gene cluster region including the *NdIS* gene determined in this study. (c) The gene cluster in *Bacillus* sp. AFS031507 containing the *NdIS*-corresponding region (indicated with a double arrow) of the 68_C3_Contig1_140404 data. Locus tags (last 5 digits following "COE25_RS") and annotated functions or domains of the gene products are shown. LacI like, putative *lac repressor-like* gene. ABC, putative *ABC transporter component protein* gene. PfkB, putative *phosphofructokinase* gene. Spo0E, putative *aspartyl-phosphate phosphatase* gene. PTS, putative *PTS transporter* gene. UK, unknown.

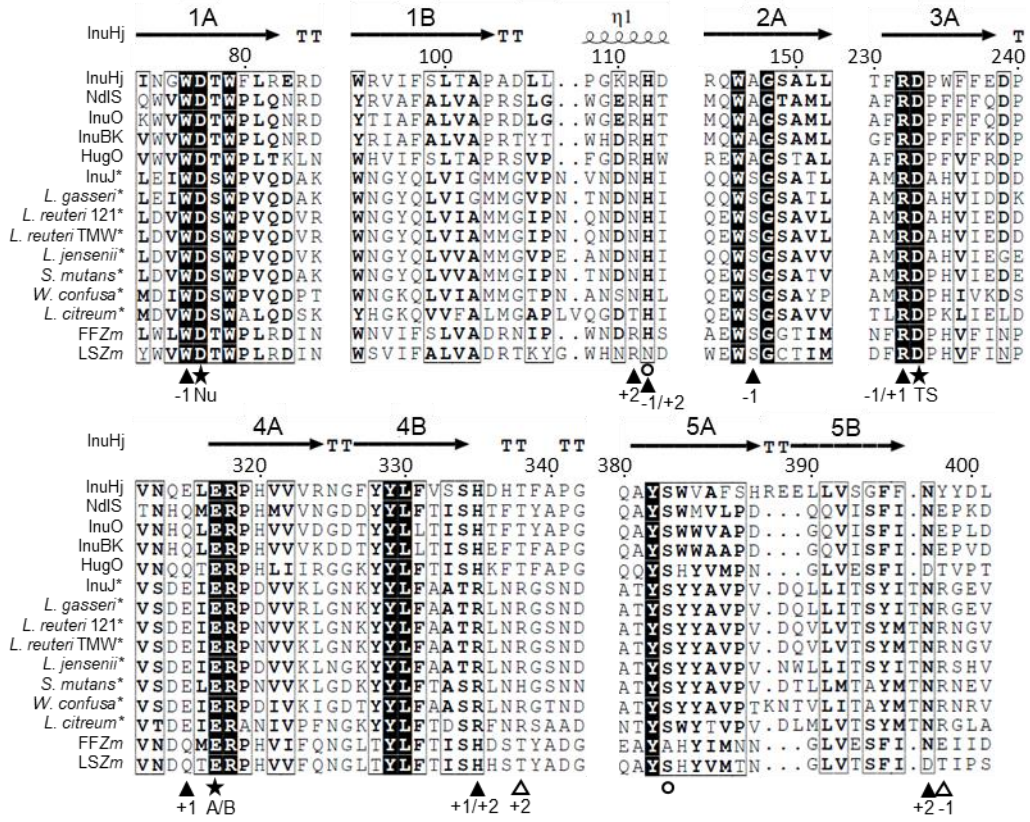

Fig. 2-7. Multiple sequence alignment of characterized inulosucrases.

InuHj, IS from the archaeon *H. jeotgali* B3T; NdIS, IS from *N. drentensis* 57N; InuO and InuBK, IS from the *Bacillales, S. agaradhaerens* WDG185 and *A. krulwichiae* JCM11691, respectively. HugO, IS from *S. viridochromogenes* DSM 40736. *Lactobacillales* IS indicated with asterisks: *L. johnsonii* NCC 533 (InuJ), *L. gasseri* DSM20604, *L. reuteri* 121, *L. reuteri* TMW 1.106, *L. jensenii* JV-V16. IS from *S. mutans* GS-5, *W. confusa* MBFCNC-2 (1), and *L. citreum* CW28. FF*Zm*, LS*Zm*, β-fructofuranosidase, and levansucrase were obtained from *Z. mobilis* ATCC29191. Stars: catalytic residues (Nu: nucleophile; TS: transition-state stabilizer; A/B: acid/base). Black triangles indicate amino acid residues that form subsites −1, +1, and +2 of InuHj for 1-kestose binding. White triangles indicate residues that form subsites −1 and +2 in InuJ from *L. johnsonii*, but are not conserved in NdIS. Circles indicate residues that determine the regioselectivity of transfructosylation in FF*Zm* and LS*Zm*. Numbers above are of NdIS. The strand notation is of InuHj (Ghauri *et al.* 2021b).

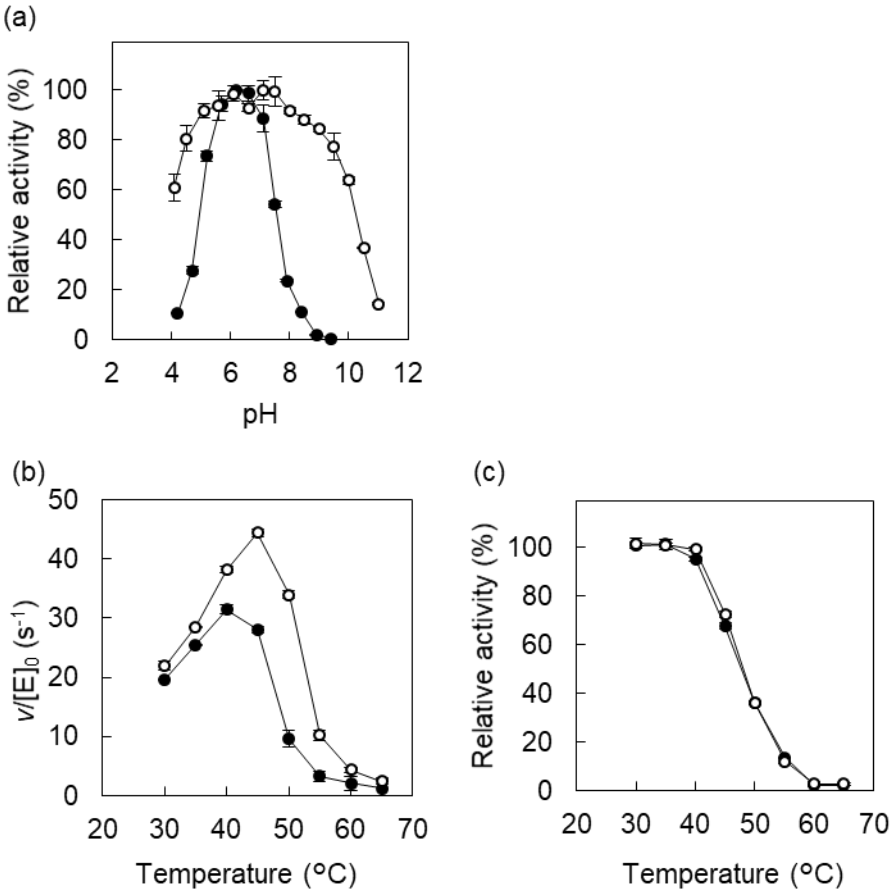

Fig. 2-8. Effects of pH and temperature on activity and stability of recombinant NdIS.

(a) Effects of pH on activity at 37°C (filled circle) and remaining activity after incubation at 4°C for 24 hours (open circle). (b) D-Glucose releasing velocity measured at the indicated temperatures at pH 6.5 in a 10-min reaction in the absence (filled circle) and presence of 10 mM $CaCl_2$ (open circle). (c) Residual activity after incubation at the indicated temperatures at pH 6.5 for 15 min in the absence (filled circle) and presence of 10 mM $CaCl_2$ (open circle). The results are presented as the means of triplicate experiments with standard deviations.

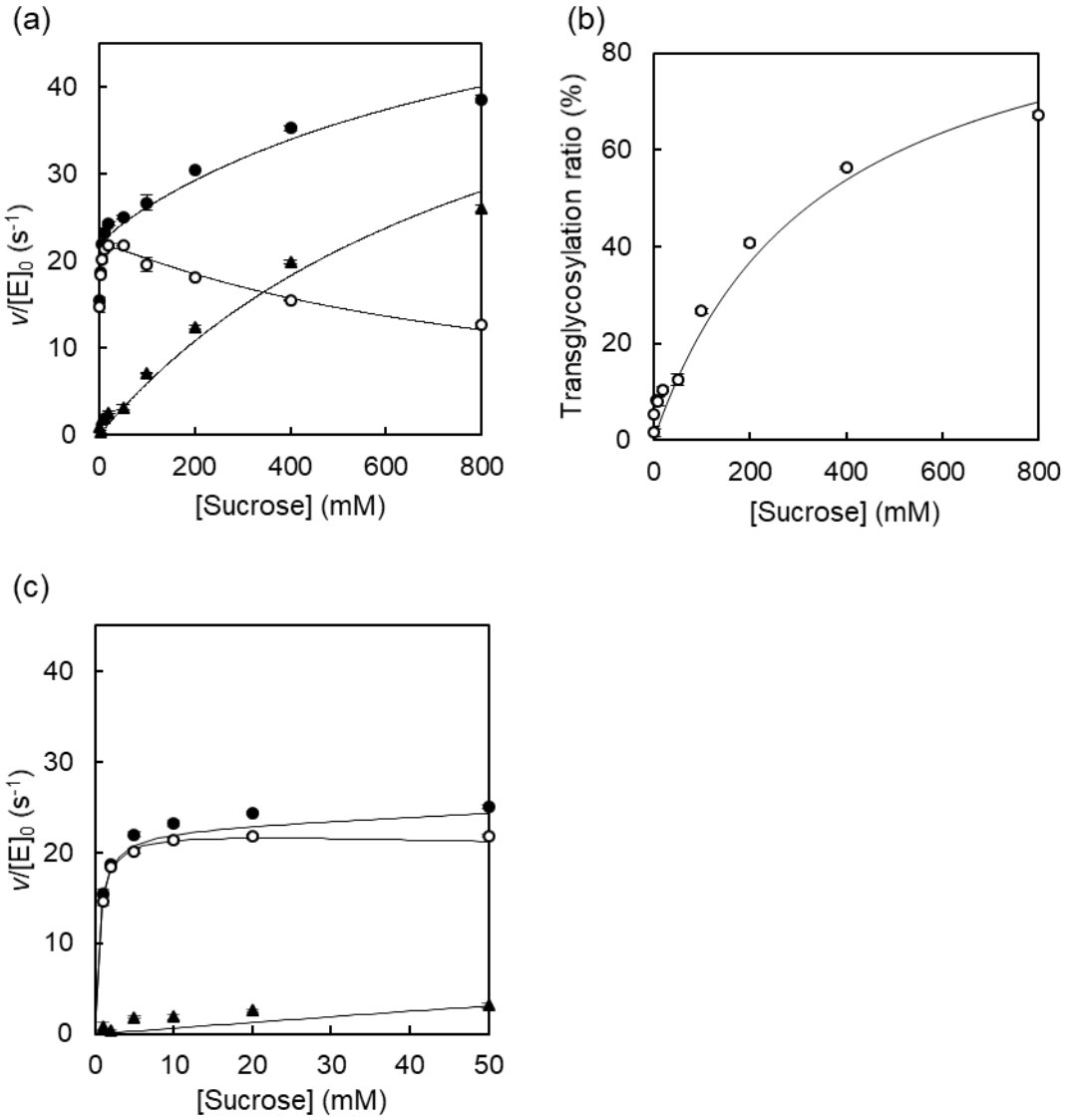

Fig. 2-9. Kinetics of catalytic reaction toward sucrose.

(a) The dependence of initial velocities of aglycone release ($v_{ag}/[E]_0$, filled circle), hydrolysis ($v_h/[E]_0$, open circle), and transglycosylation ($v_{tg}/[E]_0$, filled triangle) on sucrose concentration. (b) Dependence of transglycosylation ratio ($r_{tg} = v_{tg}/v_{ag}$) on sucrose concentration. (c) Enlarged view of panel (a) at 0 to 50 mM sucrose concentration. Theoretical curves with the kinetic parameters are drawn. The data are presented as the means of triplicate experiments with standard deviations.

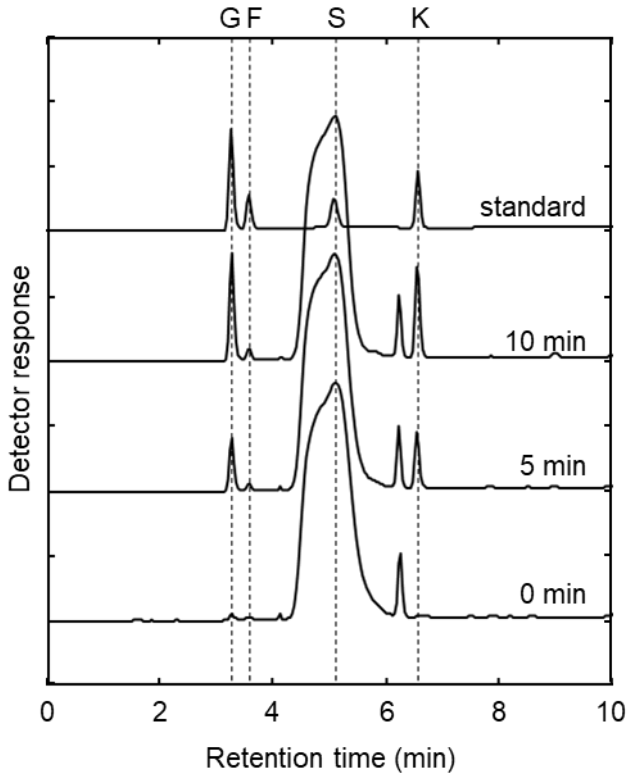

Fig. 2-10. HPAEC-PAD analysis of the initial reaction products of NdIS from 800 mM sucrose.

The reaction was performed in 800 mM sucrose and 50.4 nM recombinant NdIS. The reaction products were analyzed at 0–10 min intervals. The standards included 20 mg/L of D-glucose, D-fructose, sucrose, and 1-kestose. G, D-glucose; F, D-fructose; S, sucrose; K, 1-kestose.

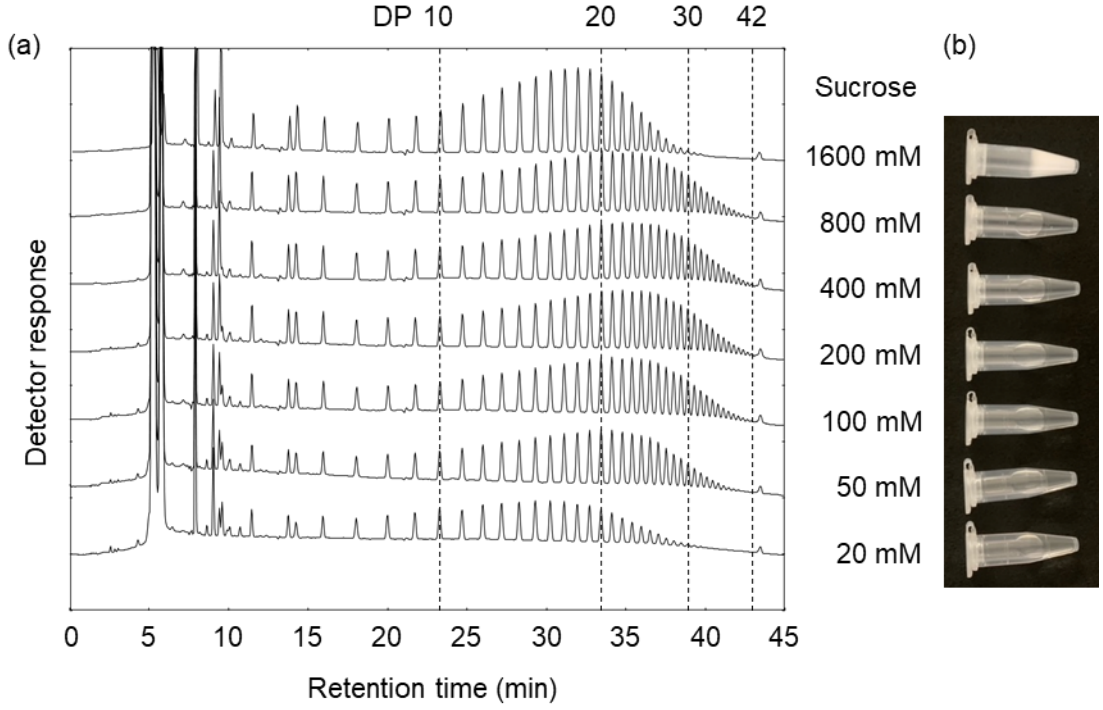

Fig. 2-11. DP of reaction products of recombinant NdIS from various concentrations of sucrose (a) and appearance of the reaction solution (b).

The reactions were carried out with 20–1,600 mM sucrose and the products were analyzed using HPAEC-PAD. DP of the reaction products are shown at the top of the figure.

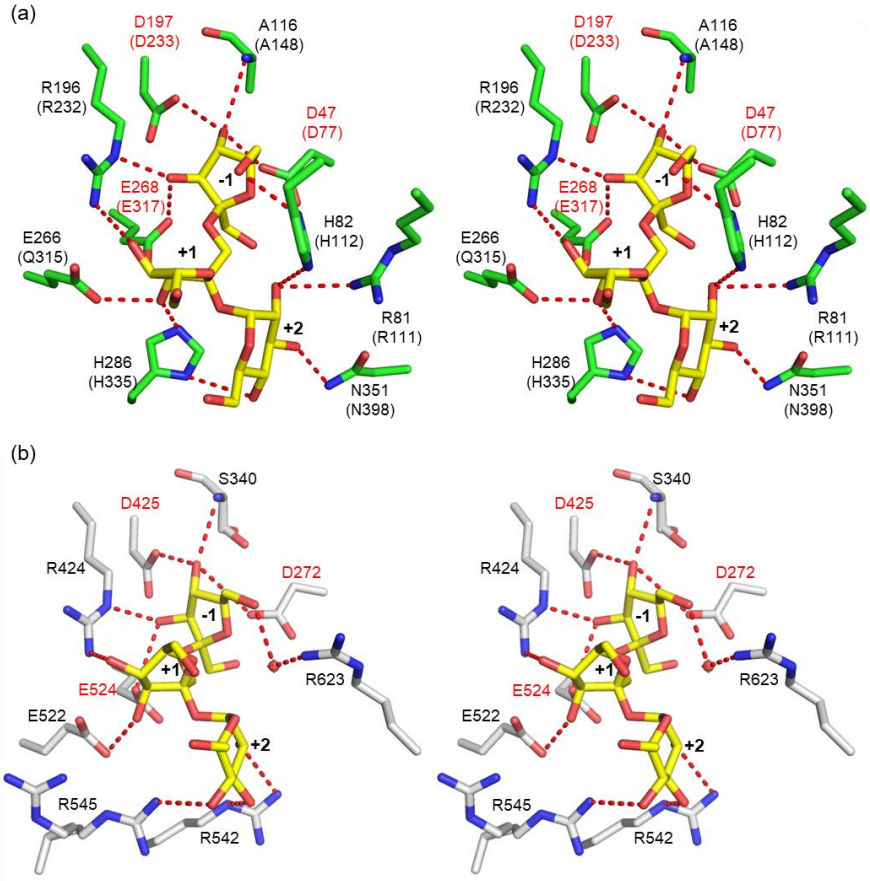

Fig. 2-12. Stereo view of 1-kestose binding site of the crystal structures of InuHj (a; Ghauri *et al.* 2021b; PDB entry, 7BJ4, molecule B) and InuJ (b; Pijning *et al.* 2011; PDB entry, 2YFT).

The structures of InuHj and InuJ in a complex with 1-kestose are shown. 1-Kestose is in yellow. The amino acid residues involved in the interaction with 1-kestose are indicated. Red ball indicates water molecule. The catalytic residues are indicated in red letters. The predicted hydrogen bonds between the residues and 1-kestose are indicated by red dashed lines. The equivalent residues of NdIS are indicated in parentheses in panel (a).

Chapter 3. Kinetic analysis of transglycosylation catalyzed by NdIS

3.1. Introduction

IS produces inulin-like polysaccharides from sucrose, but their length and structure vary among enzymes. For example, *Bacillales* IS produces linear inulin with tens of DP (Wada *et al.* 2003; Kralj *et al*. 2018; Yokoi *et al.* 2021). On the other hand, *Lactobacillales* IS produces inulin-like polymers with a branched structure and tens of thousands of DP (Rosell and Birkhed 1974; van Hijum *et al.* 2002; Anwar *et al*. 2008). As described in Chapter 1, in *L. reuteri* 121 IS, one of the *Lactobacillales* IS, some amino acid residues that are important for the formation of products with DP 6–10 have been identified (Charoenwongpaiboon *et al*. 2019a). However, the mechanism involved in chain length determination is still unclear especially in *Bacillales* IS. Even the acceptor specificity for the short-chain FOS generated in the process of producing the long-chain products, such as 1-kestose and nystose, is not known. The previous chapter described the discovery of NdIS, an inulin polysaccharide-generating enzyme secreted extracellularly by *N. drentensis* 57N, and the characteristics of inulin polysaccharide synthesis using sucrose as the initial substrate. NdIS produced inulin-type polysaccharides with an average DP of 7–18 and a maximum DP of 30–42 or higher at any starting surose concentration (20–1600 mM) (section 2.3.7). The initial reaction analysis revealed that NdIS predominantly hydrolyzes sucrose at low concentrations rather than transglycosylation (section 2.3.5). The high K_{TG} for sucrose (344 mM) clearly indicates that sucrose is not good acceptor of transglycosylation for NdIS. However, the production of inulin-type polysaccharides was apparently observed even in the reaction with low concentration of sucrose. This suggests that transglycosylation product slightly produced in the initial reaction are assumed to be used preferentially as acceptor of transglycosylation. So far, no specific evaluation of the acceptor and donor has been performed in ISs, and the molecular mechanism of inulin-type polysaccharides synthesis is unknown. Therefore, this chapter aimed to elucidate the molecular mechanism of inulin synthesis of NdIS

through detail kinetic analysis of transglycosylation. In particular, the relative acceptor specificity was quantified by a simple method using a two-substrate mixture reaction. The specificity of IS had not been evaluated by separating acceptors and donors. In this way, sucrose and FOSs were shown to be significantly better as donor and acceptor, respectively, than the other. Selective transglycosylation from sucrose to the initially produced FOS as the preferential acceptor was indicated as the molecular mechanism of NdIS for β-(2→1)-fructan chain elongation is discussed based on the donor and acceptor preference. The DP-controlled inulin synthesis by NdIS through adjusting the acceptor concentration is demonstrated.

3.2. Materials and methods

3.2.1. TLC analysis of the products from sucrose, 1-kestose, and nystose

A reaction mixture (50 μL), consisting of 50 mM substrate (sucrose, 1-kestose, or nystose), 40 mM MES-NaOH buffer (pH 6.5), 0.2 g/L BSA, and 502 nM NdIS, was incubated at 37°C. After 10 min, 1 h, and 18 h of reaction time, 10 μL of the reaction mixture was drawn held at 100°C for 10 min to stop the reaction. TLC analysis was performed as described in section 2.2.2.

3.2.2. Preparation of FOSs

A reaction mixture (12.5 mL), consisting of 600 mM sucrose, 300 mM nystose, 100 mM MES-NaOH buffer (pH 6.5), and 250 nM NdIS, was kept at 37°C for 5 h. The reaction was stopped by holding the mixture at 100°C for 10 min, and the products was separated by active carbon-celite column chromatography (50 mm i.d. × 510 mm; SW-50 [Futamura Chemical, Nagoya, Japan]/Radiolite #700 [Hayashi Kasei, Osaka, Japan], 1/1, w/w). Monosaccharides, disaccharides, and trisaccharides were washed out with 11% v/v ethanol. FOSs of DP 4–9 were eluted with 12% v/v ethanol (4.5 L) and 13%

v/v ethanol (2 L). The fractions containing DP 5–9 of FOSs were lyophilized. Sugar composition of the reaction products and the purity of the prepared FOSs were evaluated by HPLC under the following conditions: sample, 20 μL of 1 mg/mL; column, Asahipak NH2P-50 4E (4.6 mm i.d. × 250 mm; Shodex); column temperature, 25°C; mobile phase, 60% v/v acetonitrile; flow rate, 1 mL/min; detection, refractive index.

3.2.3. Kinetic analysis of two-substrate reactions with sucrose and various sugars

The reaction was performed as described in section 2.2.11, but in addition to 50 mM sucrose as the first substrate, 50 mM sugars (1-kestose, nystose, DP 5–9 FOS, and D-xylose) were contained as the second substrate. The NdIS concentration was 0.502 nM for the reactions in which 1-kestose or nystose was added as a second substrate and 1.26 nM for the others. The reactions with 50 mM sucrose and 0, 0.5, 1, 1.5, and 2 mM 1-kestose were also carried out under the same conditions. In the reactions with 50 mM 1-kestose and nystose, reaction aliquots were taken during the reaction as described in section 2.2.14, and v_{ag}, v_h, and v_{tg}, and transglycosylation ratio with sucrose were determined as described in section 2.2.13. In addition, v_{tg} with 50 mM 1-kestose and nystose was also calulated through measuring nystose and fructosylnystose by HPAEC-PAD, respectively, as described in section 2.2.18.

The acceptor preference of NdIS was evaluated using v_{tg}/v_h according to the reaction scheme shown in Fig. 3-1. In this scheme, when E-Fru is regarded as a starting enzyme, the specificity constants k'_2, for E-Fru to produce Fru via E-Fru water, k'_4, for E-Fru to produce Fru-sucrose *via* E-Fru Sucrose, and k'_6, for E-Fru to produce Fru-FOS *via* E-Fru FOS, respectively, are as follows:

$k'_2 = k_1k_2/(k_{-1} + k_2)$,

$k'_4 = k_3k_4/(k_{-3} + k_4)$,

$k'_6 = k_5k_6/(k_{-5} + k_6)$,

v_h and v_{tg} are as follows, respectively:

$v_h = k'_2$[E-Fru][water],

$v_{tg} = k'_4$[E-Fru][sucrose] + k'_6[E-Fru][FOS],

from these, v_{tg}/v_h is expressed in the following Eq. 3-1:

Eq. 3-1, $v_{tg}/v_h = (k'_4/k'_2)$ [sucrose]/[water] + (k'_6/k'_2) [FOS]/[water],

where, [water] is invariant, the [FOS]-v_{tg}/v_h plot gives a straight line with slope (k'_6/k'_2)/[water] and intersection with vertical axis (k'_4/k'_2) [sucrose]/[water] when the [sucrose] is constant. Using the v_{tg}/v_h in the presence of 50 mM FOS relative to that in the absence of FOS (Relative-v_{tg}/v_h), k'_6/k'_4 is expressed as following Eq. 3-2:

Eq. 3-2, k'_6/k'_4 = Relative-$v_{tg}/v_h - 1$,

k'_6/k'_4 indicates the affinity of FOS for E-Fru over sucrose.

3.2.4. Measurement of reaction rates for 1-kestose and nystose

The reaction conditions were the same as the two-substrate reaction (section 3.2.3), but 50 mM 1-kestose and nystose as a sole substrate. NdIS concentration was 12.6 nM. Reaction product quantification was done as described in section 2.2.18.

3.2.5. Analysis of polysaccharide products from two-substrate reaction of sucrose and 1-kestose or nystose

The reaction conditions were the same as for the two-substrate reactions (section 3.2.3), but 400 mM sucrose, 0, 10, 20, 50, and 100 mM 1-kestose or nystose, 502 nM NdIS, and 20 h reaction time. The reaction was terminated by heating the sample at 100°C for 10 min. Sucrose, D-glucose, and D-fructose in the samples were quantified by HPLC. The HPLC was done with Sugar KS-801 column (8.0 mm i.d.

× 300 mm) at 60°C and 50 μM NaOH as the eluent at a flow rate of 1.0 mL/min. Sugars were detected by monitoring the refractive index. Sucrose, D-glucose or D-fructose at 5 g/L each were measured separately as quantification standards. Molar concentrations of enzymatically liberated D-fructose $[Fru]_L$ and D-glucose $[Glc]_L$ and remaining sucrose [Suc] were determined using the samples before the acid hydrolysis. Portions of the reaction samples were incubated with 100 mM HCl at 60°C for 2 h for complete hydrolysis. Total molar concentrations of D-fructosyl units $[Fru]_T$ and D-glucosyl units $[Glc]_T$ contained in the substrates were calculated from those in the acid hydrolysates. The average DPs of the transglycosylation products were calculated from their fructose/glucose ratios using the following equation:

Eq. 3-3, Average DP = $1 + ([Fru]_T - [Fru]_L - [Suc])/([Glc]_T - [Glc]_L - [Suc])$

To analysis of polysaccharides DP distribution, the samples were diluted 10-fold and analyzed by HPAEC-PAD under the conditions described in section 2.2.18.

3.2.6. Analysis of transglycosylation with monosaccharide acceptors

Transglycosylation of NdIS with various monosaccharides was analyzed as for the two-substrate reaction (section 3.2.3), but 10 g/L inulin instead of sucrose, and 502 nM NdIS. As the second substrate, 50 mM monosaccharides (D-fructose, D-psicose, D-tagatose, L-sorbose, D-glucose, D-mannose, D-allose, D-galactose, and D-xylose) were examined. A reaction containing equimolar concentrations of D-glucose and D-xylose (10, 20, and 50 mM) as the monosaccharide acceptor was also analyzed to evaluate the acceptor preference. The reaction was terminated by heating at 100°C for 10 min. The reaction products were analyzed by HPAEC-PAD analysis as described in section 2.2.18. From the transglycosylation velocities obtained in the presence of equimolar concentrations of D-glucose and D-xylose, the difference in binding energy ($\Delta\Delta G$) was evaluated using the following Eq. 3-4 quoted from Fersht *et al.* 1985:

Eq. 3-4, $\Delta\Delta G = \Delta G_{Glc}^{\ddagger} - \Delta G_{Xyl}^{\ddagger} = -RT \ln (k'_{Glc}/k'_{Xyl})$,

where k'_{Glc} and k'_{Xyl} are specificity constants for D-glucose and D-xylose as acceptor, respectively, in the deglycosylation step for transglycosylation. In the presence of equimolar D-glucose and D-xylose (50 mM), $k'_{Glc}/k'_{Xyl} = v_{tg\ Glc}/v_{tg\ Xyl}$.

3.2.7. Preparation of D-fructosyl D-xyloside

A reaction mixture (1 mL), containing 0.54 M sucrose, 2.87 M D-xylose, 40 mM MES-NaOH buffer (pH 6.5), and 250 nM NdIS was kept at 37°C for 24 h, and then at 100°C for 10 min. The transglycosylation product was purified from the sample (300 μL) by RP-HPLC: sample injection, 100 μL; column, YMC-Pack ODS-AQ (20 mm i.d. × 250 mm; YMC, Kyoto, Japan); column temperature, 35°C; eluent, water; flow rate, 3 mL/min; detection, refractive index. In three repeated chromatographies, the peak eluted at 30–35 min was collected. The sample was lyophilized and used for structural analysis. Purity of the sample was analyzed by RP-HPLC as for the separation, but injection, 5 μL of 4 mg/mL sample; column, YMC-Pack ODS-AQ (4.6 mm i.d. × 250 mm; YMC); flow rate, 0.2 mL/min.

3.2.8. Structural analysis of D-fructosyl D-xyloside

Electrospray ionization-mass spectrometry (ESI-MS) of the transglycosylation product toward D-xylose was carried out using an Exactive mass spectrometer (Thermo Fisher Scientific). The sample was introduced by flow injection using methanol as the mobile phase solvent. The positive ion was detected under the following conditions: tube lens voltage, 80 V; skimmer voltage, 30 V. ^{13}C- and ^{1}H-NMR spectra were recorded in D_2O at 27°C using a Bruker Advance Neo. A series of two-dimensional homo- and heteronuclear correlated spectroscopy (COSY), heteronuclear single quantum coherence (HSQC), HSQC-total correlation spectroscopy (HSQC-TOCSY), heteronuclear multiple bond correlation (HMBC), and heteronuclear 2-bond correlation (H2BC) spectra were obtained.

3.3. Results

3.3.1. Reaction of NdIS on 1-kestose and nystose

The reactions of NdIS with fructooligosaccharides was investigated. The products of the reaction using 1-kestose (DP 3) or nistose (DP 4) as substrates were analyzed by TLC (Fig. 3-2). In a reference reaction using 50 mM sucrose, the products were mostly inulin-type polysaccharides and monosaccharides with trace amounts of oligosaccharides. In the reaction with 1-kestose or nystose substrates, the formation of oligosaccharides with different DP, i.e., disproportionation of these substrates, was observed (Fig. 3-2). Slight amounts of monosaccharides were formed after 18 h of reaction. Sucrose was not detected in the reactions. In the reaction with nystose, products with DP 3 to 10 or higher were produced. On the other hand, the reaction of 1-kestose produced products with DP 3 to 7 and progress was less than that of nystose. The product distribution indicates that the 1-kestose and nystose serve as both donor and acceptor in the transglycosylation, and the other FOSs serves as well. The undetectable sucrose with the formation of monosaccharide in the reaction with 1-kestose suggests that sucrose released from 1-kestose in the reaction was quicily consumed.

Initial reactions with 1-kestose and nystose were analyzed quantitatively. After the reaction with 50 mM 1-kestose, 44.8 μM D-glucose, 8.01 μM D-fructose, and 67.7 μM nystose were detected. In addition, sucrose was detected: 111 μM before the reaction as a contaminant, and 80.1 μM after the reaction, with a net reduction of 30.9 μM as a result of the reaction. The D-glucose concentration indicates that 44.8 μM sucrose was consumed mostly as a donor in transglycosylation in addition to in hydrolysis. As mentioned below, the consumption of sucrose as acceptor is negligible at the low sucrose concetration. Therefore, the consumption of 1-kestose as a donor, equivalent to the production of sucrose that was further used to form D-glucose (Fig. 3-3), was calculated from the amounts of D-glucose production and sucrose reduction, to be 13.9 μM. Under the conditions (in the presence of 0.11 mM sucrose), the $v_{ag}/[E]_0$ of 1-

kestose was estimated to be 1.84 s^{-1} (Table 3-1). It is noteworthy that sucrose was consumed more (36.8 μM) than 1-kestose (13.9 μM) as a donor even at the much lower concentration, 0.2% of 1-kestose concentration.

Negligible amounts of D-glucose formation were detected at the initial reaction stages with nystose. The formation rates of D-fructose ($v_h/[E]_0$), 1-kestose ($v_{ag}/[E]_0$), and fructosylnystose ($v_{tg}/[E]_0$) were calculated to be 0.621 ± 0.336 s^{-1}, 27.5 ± 1.6 s^{-1}, and 29.5 ± 0.9 s^{-1}, respectively (Table 3-1). The $v_{ag}/[E]_0$ value was almost equal to $v_{tg}/[E]_0$. The $v_{ag}/[E]_0$ of nystose (27.5 s^{-1}) was much higher than that of 1-kestose (1.84 s^{-1}), indicating that nystose is a better donor than 1-kestose.

3.3.2. Two-substrate reactions of NdIS with sucrose and various FOSs

The acceptors specificity of NdIS was investigated using the two-substrate reactions containing sucrose and FOSs. First, initial reaction products with 50 mM sucrose and 50 mM nystose were analyzed by HPAEC-PAD (Fig. 3-4). The increase in D-glucose and fructosylnystose concentration over time was confirmed, and no D-fructose release was observed. The content of contaminant 1-kestose was not significantly changed during the reaction (308 to 310 μM at 0 to 30 min reaction). The rate constant of fructosylnystose production was 505 ± 7 s^{-1}. The results indicate that sucrose and nystose serve as donor and acceptor, respectively in the two-substrate reaction. Next, the release rates of D-glucose ($v_{ag}/[E]_0$) and D-fructose ($v_h/[E]_0$) under the same conditions were determined from the respective product concentrations quantified by the colorimetric method, and the transglycosylation rate ($v_{tg}/[E]_0$) was calculated from their differences (Table 3-2). The addition of nystose increased the degradation rate of sucrose ($v_{ag}/[E]_0$) 25-fold, but had no effect on the rate of fructose release ($v_h/[E]_0$). Most of the D-fructosyl group derived from sucrose was transferred to nystose, and the transglycosylation percentage was 98.4%. $v_{tg}/[E]_0$ estimated to be 599 ± 6 s^{-1} was close to that calculated from fructosylnystose quantified by

HPAEC-PAD. In the reaction using 50 mM sucrose as the sole substrate, the transglycosylation percentage was 19% (Table 3-1) as described in Chapter 2, indicating that nystose was a much better acceptor molecule than sucrose.

Similarly, the transglycosylation rate v_{tg} was calculated from the production rates of D-glucose and D-fructose in the two-substrate reaction with 50 mM sucrose and 50 mM various FOSs (Table 3-2). In the presence of the second substrate FOSs, an increase in v_{tg} and a concominant increase in v_{ag} was observed. In all the two-substrate reactions, the transglycosylation percentage was 90% or higher. The relative acceptor preference over sucrose (k'_6/k'_4) calculated from the hydrolysis rate to the transglycosylation rate in the presence of FOSs were 36.5–243-fold. The highest transglycosylation, both in v_{tg} and the ratios, was observed in the reaction with nystose. These results suggest that sucrose and FOSs preferentially serve as donor and acceptor in the two-substrate reaction, respectively. In other words, sucrose and FOSs are unfavorable as acceptor and donor, respectively.

The effects of FOS concentration on the reaction were analyzed using 0.5–2 mM 1-kestose as the second substrate in the presence of 50 mM sucrose (Fig. 3-5). The v_{tg} value increased in a 1-kestose concentration-dependent manner, reaching 4.3-fold at 2 mM (Fig. 3-5a). The [1-kestose]-v_{tg}/v_h plots gave a straight line as expected from the theory, with a slope of 0.407 and an intersection with vertical axis of 0.240 (Fig. 3-5b). According to Eq. 3-1 and Eq. 3-2, k'_6/k'_4 was calculated from these values to be 83.8, which is comparable with the k'_6/k'_4 calculated from the reaction of 50 mM 1-kestose and sucrose (59.7) in Table 3-2.

3.3.3. Products polymerization dependent on FOS concentration in two-substrate reaction

Average DP of oligosaccharides (DP ≥ 3) after the 20-h of two-substrate reactions with 400 mM sucrose and 0 to 100 mM of either 1-kestose or nystose was calculated from concentrations of D-glucose,

D-fructose, and residual sucrose. The average DP was 18.0 in the reaction starting with only 400 mM sucrose, but it decreased with increasing initial concentration of the starting 1-kestose and nystose (Table 3-3). At 100 mM FOS, increase in the average DPs were almost identical to the ratio of molar concentrations of consumed sucrose over initial FOS (theoretical value). This suggests that all D-fructosyl residues of the sucrose consumed were transferred to 1-kestose and nystose, and its D-fructosyl products to increase DP of the chains. At FOS concentrations below 100 mM, the measured average DPs were lower than the theoretical value, suggesting that transglycosylation to sucrose occurs to a significant extent under these reaction conditions to increase the acceptor FOS concentration. HPAEC-PAD analysis indicated that the reaction products were distributed in a wide range of DP, the chain-length distribution was dependent on the initial FOS concentration (Fig. 3-6). The highest DP detected was 42 starting with only sucrose, but decreased depending on the initial concentration of 1-kestose and nystose to 22 and 23, respectively, at 100 mM.

3.3.4. Evaluation of acceptor specificity of NdIS for monosaccharides

Transglycosylation activity of NdIS toward various monosaccharides was investigated in reactions with 50 mM monosaccharide and 10 g/L inulin. In the HPAEC-PAD analysis, transglycosylation products were detected only in the reactions with D-glucose and D-xylose (Fig. 3-7), but not with D-psicose, D-fructose, D-sorbose, D-tagatose, D-mannose, D-allose, or D-galactose under the conditions. The product from D-glucose was only sucrose with the same retention time as authentic sucrose, and the amounts of 1-kestose and nystose did not change before and after the reaction. The product from D-xylose was also only Fruβ2-1αXyl (see section 3.3.6). The rates of the product formation from 50 mM D-glucose (2.51 ± 0.20 s^{-1}) and 50 mM D-xylose (2.89 ± 0.12 s^{-1}) were almost equal (Table 3-4). However, in reactions containing both D-glucose and D-xylose at equimolar concentrations (10–50 mM), the rates for D-glucose

were 1.4-fold higher than for D-xylose, regardless of their concentrations (Table 3-4). This result indicates that the specificity constant of NdIS to D-glucose is 1.4-fold higher than to D-xylose. $\Delta\Delta G$ between acceptor D-glucose and D-xylose was calculated to be 0.88 kJ/mol from Eq. 3-4. The relative acceptor preference for D-xylose over sucrose was also evaluated in the two-substrate reactions with sucrose as done for FOSs (Table 3-2). The presence of D-xylose increased $v_{tg}/[E]_0$ 42.6-fold to 201 ± 2 s^{-1} compared with the reaction with sucrose only, and k'_6/k'_4 was 39.9-fold. These results indicate that NdIS has a higher preference for the monosaccharides D-glucose and D-xylose than for sucrose as acceptors.

3.3.5. Preparation of a series of FOSs

FOSs of DP 5, 6, 7, 8 and 9 were prepared. A 20-mL reaction mixture contained 600 mM sucrose and 300 mM nystose (2.5 g each) as starting materials and 250 nM NdIS as catalyst. After the 5-h reaction, sugar composition was analyzed by HPLC: DP 1–2 (D-glucose, D-fructose, and sucrose), 30.5%; DP 3, 1.4%; DP 4, 7.8% DP 5, 12.2%; DP 6, 14.5% DP 7, 13.9%; DP 8, 10.3%; DP 9, 6.0%; DP 10, 2.6%: and DP 11, 0.8% (Fig. 3-8). Through the active carbon-celite column chromatography, the lyophilized FOSs were obtained: DP 5, 281 mg; DP 6, 150 mg; DP7, 69 mg; DP 8, 154 mg; and DP 9, 81 mg, with purity of 99.9, 87.1, 76.1, 83.1%, and 88.8%, respectively. The total yield (735 mg, FOSs of DPs 5–9) was 15% of the total starting materials (5.0 g). This low recovery was due to the partial overlap of the FOS of each DP eluted (data not shown).

3.3.6. Preparation and structural analysis of D-fructosyl D-xyloside

The transfructosylation product, D-fructosyl D-xyloside, was analyzed, resulting from the combination of inulin or sucrose with xylose. The D-fructosyl D-xyloside was produced and its structure was analyzed. A 1-mL reaction mixture containing 2.87 M D-xylose, 0.54 M sucrose, and 250 nM NdIS

as starting materials. After 24-h reaction, 0.45 M D-fructosyl D-xyloside was produced with an yield of 83% on a molar basis from sucrose. From 0.3 mL of the above reaction mixture, 37.5 mg of D-fructosyl D-xyloside was obtained by purification using RP-HPLC with 96.2% purity and 89.0% recovery. The ESI-MS analysis of D-fructosyl D-xyloside gave a signal at 335.09 *m*/*z* $[M + Na]^+$. The chemical shifts in the ^{1}H- and ^{13}C-NMR analyses are summarized in Table 3-5. The coupling constant of $J_{H1, H2}$ of the D-xylosyl residue was 3.8 Hz, characteristic of a pyranose-type α-bond. HMBC showed a correlation between C-2 of D-fructose and H-1 of D-xylose moieties, indicating that D-fructosyl D-xyloside has the Fru2-1Xyl bond. HMBC also showed a correlation between C-2 and H-5 of the D-fructose moiety, indicating that D-fructose is in the furanose form. Based on the chemical shifts of ^{13}C spectrum of D-fructose (Agrawal 1992), D-fructosyl residue was β-form. Taken together, the structure of the product was β-D-fructofuranosyl α-D-xylopyranoside (Fruβ2-1αXyl).

3.4. Discussion

In this chapter, molecular mechanism for β-(2→1)-fructan synthesis was investigated by analyzing transglycosylation of NdIS. In the single-substrate reaction of NdIS with sucrose, 1-kestose, and nystose, were analyzed. This enzyme produced inulin-type β-(2→1)-fructan only from sucrose through successive transfructosylation (Fig. 3-2), and catalyzed disproportionation for the oligosaccharide substrates 1-kestose and nystose (Fig. 3-2). The results suggest that 1-kestose and nystose are more favorable acceptors than sucrose (acceptor preference discussed in detail later). Thus, the reaction rates to these substrates were suggested to be limited by donor capacities. Sucrose produced as an aglycone in the 1-kestose donor reaction was used as a donor in the reaction, and its concentration decreased, suggesting that sucrose is preferential donor over 1-kestose.

In the two-substrate reaction of sucrose and nystose, sucrose predominantly acted as the donor and

nystose as the acceptor in the transglycosylation (Fig. 3-3). Rate for sucrose hydrolysis was very low in this reaction. This indicates that sucrose is much better donor than nystose, and nystose is much better acceptor than sucrose. Higher preference of nystose as acceptor than sucrose was also suggested in the single-substrate reaction (section 3.3.1). Acceptor specificity of various DP of FOS was estimated by the two-substrate reaction. As indicated in Fig. 3-1, two acceptors competitively act as substrate with the fructosyl enzyme in the theory (section 3.2.3). k_4' and k_6' are regard as specificity constants for sucrose and FOS as acceptor. From v_{tg}/v_h determined in only sucrose and the both (50 mM each), the relative specificity constants (k_6'/ k_4') were calculated (Table 3-2). With 1-kestose and nystose, transglycosylation to the FOSs mostly occurred and transglycosylation to sucrose acceptor hardly occurred under the analytical conditions (Fig. 3-4, Table 3-2). The validity of the relative k'_6/k'_4 was confirmed from the fact that even the concentration of FOS (1-kestose) was greatly varied from sucrose (50 mM sucrose and 0–2 mM 1-kestose), k'_6/k'_4 was not significantly different from the value at 50 mM 1-kestose. A quantitative comparison of acceptor specificity was reasonable. The k'_6/k'_4 to 1-kestose was estimated to be 59.7-fold (Table 3-2). Among the FOS tested, k'_6/k'_4 was maximal for nystose, 243-fold, but remained high even at higher DP. These results suggest that elongated transglycosylation products are also preferentially used as acceptors for transglycosylation and β-(2→1)-D-fructosyl chain is elongated.

Monosaccharide acceptor screening revealed that NdIS utilized D-glucose and D-xylose as acceptor of transglycosylation and produced sucrose and Fruβ2-1αXyl, respectively. This means that D-xylose binds to +1 subsite in similar manner to D-glucose during the transfrucosylation. Kinetic analysis of transglycosylation to these monosaccharides using inulin as a donor substrate showed that acceptor specificity of NdIS is 1.4-fold higher for D-glucose than for D-xylose, and $\Delta\Delta G$ between D-glucose and for D-xylose was only 0.88 kJ/mol, which is less than the energy difference due to hydrogen bonding with uncharged amino acid residues (2.1–6.3 kJ/mol; Fersht *et al.* 1985). The result suggests that NdIS did not

strictly recognize the 6-hydroxymethylen group of D-glucosyl residue of sucrose in +1 subsite, although Trp residue (Trp115 and Trp146 of InuHj and NdIS, respectively) is located near C-6 of the D-glucosyl residue in subsite +1. As D-mannose, D-allose, and D-galactose were inert as acceptor of NdIS, this enzyme strictly recognizes O-2, O-3, and O-4 of D-glucose in +1 subsite. In InuHj complexed with sucrose (PDB entry, 7BJC, molecule A), O-2, O-3, and O-4 of the D-glucosyl residue are predicted to form hydrogen bonds with surrounding residues including Arg196, Glu266, Glu268, and His286 (Fig. 3-9). Although the residue corresponding to Glu266 of InuHj is Gln315 in NdIS, hydrogen bonding interactions with O-2, O-3, and O-4 of the D-glucosyl residue, observed in InuHj, were also assumed in NdIS, and are thought to be essential for the acceptor binding (Fig. 3-9). NdIS did not use D-fructose as acceptor of transglycosylation, indicating that the high acceptor specificity to FOS is due to the high affinity of the +2 or more subsites for D-fructosyl units.

In the single-substrate reaction, v_{ag} for 1-kestose was much lower than those for sucrose and nystose, suggesting that binding of D-glucosyl residue to +2 subsite is unfavorable for NdIS. This is consistent with the fact that sucrose is a poor acceptor for the transglycosylation as described above (section 2.3.5). The difficulty of D-glucosyl residue to bind +2 subsite is thought to be important for the preferential use of sucrose as donor. Preference for sucrose as acceptor in transglycosylation is different between NdIS and *L. reuteri* 121 IS, because *L. reuteri* 121 IS catalyzes distributive oligosaccharide (DP 3 to 10) synthesis from sucrose (Ozimek *et al.* 2006). *L. reuteri* 121 IS is predicted to have higher affinity to D-glucosyl residue in +2 subsite than NdIS. As shown in Chapter 2, NdIS lacks residues corresponding to Arg542 and Arg545 of InuJ, which are widely conserved in *Lactobacillales* IS, including *L. reuteri* 121 IS. As these Arg residues of InuJ provide hydrogen bonding interactions with D-glucosyl residue of 1-kestose in +2 subsite (Fig. 2-12), lacking the Arg residues in NdIS may cause low affinity to D-glucosyl residue in +2 subsite.

The mechanism of long-chain inulin formation from sucrose is discussed based on donor and acceptor specificity. Quantitative evaluation of relative acceptor specificity, mainly by two-substrate reaction, revealed that sucrose acts as a much better donor and poorer acceptor than FOS, and that FOS maintains high k'_6/k'_4 even when the DP of FOS increased. Therefore, the following inulin synthesis mechanism from sucrose is proposed: Even if sucrose, which has low acceptor capacity, is used as a substrate, once 1-kestose is formed through the transglycosylation, it becomes an acceptor, forming a nystose. The nystose that excelled as an acceptor is further fructosylated. This sequential reaction is likely a key mechanism for the elongation of the D-fructosyl chain.

Table 3-1. Reaction velocities of NdIS toward 50 mM sucrose, 1-kestose and nystose.

Substrate	$v_{ag}/[E]_0$ (s^{-1})	$v_h/[E]_0$ (s^{-1})	$v_{tg}/[E]_0$ (s^{-1})
Sucrose	24.8 ± 0.4	20.1 ± 0.2	4.71 ± 0.33
1-Kestose	1.86[a]	N.D.	N.D.
Nystose	27.5 ± 1.6	0.621 ± 0.336	29.5 ± 0.9

[a] v_{ag} of 1-kestose is estimated by subtracting net sucrose consumption from D-glucose production from 50 mM 1-kestose, in the presence of 0.11 mM contaminant sucrose (Fig. 3-3). N.D., not determined due to rapid degradation of sucrose. The results are presented as the means of triplicate experiments with standard deviations.

Table 3-2. Two-substrate reaction rates with 50 mM sucrose and 50 mM various sugars of NdIS.

Acceptor	$v_{ag}/[E]_0$ (s^{-1})	$v_h/[E]_0$ (s^{-1})	$v_{tg}/[E]_0$ (s^{-1})	r_{tg} (%)	k'_6/k'_4 (Relative-v_{tg}/v_h[a] – 1)
Sucrose[b]	24.8 ± 0.4	20.1 ± 0.2	4.71 ± 0.33	19.0	1[d]
1-Kestose	308 ± 12	20.3 ± 1.2	288 ± 12 (242 ± 14)[c]	93.5	59.7
Nystose	609 ± 4	10.5 ± 2.1	599 ± 6 (505 ± 7)[c]	98.4	243
Fru-nystose (DP5)	422 ± 4	16.5 ± 1.6	406 ± 6	96.1	104
Fru_2-nystose (DP6)	189 ± 3	8.54 ± 0.64	180 ± 3	95.5	89.2
Fru_3-nystose (DP7)	169 ± 1	9.28 ± 1.29	160 ± 1	94.5	72.7
Fru_4-nystose (DP8)	205 ± 4	14.5 ± 1.9	190 ± 3	92.9	55.0
Fru_5-nystose (DP9)	152 ± 13	15.6 ± 1.1	137 ± 13	89.7	36.5
D-Xylose	222 ± 2	21.0 ± 2.1	201 ± 2	90.5	39.9

v_{ag} and v_h were rates of the D-glucose and D-fructose formation, respectively. $v_{tg} = v_{ag} - v_h$. The results are presented as the means of triplicate experiments with standard deviations.

[a] Relative v_{tg}/v_h to that with 50 mM sucrose.

[b] Only sucrose (50 mM) and no second substrate.

[c] v_{tg} values in parenthesis are determined through direct quantification of transglycosylation products by HPAEC-PAD.

[d] k'_4/k'_4 value.

Table 3-3. Average DPs of reaction products of NdIS from 400 mM sucrose and various concentrations of 1-kestose/nystose.

	Average DP		Theoretical value[a] ([Suc]/[FOS]) + DP_{FOS}[b]	
FOS (mM)	1-Kestose	Nystose	1-Kestose	Nystose
0	18.0	18.0	N.A.	N.A.
10	15.6	15.7	43	44
20	15.3	16.0	23	24
50	9.2	10.5	11	12
100	6.4	7.7	7	8

The average DPs were calculated from concentrations of D-glucose, D-fructose, and residual sucrose according to Eq. 3-3. N.A., not applicable.

[a] Theoretical value of the average DP when all D-fructose unit of sucrose is transglycosylated to FOS.

[b] DP_{FOS} means DP of initial FOS (1-kestose or nystose).

Table 3-4. Transglycosylation velocities of NdIS toward D-glucose and D-xylose in the presence of 10 g/L inulin.

Acceptor substrate	$v_{tg\ Glc}$[a]/$[E]_0$ (s^{-1})	$v_{tg\ Xyl}$[b]/$[E]_0$ (s^{-1})	$v_{tg\ Glc}/v_{tg\ Xyl}$
50 mM Glc	2.51 ± 0.20	N.A.	N.A.
50 mM Xyl	N.A.	2.89 ± 0.12	N.A.
10 mM Glc and Xyl	1.43 ± 0.09	1.07 ± 0.07	1.34 ± 0.01
20 mM Glc and Xyl	1.82 ± 0.21	1.32 ± 0.14	1.38 ± 0.01
50 mM Glc and Xyl	1.77 ± 0.16	1.24 ± 0.12	1.43 ± 0.02

N.A., not applicable. The results are presented as the means of triplicate experiments with standard deviations.

[a] $v_{tg\ glc}$, [b] $v_{tg\ xyl}$: rates of the of the sucrose and Fru-Xyl formation in transglucosylation with D-glucose and D-xylose, respectively. The products were directly quantified by HPLC.

Table 3-5. Chemical shifts of β-D-fructofuranosyl α-D-xylopyranoside in the ^{1}H- and ^{13}C-NMR spectra.

Residue	Number	δ_C (ppm)	δ_H (ppm)	*J* (Hz)	
α-Xyl*p*	1	93.22	5.38	d	3.8
	2	71.94	3.57	dd	9.8, 3.8
	3	73.67	3.72	m	
	4	70.07	3.64	m	
	5	62.64	3.73	m	
β-Fru*f*	1	61.77	3.70	brs	
	2	104.60			
	3	77.13	4.25	d	8.8
	4	74.54	4.14	dd	8.6, 8.6
	5	82.27	3.92	ddd	8.6, 8.5, 2.8
	6	62.70	3.85	dd	12.4, 2.8

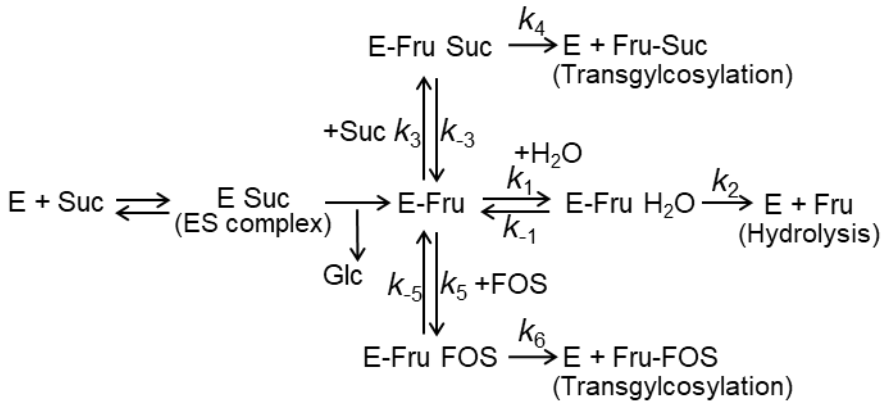

Fig. 3-1. Reaction scheme for two-substrate reaction of sucrose and FOS.

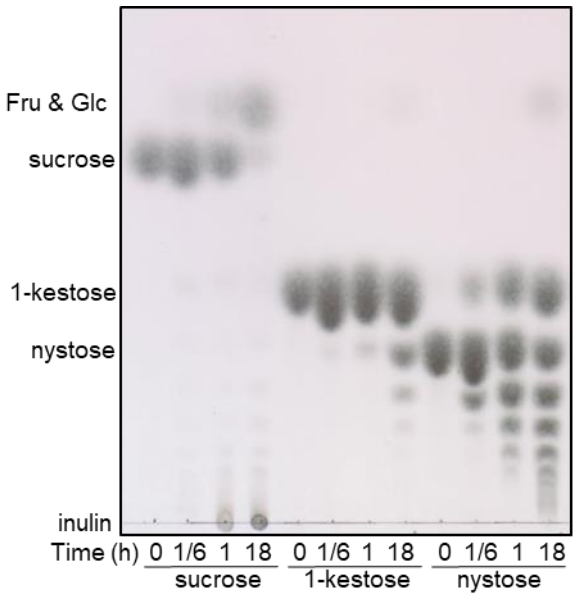

Fig. 3-2. TLC analyses of the reaction products of NdIS from 50 mM sucrose, 1-kestose, and nystose.

Reaction mixtures consisting of 50 mM substrate, 40 mM MES-NaOH buffer (pH 6.5), 0.2 g/L BSA, and 502 nM NdIS were incubated at 37°C. Samples were taken at the indicated times, and the reaction was stopped by heating at 100°C for 10 min.

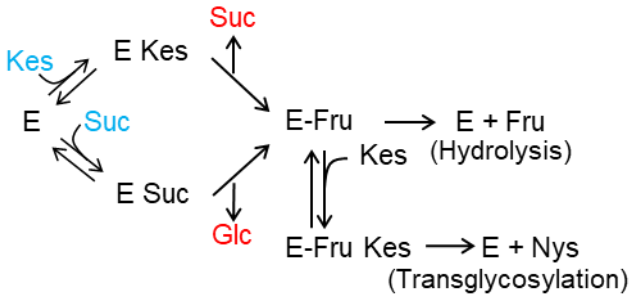

Fig. 3-3. Proposed NdIS reaction scheme when using 1-kestose with a small amount of sucrose contaminated as a substrate.

Donors and liberated aglycones are shown by light blue and red letters, respectively.

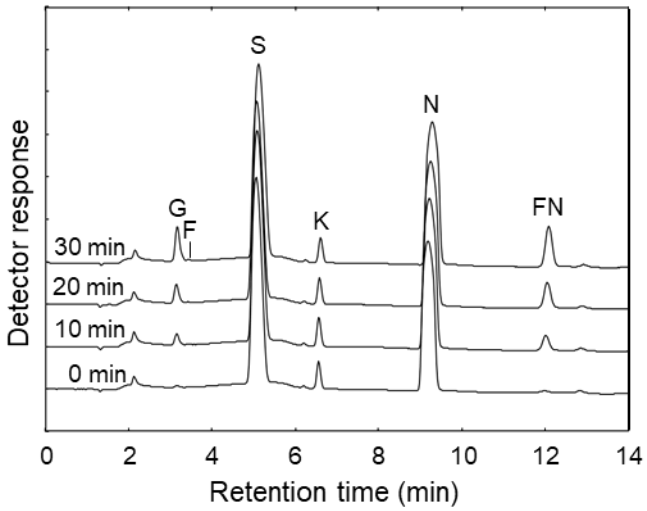

Fig. 3-4. HPAEC-PAD analysis of the initial reaction products of NdIS from 50 mM sucrose and nystose. The reaction was performed in 50 mM sucrose, 50 mM nystose, and 0.502 nM NdIS. The reaction products were analyzed at 10 min intervals for up to 30 min. G, D-glucose; F, D-fructose; S, sucrose; K, 1-kestose; N, nystose; FN, fructosylnystose.

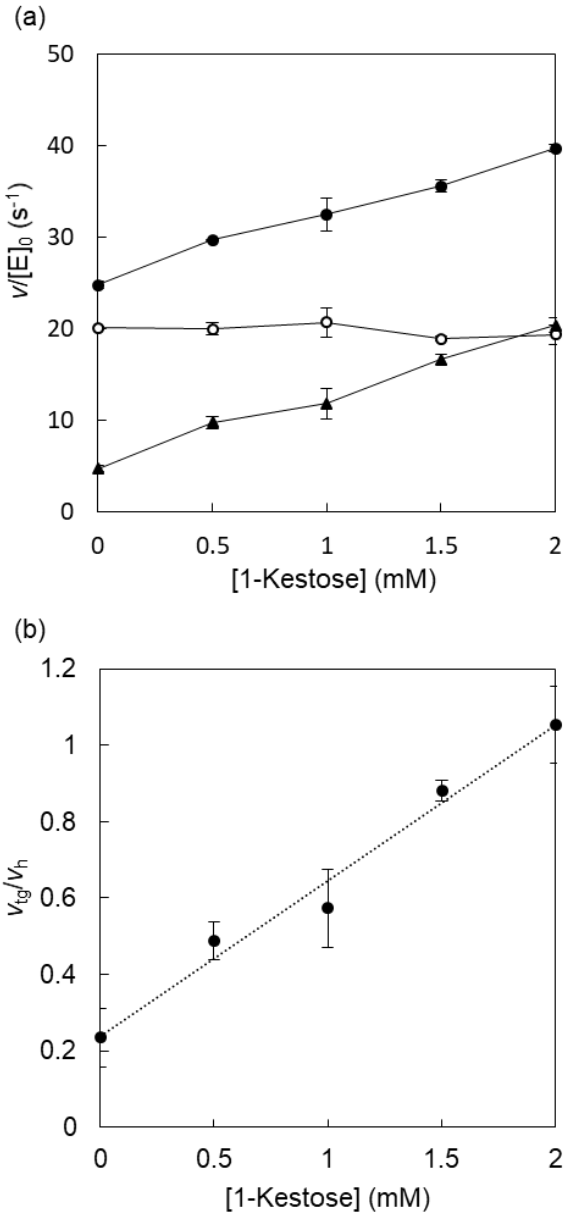

Fig. 3-5. Reaction velocities of NdIS to 50 mM sucrose and 0-2 mM 1-kestose.

(a) Initial velocities of aglycone (D-glucose) release ($v_{ag}/[E]_0$, filled circle), hydrolysis ($v_h/[E]_0$, open circle), and transglycosylation ($v_{tg}/[E]_0$, filled triangle) on 1-kestose concentration. (b) v_{tg}/v_h at various 1-kestose concentrations. Approximate curve is shown as a dashed line.

The results are presented as the means of triplicate experiments with standard deviations.

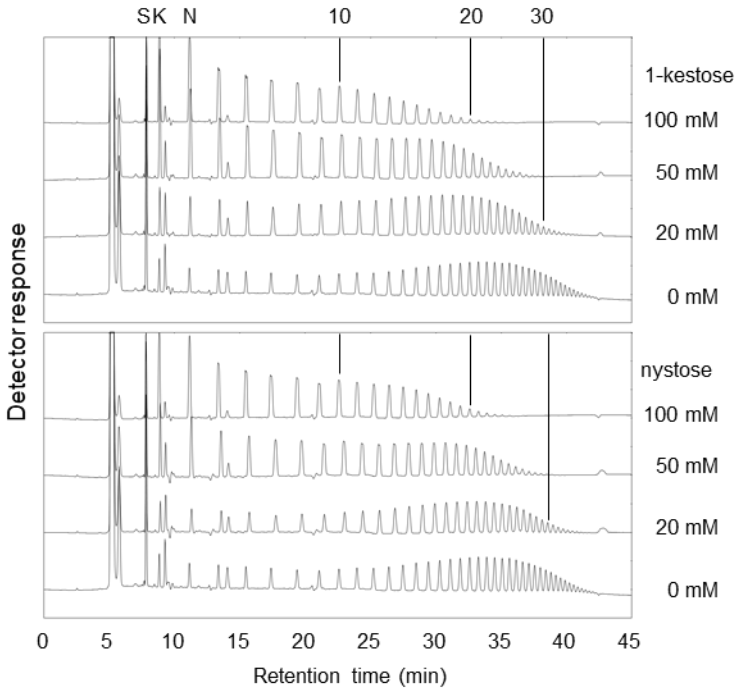

Fig. 3-6. DP distributions of reaction products of NdIS from 400 mM sucrose and 0-100 mM 1-kestose and nystose.

The reaction product distributions were analyzed by HPAEC-PAD. Initial FOS and its concentrations are shown on the right. Numbers above are shown DP. S, sucrose; K, 1-kestose; N, nystose.

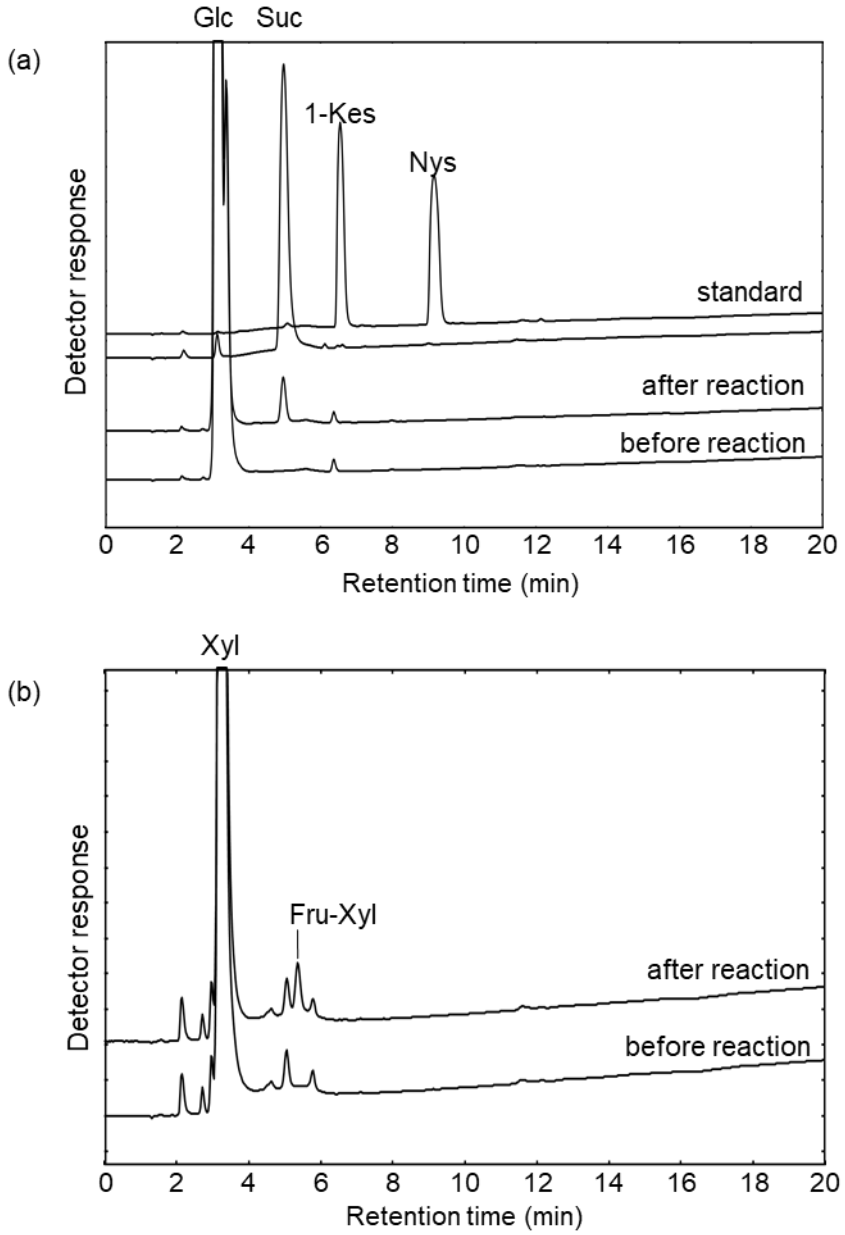

Fig. 3-7. HPAEC-PAD analysis of transglycosylation product from 10 g/L inulin and 50 mM monosaccharides, catalyzed by NdIS.

(a) Product analysis of transglycosylation toward D-glucose. (b) That toward D-xylose.

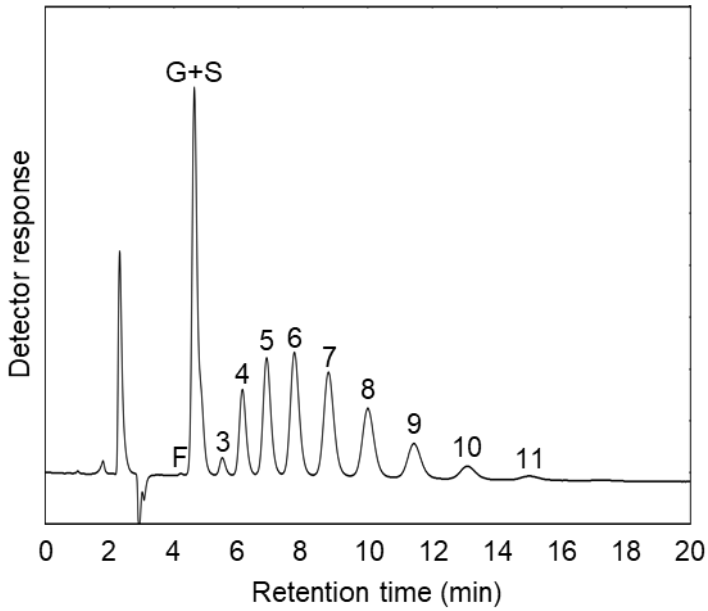

Fig. 3-8. HPLC analysis of the reaction products from 600 mM sucrose and 300 mM nystose by NdIS. HPLC analysis was done using an Asahipak NH2P-50 4E column with 60% (v/v) acetonitrile at 25°C. The refractive index was monitored. G, D-glucose; F, D-fructose; S, sucrose; 3–11, FOS with DP 3–11.

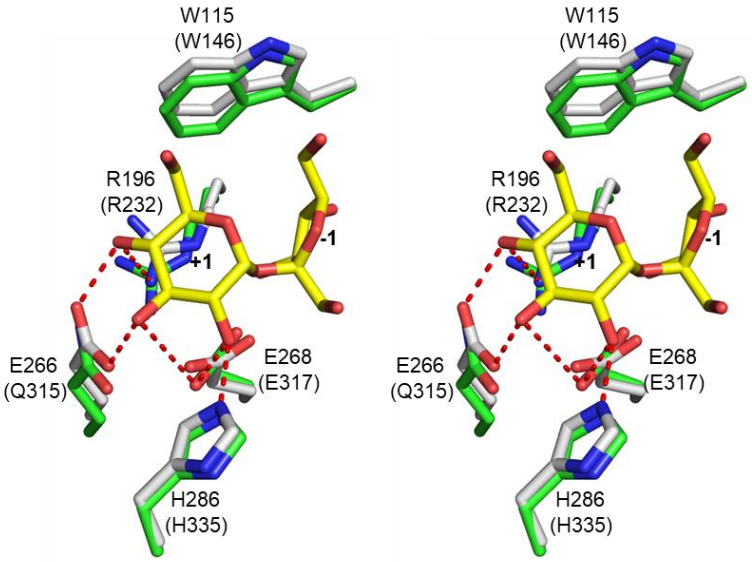

Fig. 3-9. Comparison of three-dimensional structure prediction model of NdIS and crystal structure of InuHj (Ghauri *et al.* 2021b; PDB entry, 7BJC, molecule A).

Bold letters indicate subsite numbers. Sucrose is shown with yellow sticks. Amino acid residues of NdIS and InuHj are shown with green and gray sticks, respectively. Parenthesized and unparenthesized amino acid residues are from NdIS and InuHj, respectively. Predicted hydrogen bonds of sucrose and InuHj at +1 subsite are shown as broken red lines.

Chapter 4. Characterization of NdFosA from *N. drentensis* 57N

4.1. Introduction

The enzymes known to modify inulin are 6-SFT, which introduces branching by β-(2→6)-D-fructosyltransfer to inulin, and 1-FFT, which elongates the branching structure to form graminan-type fructans. (Sprenger et al 1995; Duchateau et al 1995; Kawasaki and Yoshida 2005). Both these enzymes belong to GH32. A GH68 enzyme that catalyzes the introduction of branching into inulin as the main reaction has not been reported so far, although *Lactobacillales* IS introduces a β-(2→6)-branch into inulin by a side reaction (Rosell and Birkhed 1974; van Hijum *et al.* 2002; Anwar *et al*. 2008). As described in Chapter 2, the culture supernatant of *N. drentensis* 57N grown on sucrose as a carbon source contained two sucrose-degrading activities. One of them was identified to be NdIS in the previous chapters. This chapter identifies the other uncharacterized sucrose-degrading enzyme as NdFosA, expressed from the gene adjacent to the *NdIS* gene, and investigates its enzymatic functions using *E. coli* recombinant enzyme. Product analysis of NdFosA from various substrates revealed that NdFosA is a novel β-fructosyltransferase in GH68 whose main reaction is β-(2→6)-D-fructosyl transfer from sucrose to the internal D-fructosyl moiety of the inulin chain.

4.2. Materials and methods

4.2.1. Partial purification of native NdFosA and analysis of its N-terminal sequence

The culture of *N. drentensis* 57N and purification of the proteins from the culture supernatant were performed as described in section 2.2.3. Of the two sucrose-acting peaks identified by hydrophobic column chromatography, the later eluted peak was recovered. N-terminal amino acid sequence analysis was performed as described in section 2.2.6.

4.2.2. Preparation of recombinant NdFosA

The *NdFosA* gene excluding the region encoding signal peptide sequence (91–1341-nt in Fig. 4-1) was amplified by PCR using Primestar Max DNA polymerase and the following primers: 5´-GGAGATATACATATGGAAGACGTAGGGCAAACG-3´ (sense) and 5´-GTGGTGGTGGTGGTGTTGTTTAATCCAGCCAGG-3´ (antisense). The nucleotide sequence encoding mature NdFosA was inserted into a pET-22b vector and the DNA insert and conjunctive regions were sequenced as in section 2.2.8. The deduced sequence corresponds to Glu31–Gln446 of NdFosA with Met and His_6 attached at N- and C-termini, respectively. A transformant of *E. coli* BL21 (DE3) harboring the pET-22b-derived expression plasmid was cultured as described in section 2.2.8, but the volume of the culture medium was 1 L. The recombinant NdFosA was purified by immobilized Ni^{2+} affinity column chromatography as described in section 2.2.8. The purified enzyme was stored at −80°C. The protein concentration of the chromatographic fraction and the molar concentration of purified enzyme were determined by the same method as described in section 2.2.9.

4.2.3. HPAEC-PAD analysis of the reaction products under various reaction conditions

A reaction mixture (100 μL) consisting of each substrate [0.5 M sucrose, 50 mM 1-kestose, 50 mM nystose, 12.5 mM inulin (50 g/L raftiline HP; molar concentration was calculated from average DP 25), or 12.5 mM inulin + 0.5 M sucrose], 40 mM MES-NaOH buffer (pH 6.5), 0.2 g/L BSA, and 198 nM recombinant NdFosA was incubated at 37°C for 20 h. For another reaction, a single enzyme (198 nM recombinant NdFosA or 314 nM recombinant NdIS), two enzymes (198 nM recombinant NdFosA and 314 nM recombinant NdIS), culture supernatant of *N. drentensis* 57N prepared as in section 2.2.5 (final 0.627 U/mL) were used as enzyme, and 1.46 M sucrose as substrate. After the reactions were completed, reaction products were analyzed by HPAEC-PAD as described in section 2.2.18. In the reactions of 12.5

mM inulin and 12.5 mM inulin + 0.5 M sucrose, 10 μL of 70 U/mL IFT from *Arthrobacter* sp. H65-7 (Nippon Beet Sugar Mfg., Tokyo, Japan) was added to a portion (20 μL) after the reaction, and held at 60°C for 18 h, followed by incubation at 100°C for 5 min to stop the reaction and the HPAEC-PAD analysis.

4.2.4. Methylation analysis of the polysaccharide products of recombinant NdFosA and NdIS from sucrose

Sucrose (1.46 M) was incubated with two enzymes, 3 μM recombinant NdIS and 3 μM recombinant NdFosA, or only 3 μM recombinant NdIS under the conditions described in the previous section 4.2.3. The reaction mixtures (100 μL) were mixed with four volumes of cold ethanol (400 μL) and kept at -35°C for 18 h. The precipitate was collected by centrifugation (1,500 × *g*, 25°C, 5 min). Cold ethanol (400 μL) was again added to the precipitate, which was held and collected in the same manner. This process was repeated two more times. After that, methanol (200 μL) was added to the precipitate and it was dehydrated at 60°C *in vacuo*. Methylation analysis was performed as in the method of Pettolino *et al.* 2012. Superhydrated dimethyl sulfoxide (500 μL; Fujifilm Wako Pure Chemical) containing 100 mg NaOH was added to 20 mg precipitate. For methylation of carbohydrates, 200 μL of methyl iodide (Fujifilm Wako Pure Chemical) was added and the mixture was stirred for 1 h. The reaction was stopped by adding 2 mL of H_2O, and 500 μL of dichloromethane was added and stirred. The dichloromethane phase was washed three times with 2 mL of water. Toluene (200 μL) was added to the dichloromethane phase, and the solvent was removed by heating at 40°C *in vacuo*. The dried sample was mixed (dissolved) with 2 M trifluoroacetic acid (500 μL) and kept at 121°C for 90 min. Toluene (200 μL) was added to the sample and it was dehydrated by heating at 40°C *in vacuo*. 15 M NH_4OH (50 μL) was added to the sample to dissolve, and then 50 μL of 1 M $NaBD_4$ in 2 M NH_4OH was added. The sample was sonicated for 1 min

and kept overnight at 25°C. Acetic acid was added until no gas was produced (50 μL in this case), and toluene (200 μL) was added and dehydrated by heating at 40°C *in vacuo*. Methanol (200 μL) was added to remove the boric acid. Acetic anhydride (250 μL) was added and kept at 100°C for 2.5 h. Water (2 mL) was added to stop the reaction, then dichloromethane (1 mL) was added, and the aqueous phase was removed. Toluene (1 mL) was added to the dichloromethane fraction, and dried by heating at 40°C *in vacuo*. Dichloromethane (200 μL) was added to dissolve the dried sample and stored at -35°C (analytical sample).

The analytical samples were analyzed by gas chromatography-mass spectrometry (GC-MS) under the following conditions: GC, GC-2010 Plus (Shimadzu); MS, GCMS-QP2010 (Shimadzu); column, BPX70 (0.22 mm i.d. × 25 m; film, 0.25 μm; Trajan Scientific and Medical, Melbourne, Australia); mobile phase, helium; flow rate, 1 mL/min; injection volume, 1 μL with split 1/10; injection temperature, 240°C; column temperature, 170–260°C for 30 min.

4.2.5. Kinetic parameters of the reaction with sucrose of recombinant NdFosA in the presence or absence of inulin

The velocities of NdFosA for D-glucose and D-fructose release from sucrose were measured by the same method as described in section 2.2.13, but enzyme concentration was 7.49 nM. The velocities in the presence of 2.5 mM inulin (raftiline HP) were determined in the same manner. In the reactions with 2–800 mM sucrose and 2.5 mM inulin, based on the reaction scheme shown in Fig. 3-1, reaction using sucrose as donor is considered as in the following Eq. 4-1:

Eq. 4-1, $v_{tg}/v_h = (k'_4/k'_2)$ [sucrose]/[water] + (k'_6/k'_2) [inulin]/[water],

the background to this equation was given in the previous chapter. According to this, At constant inulin concentration (2.5 mM), the [sucrose]-v_{tg}/v_h plots give a straight line with a slope of (k'_4/k'_2)/[water] and

an intersection with the vertical axis of (k'_6/k'_2)[inulin]/[water]. These values give k'_6/k'_4, the relative acceptor preference of inulin over sucrose.

4.2.6. Standard activity assay of NdFosA

The D-glucose-releasing activity toward sucrose was measured. Reaction conditions were the same as in section 2.2.11. One unit of sucrose-degrading activity was defined as the amount of enzyme yielding a D-glucose- releasing rate of 1 μmol/min under these conditions.

4.2.7. Effects of pH, temperature, and metal ions on the activity and stability of NdFosA

To determine the optimum pH and temperature, a standard activity assay as described in section 4.2.6 was used, but 40 mM Britton-Robinson buffer (pH 4.2–9.4) was used for the reaction buffer, and various temperatures (30–60°C) were used. Optimal temperature was also evaluated in the presence of 10 mM $CaCl_2$. Other conditions were the same as in the absence of $CaCl_2$. For pH stability measurements, 7.5 μM of the enzyme was kept in 80 mM potassium chloride buffer (pH 0.6–1.1), 80 mM sodium phosphate buffer (pH 1.7–2.6, 11.5–12.3), and 80 mM Britton-Robinson buffer (pH 3.1–11.0) at 4°C for 24 h, and residual activities were measured. To assess temperature stability, 37.4 nM of the enzyme was maintained in 10 mM MES-NaOH buffer (pH 6.5) containing 1 g/L BSA, in the presence or absence of 10 mM $CaCl_2$ at 30-60°C for 15 min. The effects of metal ions were measured in the presence of 10 mM LiCl, NaCl, KCl, NH_4Cl, $MgCl_2$, $CaCl_2$, $CoCl_2$, $NiCl_2$, and EDTA under standard conditions.

4.3. Results

4.3.1. Partial purification and gene identification of NdFosA

NdFosA was partially purified from 400 mL of the culture supernatant of *N. drentensis* 57N by

ammonium sulfate precipitation and two column chromatographies. In hydrophobic column chromatography, two sucrase activity peaks were observed in the adsorbed fractions as described in section 2.3.2 (Fig. 2-3). The active fractions eluted later were collected, and the partially purified NdFosA was obtained, with 20% yield of activity (11.9 mg, 261 U). The sample showed a single protein band of 44 kDa in the SDS-PAGE analysis (Fig. 4-2a). Two amino-acid derivatives were obtained in each cycle of Edman degradation: E/A, D/E, V/I, S/G, S/Q, D/T, T/Y, N/T, and S/W. One of them corresponded to the N-terminal sequences of mature NdIS (AEISSDYTS). The other sequence EDVGQTTNW corresponds to Glu31 to Trp39 of the deduced sequence of NdFosA, the product of the *NdFosA* gene, located downstream of the *NdIS* gene (Fig. 2-6). Full length of the *NdFosA* gene sequence is shown in Fig. 4-1. The 1,341-nt-long the *NdFosA* gene encoded a precursor protein comprising 446 amino acids. The N-terminal amino-acid sequence of the purified NdFosA indicated that N-terminal Met1–Ala30 is a signal peptide for secretion. This is also suggested by the SignalP-5.0 program (Armenteros *et al.* 2019). Therefore, the mature NdFosA was composed of 416 residues. The calculated molecular mass of the mature NdFosA was 46.1 kDa, which is close to the molecular mass of purified NdFosA (44 kDa, Fig. 4-2b).

4.3.2. Sequence comparison and prediction of catalytic amino acids on the putative sequence of NdFosA

A sequence similarity search using the BLAST program (Altschul *et al.* 1990) indicated that NdFosA is 98.7% identical to a putative GH68 fructosyltransferase from *Bacillus* sp. AFS031507 (NCBI, WP_098930308.1, COE25_RS01265, shown in Fig. 2-6c), 66% to *S. agaradhaerens* WDG185 FosA (SaFosA), 45% to *H. jeotgali* B3T InuHj, and 40% to NdIS. Partial amino acid sequence alignments of the GH68 enzymes, NdFosA, NdIS, *S. agaradhaerens* FosA, and two IS enzymes with known ternary structures (*H. jeotgali* B3T InuHj and *L. johnsonii* NCC 533 InuJ) are shown in Fig. 4-3. This alignment

revealed that the three possible catalytic residues acting as nucleophile, general acid/base, and transition-state stabilizer of NdFosA were Asp74, Glu312, and Asp226, respectively. The other residues involved in the formation of −1 to +2 subsites of InuHj and NdIS are partially conserved in NdFosA, with His109, Ala144, Arg225 and His330 common to both and Glu310 to InuHj. NdFosA has Val108 and His392 at the position of Arg81 and Asn351 of InuHj and Arg111 and Asn398 of NdIS, respectively, which are hydrogen-bonded to the D-glucosyl moiety in +2 subsite. The corresponding residues of SaFosA were Val108 and Gln386.

4.3.3. Purification of the recombinant NdFosA

Recombinant NdFosA with a C-terminal His_6 tag was produced in *E. coli* BL21 (DE3) transformants and purified by Ni^{2+}-immobilized affinity column chromatography. A total of 137 mg of recombinant NdFosA with 53.8 U/mg was obtained from 1 L of shake-flask culture cells. Purified recombinant NdFosA showed a single protein band of 44 kDa on SDS-PAGE (Fig. 4-2b). The determined molecular mass is the same as the native NdFosA and close to the calculated one from the amino acid sequence (46.9 kDa).

4.3.4. Reaction of NdFosA with various substrates

Substrate and product specificity of recombinant NdFosA was evaluated. The 20-h reaction products were analyzed by HPAEC-PAD (Fig. 4-4). Reaction with 0.5 M sucrose produced mainly 1-kestose, D-fructose, and D-glucose, with trace amounts of oligosaccharides, but no longer-chain FOSs (Fig. 4-4a). From 1-kestose, small amounts of D-fructose and D-glucose were produced without any detectable increase in sucrose (Fig. 4-4b). No obvious product was detected with nystose or inulin alone (Fig. 4-4c, d). These results indicated that NdFosA catalyzed hydrolysis and β-(2→1)-transfructosylation

with sucrose like NdIS, but the FOS chain elongation is limited to 1-kestose under the conditions. NdFosA hydrolyzed 1-kestose but did not transglycosylated under the conditions. Inulin and nystose were not substrates for NdFosA under the conditions. The two-substrate reaction with 0.5 M sucrose and 12.5 mM inulin significantly consumed sucrose, and produced monosaccharides, D-glucose and D-fructose, 1-kestose, and a series of unknown products, detected after every DP of inulin (DP ≥ 8) in the HPAEC-PAD chromatography (Fig. 4-4e). The inulin-associating products in the HPAEC profile were accumulated more in a DP dependent manner. These results suggest that NdFosA catalyzes transfructosylation from sucrose to inulin of DP 8 or higher, resulting in modification of inulin molecules. The treatment with IFT almost completely degraded linear inulin to DFA III and short-chain FOSs (nystose and fructosylnystose) through intramolecular transfer from D-fructosyl termini of the D-fructan moieties under the conditions (Fig. 4-4d). Contrary, the NdFosA products were partially degraded. The IFT treatment reduced their DP, but not completely degraded them and a series of peaks are remained (Fig. 4-4e). This result suggests that NdFosA attaches the branched D-fructosyl residue. These branched products were found in the reaction even with sucrose as a sole starting material when the *N. drentensis* culture supernatant was used as the enzyme source (Fig. 4-5, "culture supernatant"). The reaction with sucrose by the combination of purified recombinant NdIS and NdFosA also produced the series of branched inulin (Fig. 4-5, "NdIS + NdFosA"), but not by one of the enzymes only. The unknown products are the result of the cooperative action of NdIS and NdFosA to sucrose. In the reaction of NdIS with 1.46 M sucrose, some of the product precipitated. The other reaction products did not precipitated.

4.3.5. Methylation analyses of the unknown products of NdFosA and NdIS for sucrose

The chemical structure of the unknown products by NdFosA was analyzed through the methylation analysis. Samples for methylation analysis were prepared from sucrose using NdIS and NdFosA. As a

control, polysaccharides obtained by treating sucrose with NdIS only were also prepared. Polysaccharides recovered from the reaction solution by ethanol precipitation were converted to the partially methylated alditol acetates (PMAAs) for the methylation analysis. Two small peaks, which were not detected in the control, were observed in the GC of PMAAs that was derived from polysaccharides using two enzymes (Fig. 4-6b, peaks 1 and 2). These peaks were identified to be 1,2,5,6-tetra-*O*-acetyl-(2-deuterio)-3,4-di-*O*-methylmannitol and 1,2,5,6-tetra-*O*-acetyl-(2-deuterio)-3,4-di-*O*-methylglucitol based on the characteristic fragments *m/z* 189 and 190 as the major primary fragments, *m/z* 233 and 234 as the minor fragments, and *m/z* 129 as the sole secondary fragment (Fig. 4-6c). The secondary fragment observed here is the result of the loss of deuterium from C-2 following the β-depletion of acetic acid from *m/z* 190 and is distinct from that of 1,2,5,6-tetra-*O*-acetyl-(1-deuterio)-3,4-di-*O*-methylmannitol and 1,2,5,6-tetra-*O*-acetyl-(1-deuterio)-3,4-di-*O*-methylglucitol. The paper (Pettolino *et al.* 2012) indicated that under the similar analytical conditions, 1,2,5,6-tetra-*O*-acetyl-(2-deuterio)-3,4-di-*O*-methylmannitol is detected earlier than 1,2,5,6-tetra-*O*-acetyl-(2-deuterio)-3,4-di-*O*-methylglucitol. This also suggests that that peak 1 is of the modified mannitol and peak 2 is of the modified glucitol. Both of these are generated from D-fructosyl residue with glycosidic linkages at positions 1, 2, and 6. The peaks of 2,5,6-tri-*O*-acetyl-(2-deuterio)-1,3,4-tri-*O*-methylglucitol and 2,5,6-tri-*O*-acetyl-(2-deuterio)-1,3,4-tri-*O*-methylmannitol were not detected, indicating no bond at the 6-position of the terminal D-fructosyl residue. These results revealed that modification of inulin by NdFosA is 6-*O*-D-fructosylation of inner D-fructosyl moieties.

4.3.6. Basic properties of the recombinant NdFosA

Recombinant NdFosA was most active at pH 7.0 and stable in a pH range of 1.7–10.5 at 4°C for 24 h (Fig. 4-7a). Its optimum temperature for the reaction rate was 40°C, but 50°C in the presence of 10 mM $CaCl_2$ (Fig. 4-7b). The maximum reaction rates in the absence and presence of 10 mM $CaCl_2$ were 41.5

± 1.6 and 149 ± 3 s^{-1}, respectively. The temperature stability range at ≤ 40°C was also increased to ≤ 45°C by the addition of 10 mM $CaCl_2$ (Fig. 4-7c). The effects of various metal ions on enzyme activity were examined (Table 4-1). The NdFosA activity decreased to 10% and 3.3% in the presence of 10 mM $CoCl_2$ and $NiCl_2$, respectively, and increased to 173% in the presence of 10 mM $CaCl_2$. The monovalent cations tested and $MgCl_2$ had no obvious effect on NdFosA activity (Table 4-1). As the addition of 10 mM EDTA only slightly reduced the activity of NdFosA to 89% of the original activity. These results suggest that Ca^{2+} contributes to the activation and thermal stabilization of NdFosA.

4.3.7. Kinetic analysis of the reaction of NdFosA with sucrose in the absence and presence of inulin

Using sucrose at various concentrations as a substrate, D-glucose released as an aglycone and D-fructose produced by hydrolysis were determined by a colorimetric method, and the aglycone release rate, hydrolysis rate, and transglycosylation rate obtained from these were calculated. The aglycone release and hydrolysis rates were almost identical up to 20 mM sucrose (Fig. 4-8a), indicating that the enzyme mainly catalyzed hydrolysis with ≤ 20 mM sucrose. The reaction rate for transglycosylation increased with increasing substrate concentration. The three reaction rates followed the rate equations (Eq. 2-1–3) obtained from the reaction scheme shown in Fig. 2-1 (Fig. 4-8a). The kinetic parameters determined were as follows: k_{cat1}, 44.0 ± 0.7 s^{-1}; k_{cat2}, 92.4 ± 7.5 s^{-1}; K_{m1}, 5.89 ± 0.33 mM; and K_{m2}, 1350 ± 260 mM. The r_{tg} values determined at various sucrose concentrations followed Eq. 2-4, with a transglycosylation parameter K_{TG} of 650 ± 162 mM (Fig. 4-8b). The three reaction rates in the presence of 2.5 mM inulin are shown in Fig. 4-8c. [Sucrose]-v_{tg}/v_h plots gave a straight line as in the theory, with a slope of 0.00228 and an intersection with vertical axis of 0.107 (Fig. 4-8d). According to Eq. 4-1, based on these value and the inulin concentration (2.5 mM), the acceptor preference for inulin over sucrose was calculated to be 18.8-fold.

4.4. Discussion

Kinetic analysis of the single substrate reaction with sucrose revealed that NdFosA catalyzes both hydrolysis and β-(2→1)-transfructosylation with the high K_{TG} 650 mM. This indicates that hydrolysis is predominant at lower concentrations of sucrose in the single substrate reaction, as observed in NdIS (K_{TG}, 344 mM). As discussed in Chapter 2, the high K_{TG} for sucrose is suitable to use sucrose as donor in the transglycosylation. Through discriminating donor and acceptor clearly, D-fructosyl units of sucrose are efficiently utilized in the formation of the target products. This functional similarity of NdFosA to NdIS in the reaction with sucrose is consistent with the high conservation of residues in the +1 and +2 subsites of NdFosA and NdIS (Fig. 4-9; predicted by ColabFold using the default parameters; Mirdita *et al.* 2022). However, in contrast to NdIS, the chain elongation by NdFosA through β-(2→1)-transglycosylation was limited to 1-kestose, and nystose and longer FOS were not produced. Its nystose-degrading activity was not detected, either. In FOS tested, NdFosA only acts on 1-kestose. According to the structural model of NdFosA, the protein structure is in a typical 5-blade propeller fold, and its long 5B-5C loop (the loop connecting β-strands B and C in the fifth propeller) forms a bulky structure near the active site (Fig. 4-10). Its superposition with the 1-kestose complex suggests that the 5B-5C loop provides steric hindrance to the D-glucosyl moiety of 1-kestose binding (Fig. 4-10). Therefore, this 5B-5C loop-forming bulky structure is probably responsible for the limited elongation of the β-(2→1)-linked chains by NdFosA.

The reaction of NdFosA to introduce the β-(2→6)-D-fructosyl side chain into the inulin chain is discussed. In the β-(2→6)-D-fructosyl transfer, DP 8 or higher, especially long-chain inulin, is used as the acceptor (Fig. 4-4e), and its internal D-fructosyl residues is D-fructosylated. To form this β-(2→6)-linked D-fructosyl branch, an internal fructosyl residue of the inulin suffers β-(2→6)-fructosylation, and this fructosyl needs to bind to subsite +1. Therefore, NdFosA should have binding sites for D-fructosyl residues of the D-fructosyl-terminal side of the target D-fructosyl group and those for D-fructosyl residues

on the D-glucosyl-terminal side. Acceptor inulin binding mode is predicted. Acceptor inulin binding subsites are defined as follows: +1 subsite for D-fructosyl residue for D-fructosylation, +2 and +3 subsites towards the D-glucosyl ends, -1', -2', and -3' subsites towards the D-fructosyl ends. For the β-(2→6)-D-fructosyl transfer, the binding manner of the D-fructosyl residue in the +1 subsite is expected to be similar to that in +1 subsite of β-(2→6)-fructosyltransferase, levansucrase. In the levanhexaose complex of *B. subtilis* 168 levansucrase (SacB), +2 subsite is in the space formed by short 2B-2C, on the other side of 5B-5C loop, due to the position of the D-fructosyl residue, particularly its 2-O (Fig. 4-11d, e; Raga-Carbajal *et al.* 2021; PDB entry 6VHQ). NdFosA also possesses the space in the corresponding position, which is in a cleft-like structure (indicated by the yellow oval) formed by short 2B-2C (Fig. 4-11a). Therefore, +2 and further positive subsites for inulin binding are predicted to be formed in the cleft-like structure. This cleft-like structure is not found in the predicted structure of NdIS carrying long 2B-2C loop (Fig. 4-11b), but found in InuJ is known to possess both the activities of β-(2→6)-branching and elongation of β-(2→1)-linked inulin chains, and carries short 2B-2C loop, responsible for the formation of the cleft structure. Although the mechanism of branch formation of InuJ remains unknown, InuJ may also use this cleft for acceptor binding in the β-(2→6)-branch formation. The 2B-2C loop is short in *Lactobacillales* IS, which produces inulin with a branched structure, but contains 5–10 extra residues in linear-inulin producer, *Bacillales* IS including NdIS, InuO, and InuBK, compared with NdFosA (Fig. 4-12). This also supports the presumption that the cleft structure is dependent on the short loop and is used for acceptor inulin binding for β-(2→6)-transfructosylation. The surface of the cleft structure of NdFosA is formed by polar side chains of residues such as Glu172, Gln173, and Tyr222 as well as Phe171 which allows hydrophobic interactions with sugar (Fig. 4-13). These residues may interact with inulin.

Next, the binding of the D-fructosyl terminal side of β-(2→1)-fructan chain to minus prime subsites in NdFosA is predicted. In SacB, 1-O of D-fructosyl residue at the +1 subsite faces down in Fig. 4-11e.

Assuming D-fructosyl residue binds similarly to this residue in NdFosA in β-(2→6)-transfructosylation, one candidate for the formation of the minus prime subsites is another cleft structure indicated by red oval in Fig. 4-11a. Although this position is near where the 5B-5C loop was predicted to prevent nystose binding, inulin may be able to bind because of the different orientation of the β-(2→1)-D-fructosyl chain. Polar amino acid residue such as Gln412 is present in this cleft and may interact with the inulin chain (Fig. 4-13). Taken together, binding mode of acceptor inulin is predicted as indicated by the white dashed line in Fig. 4-11a.

Physicochemical property of the branched inulin is discussed. Although linear inulin, produced in reaction with 1.46 M or higher concentration of sucrose by recombinant NdIS, contains water-insoluble polysaccharides, such insoluble polysaccharide was not formed by the cooperative action of recombinant NdIS and NdFosA. As no significant difference was observed in the chain length distribution of these products (Fig. 4-5, "NdIS" and "NdIS + NdFosA"), the β-(2→6) branched structure introduced by NdFosA presumably suppressed the aggregation and precipitation of inulin. FOSs of ≥DP 9 form a single helical structure, which decreases their compatibility with water (Mensink *et al.* 2015), and the introduction of branch in inulin may suppress the formation of the single helical structure, resulting in increased water solubility.

It is known that the GH32 enzymes 1-FFT and 6-SFT modify inulin and synthesize β-(2→6)-branched graminan-type inulin in plants, but no microbial enzyme that introduce β-(2→6)-branch to inulin has been reported so far. This chapter shows that NdFosA, secreted by *N. drentensis* 57N, is a novel enzyme that transfers the D-fructosyl residue of sucrose to the internal D-fructosyl residue of inulin to form β-(2→6)-D-fructosyl linkage. The branching of inulin by NdFosA may provide the new function and physical and beneficial properties to inulin.

Table 4-1. Effects of 10 mM metal ions and EDTA on NdFosA activity.

10 mM additive	Activity (%)[a]
LiCl	101 ± 3
NaCl	106 ± 10
KCl	100 ± 4
NH_4Cl	99 ± 1
$MgCl_2$	98 ± 2
$CaCl_2$	173 ± 2
$CoCl_2$	10 ± 3
$NiCl_2$	3.1 ± 0.0
EDTA	89 ± 3

[a] Relative to activity in the absence of the metal ions.

Fig. 4-1. Nucleotide sequence of the *NdFosA* gene and its deduced amino-acid sequence.

Amino-acid sequence determined by Edman degradation is underlined. The catalytic residues are in bold.

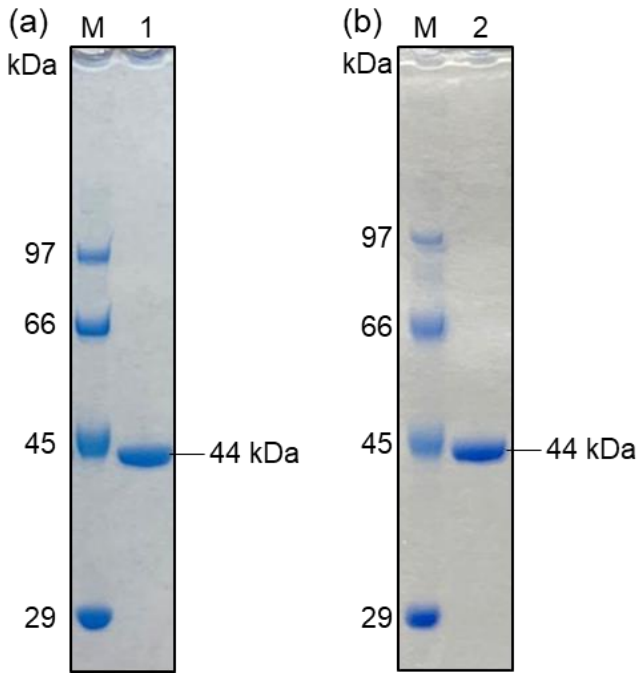

Fig. 4-2. SDS-PAGE of protein partially purified NdFosA (a) and recombinant NdFosA (b).

Lane 1, partially purified NdFosA (1 μg); lane 2, recombinant NdFosA (1 μg); lane M, size markers. The molecular masses of the standards are shown on the left.

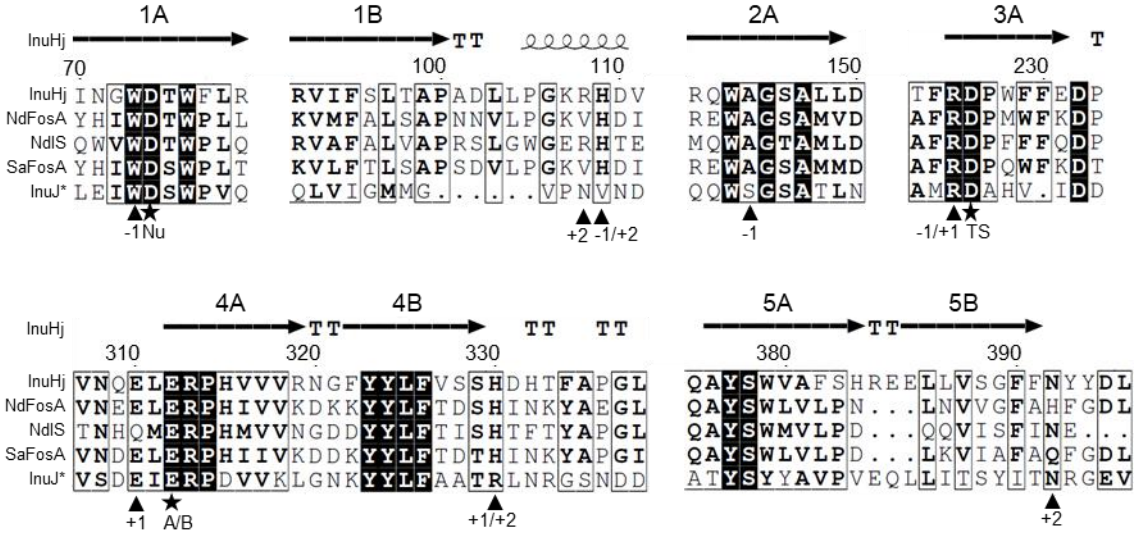

Fig. 4-3. Comparison of catalytic and subsite-forming residues of characterized GH68 enzymes.

InuHj, IS from *H. jeotgali* B3T; NdFosA, fructosyltransferase from *N. drentensis* 57N; NdIS, IS from *N. drentensis* 57N; SaFosA, β-fructofuranosidase from *S. agaradhaerens* WDG185; InuJ, IS from *L. johnsonii* NCC 533. *Lactobacillales* IS indicated with asterisks. Stars: catalytic residues (Nu: nucleophile; TS: transition-state stabilizer; A/B: acid/base). Triangles indicate amino acid residues that form subsites −1, +1, and +2 of InuHj for 1-kestose binding. Numbers above are of NdFosA.

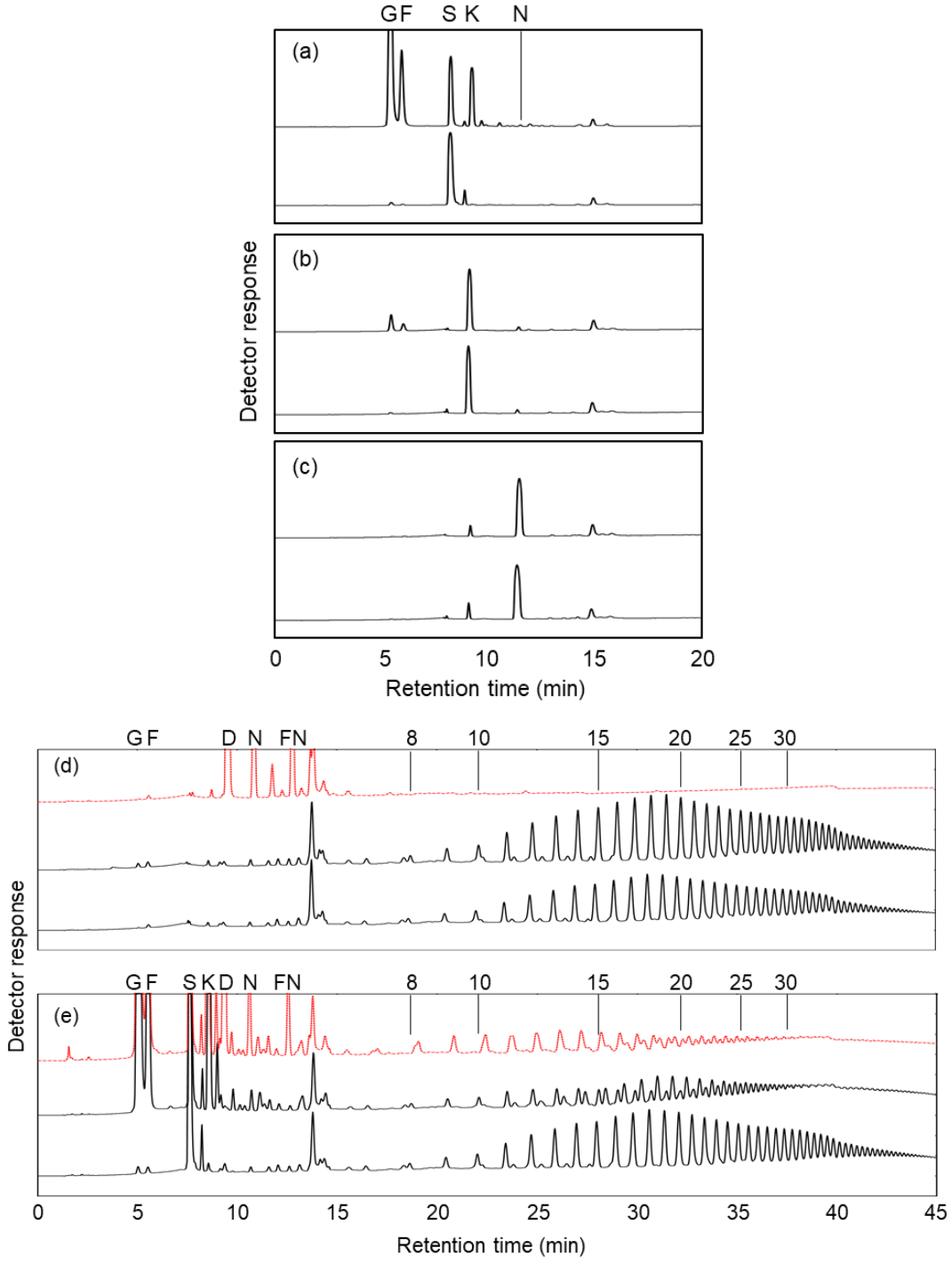

Fig. 4-4. HPAEC-PAD analysis of NdFosA-catalyzed long-term reactions with various substrates..

Product analysis of NdFosA from a prolonged reaction of (a) 0.5 M sucrose, (b) 50 mM 1-kestose, (c) 50 mM nystose, (d) 12.5 mM inulin, and (e) 0.5 M sucrose and 12.5 mM inulin. HPAEC-PAD charts above and below show post- and pre-reaction, respectively. Profiles with red dashed lines in panel (d) and (e) are of the post-reaction sample after digested with IFT. G, D-Glucose; F, D-fructose; S, sucrose; K, 1-kestose; N, nystose; FN, fructosyl-nystose; D, DFA III. Numbers 8–30, FOS with DP8–30.

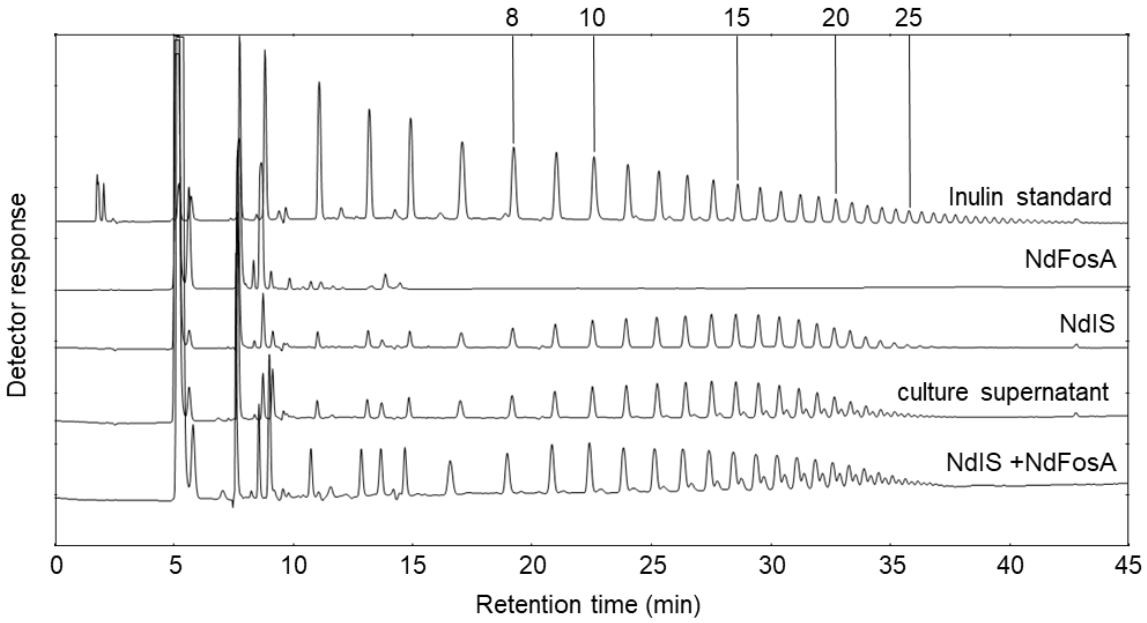

Fig. 4-5. HPAEC-PAD analysis of reaction products of various enzymes to sucrose.

HPAEC-PAD charts show inulin standard (raftiline ST), the reaction products of NdFosA, NdIS, culture supernatant of *N. drentensis* 57N, and NdIS + NdFosA from 1.46 M sucrose, respectively. Numbers above are DP.

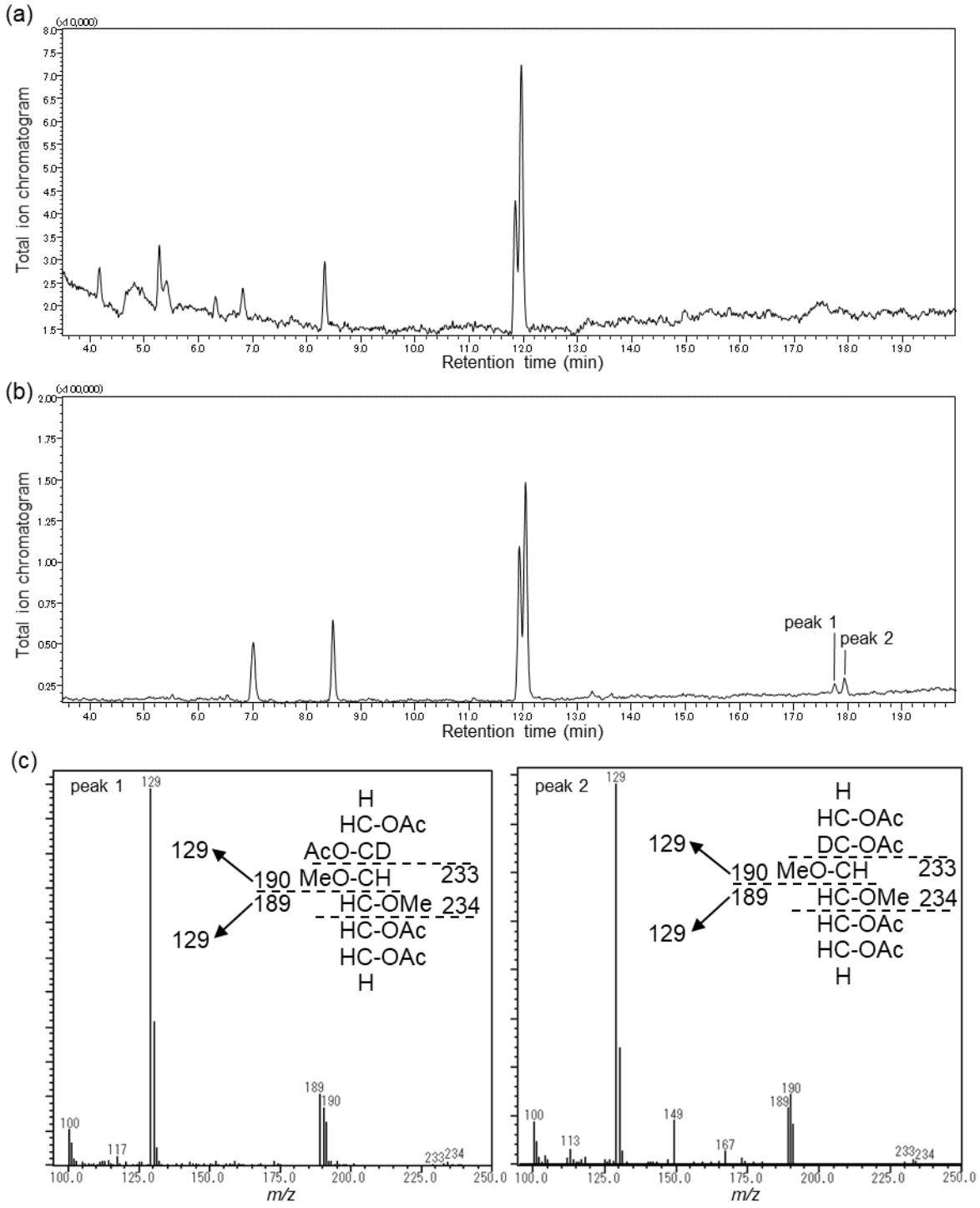

Fig. 4-6. GC-MS profile of partially methylated alditol acetates (PMAAs).

PMAAs from the reaction products from 1.46 M sucrose of (a) 3 μM NdIS and (b) 3 μM NdIS and 3 μM NdFosA are analyzed. (c) MS fragments and deduced structures of peak 1 and 2, identified as 1,2,5,6-tetra-*O*-acetyl-(2-deuterio)-3,4-di-*O*-methylmannitol and 1,2,5,6-tetra-*O*-acetyl-(2-deuterio)-3,4-di-*O*-methylglucitol, respectively.

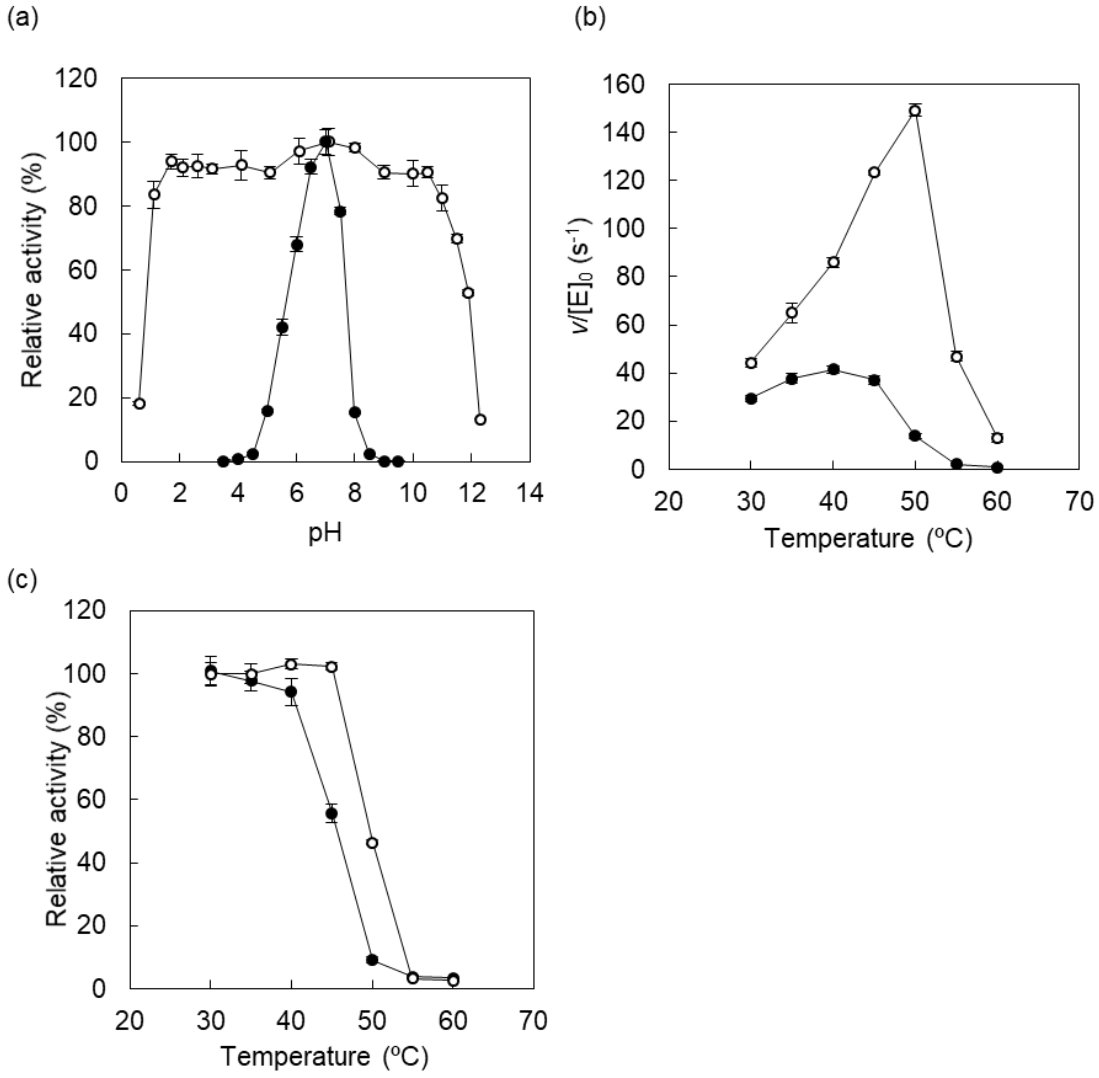

Fig. 4-7. Effects of pH and temperature on activity and stability of recombinant NdFosA.

(a) Effects of pH on activity at 37˚C (filled circle) and remaining activity after incubation at 4˚C for 24 h (open circle). (b) D-Glucose releasing velocity measured at the indicated temperatures at pH 6.5 in a 10-min reaction in the absence (filled circle) and presence of 10 mM $CaCl_2$ (open circle). (c) Residual activity after incubation at the indicated temperatures at pH 6.5 for 15 min in the absence (filled circle) and presence of 10 mM $CaCl_2$ (open circle). The results are presented as the means of triplicate experiments with standard deviations.

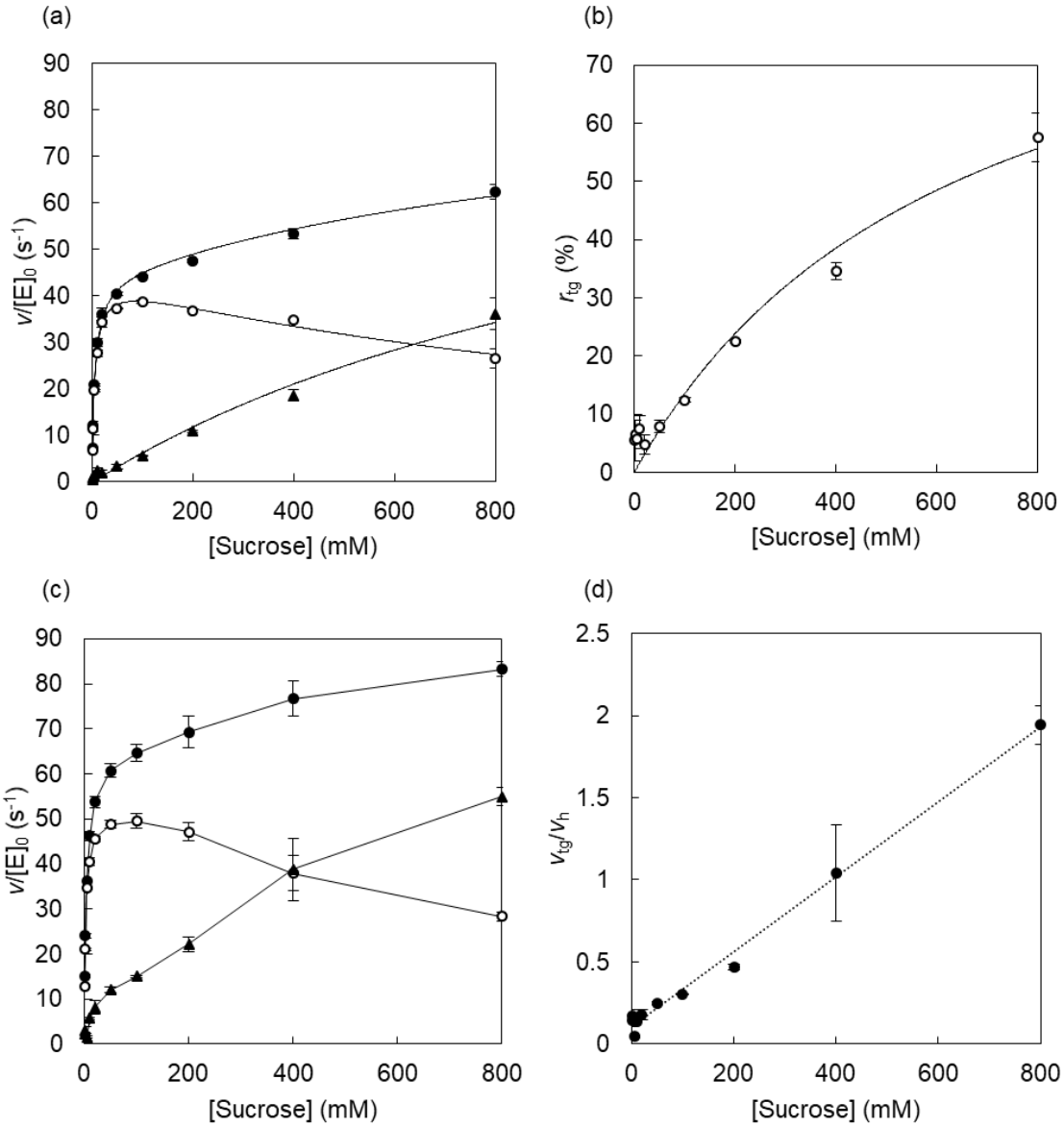

Fig. 4-8. Kinetics of catalytic reaction toward sucrose of recombinant NdFosA in the presence and absence of 2.5 mM inulin.

(a) The dependence of initial velocities of aglycone release ($v_{ag}/[E]_0$, filled circle), hydrolysis ($v_h/[E]_0$, open circle), and transglycosylation ($v_{tg}/[E]_0$, filled triangle) on sucrose concentration in the absence of 2.5 mM inulin. (b) Dependence of transglycosylation ratio ($r_{tg} = v_{tg}/v_{ag}$) on sucrose concentration calculated from the data shown in (a). (c) The dependence of v_{ag}, v_h, and v_{tg} on sucrose concentration in the presence of 2.5 mM inulin. (d) v_{tg}/v_h-[Sucrose] plot in the presence of 2.5 mM inulin. Theoretical curves from the kinetic parameters are shown in panel (a) and (b). Approximated curve is shown in panel (d) as dashed line. The data are presented as the means of triplicate experiments with standard deviations.

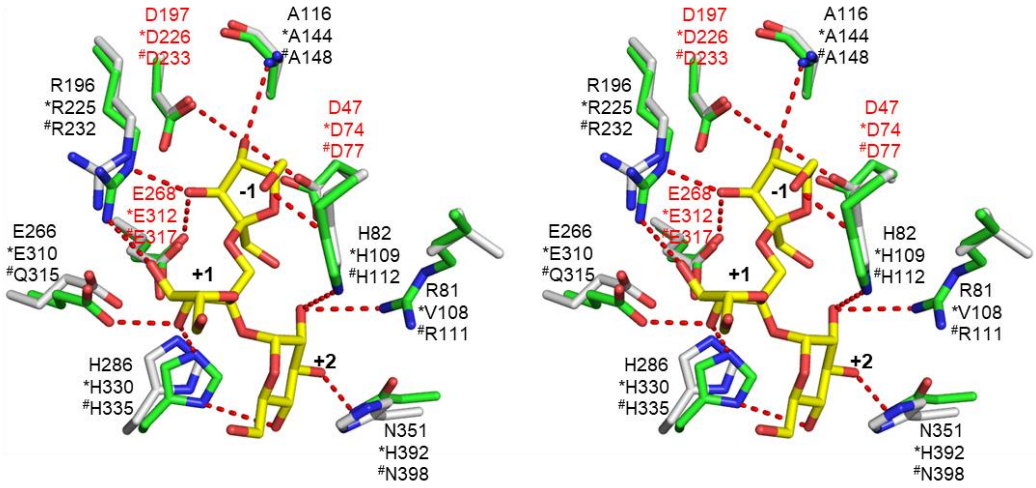

Fig. 4-9. Comparison of the crystal structure of InuHj (7BJ4, Ghauri *et al.* 2021b) and the three-dimensional structure prediction model of NdFosA.

Green and white sticks indicate amino acid residues of InuHj and NdFosA, respectively. Yellow sticks indicate 1-kestose in the structure of InuHj. The catalytic residues are indicated in red letters. The predicted hydrogen bonds between the residues of InuHj and 1-kestose are indicated by red dashed lines. Amino acid residues of NdFosA and the corresponding residues of NdIS are marked with an asterisk and a sharp, respectively.

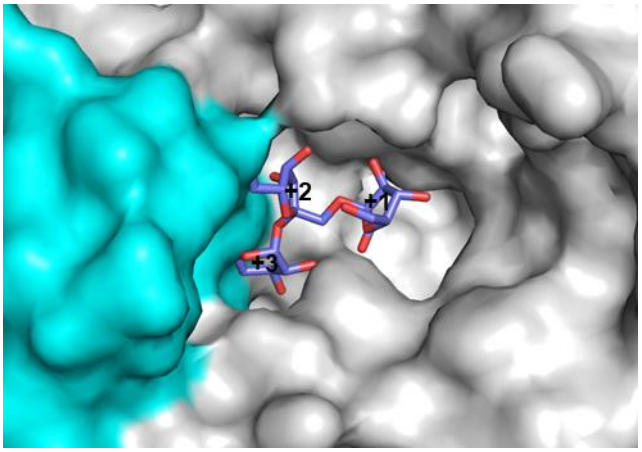

Fig. 4-10. Three-dimensional structure prediction model of NdFosA complexed with acceptor 1-kestose. Violet stick indicates 1-kestose in the structure of InuHj (Terminal D-fructosyl residue overlaid on the +1 Fru position). 5B-5C loop is colored with cyan.

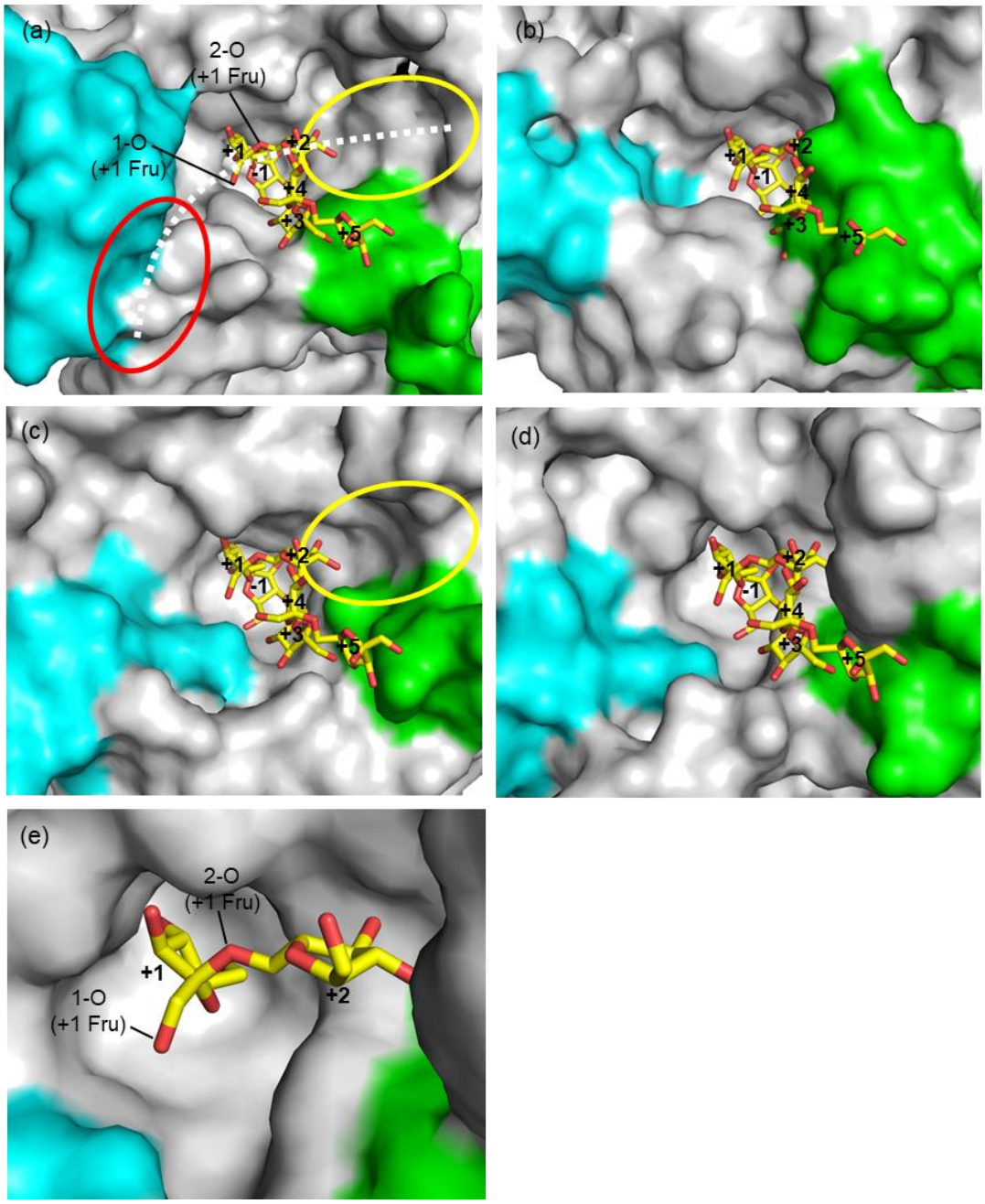

Fig. 4-11. Comparison of the molecular surfaces of NdFosA with NdIS, InuJ (2YFT, Pijning *et al.* 2011), and *B. subtilis* levansucrase (SacB; 6VHQ, Raga-Carbajal *et al.* 2021).

Three-dimensional structure prediction model of (a) NdFosA and (b) NdIS. Crystal structure of (c) InuJ, and (d) SacB (levanhexaose complex). (e) Enlarged view of panel (d), showing only +1 Fru and +2 Fru. Yellow sticks indicate levanhexaose in the structure of SacB. 2B-2C and 5B-5C loops are colored with green and cyan, respectively. Yellow and red ovals indicate cleft structures that possibly accommodate D-glucosyl and D-fructosyl terminal residues, respectively. White dashed line in panel (a) shows the presumed inulin binding position.

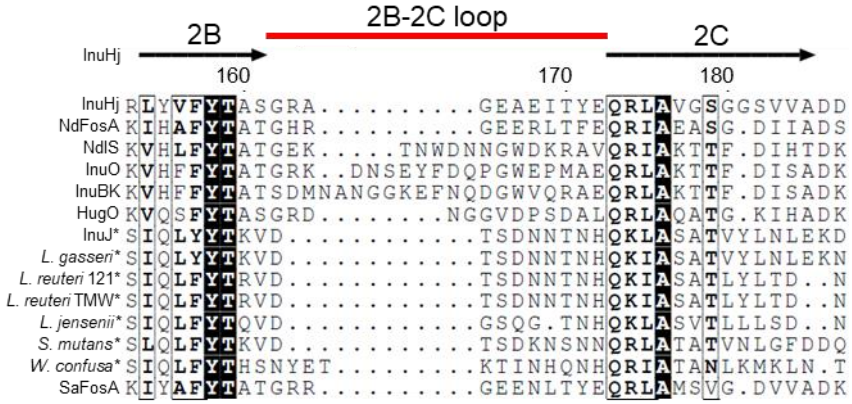

Fig. 4-12. Multiple sequence alignment of NdFosA, SaFosA, and characterized ISs around the 2B-2C loop.

InuHj, *H. jeotgali* B3T IS; NdFosA, fructosyltransferase from *N. drentensis* 57N; NdIS, *N. drentensis* 57N IS; InuO, *S. agaradhaerens* WDG185 IS; InuBK, *A. krulwichiae* JCM11691 IS; HugO, *S. viridochromogenes* DSM 40736 IS. *Lactobacillales* IS indicated with asterisks: *L. johnsonii* NCC 533 (InuJ), *L. gasseri* DSM20604, *L. reuteri* 121, *L. reuteri* TMW 1.106, and *L. jensenii* JV-V16. IS from *S. mutans* GS-5, and *W. confusa* MBFCNC-2 (1). SaFosA, β-fructofuranosidase from *S. agaradhaerens* WDG185. Numbers above are of NdFosA.

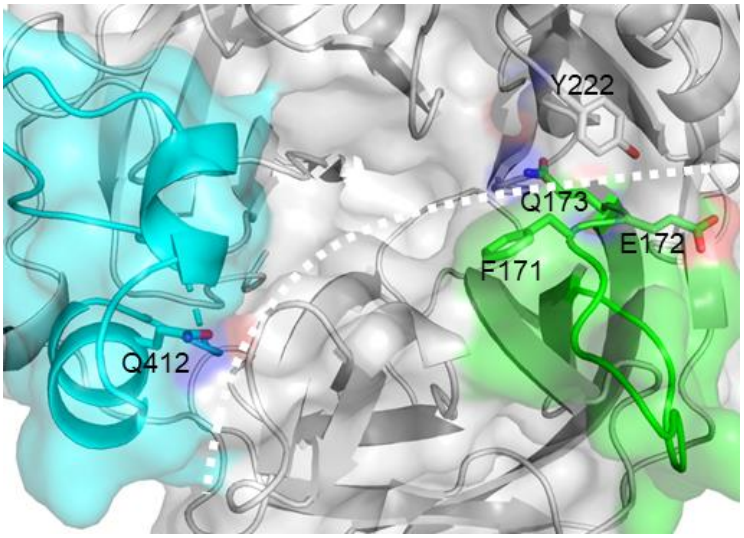

Fig. 4-13. Amino acid residues located around the putative inulin binding position of NdFosA.

2B-2C and 5B-5C loops are colored with green and cyan, respectively. White dashed line shows the presumed inulin binding position.

Chapter 5. General discussion

Inulin is used not only as a prebiotic but also as a material for the synthesis of useful oligosaccharides, and its industrial use is expanding. For efficient production and diversification of inulin and related oligosaccharides, IS and inulin-acting enzymes are useful. Furthermore, a deep understanding of the mechanism of inulin synthesis by IS is also important for efficient production of inulin from sucrose.

N. drentensis 57N, isolated from soil based on inulin producing activity, produced two extracellular sucrose-acting enzymes, NdIS and NdFosA. Functional analysis of each enzyme revealed that NdIS synthesizes inulin from sucrose and NdFosA is a novel inulin branching enzyme that transfers the D-fructosyl residue of sucrose to the 6-hydroxy group of internal D-fructosyl residue of inulin, and that these two enzymes cooperatively synthesize inulin type polysaccharide with β-(2→6) branches from sucrose extracellularly. In *Bacillales*, the role of inulin type polysaccharide is unknown, while in *Lactobacillales*, inulin type polysaccharide is used for binding to the gastrointestinal tract and formation of biofilms (Walter *et al.* 2008; Birkhed *et al.* 1979). The determined sequence of *N. drentensis* 57N is highly consistent with the sequence of *Bacillus* sp. AFS031507, whose genome sequence has already been determined, and is considered a closely related species, with a similar cluster of enzymes related to sucrose metabolism (Fig. 2-5). The sucrose metabolism-related enzyme genes of *Bacillus* sp. AFS031507 contains three genes, COE25_RS31310, COE25_RS01290, and COE25_RS01275. COE25_RS31310 encodes protein with extracellular CFT-like and β-fructofuranosidase-like sequences. COE25_RS01290 and COE_RS01275 encode intracellular CFT-like sequences in the both. Based on these possible functions of the proteins (COE25_RS31310, COE25_RS01290, and COE25_RS01275) and the clarified functions of NdIS and NdFosA in this study, the following sucrose metabolic pathway of *N. drentensis* 57N was proposed: NdIS and NdFosA synthesize inulin-type polysaccharide with β-(2→6) branching structure from sucrose. One of the two GH32 domains in the COE25_RS31310 equivalent (β-fructofuranosidase-

like) cleaves the β-(2→6)-branched D-fructosyl residue of inulin type polysaccharide and the other domain (CFT-like) synthesizes cycloinulooligosaccharides or inulooligosaccharides. The synthesized product is transferred into the bacterial cell by an ABC transporter, and further degraded by COE25_RS01275 and COE25_RS01290 like protein in the cell (Fig. 5-1). The reason why *N. drentensis* 57N synthesizes inulin type polysaccharide with β-(2→6) branching structure may be to reduce the capitalization of other microorganisms. To prove the metabolic pathway, it is necessary to determine the presence of COE25_RS31310, COE25_RS01275, and COE25_RS01290-like proteins in *N. drentensis* 57N and to characterize them. BLAST analysis showed that all microorganisms harboring NdIS homologues with sequences more than 68% identical with NdIS, had the gene encoding NdFosA homologues with more than 66% identity to NdFosA downstream of the NdIS-like gene (Table 5-1). Synthesis of inulin type polysaccharides with branched structures may be a common feature of IS producing *Bacillales*.

NdIS showed high sequence similarity to reported ISs from *Bacillales*, but produced fructan with a higher DP than these enzymes. Long-chain fructans are useful materials for DFA III synthesis, because IFT from *Arthrobacter* sp. H65-7 use DP 6 or higher FOSs as substrates (Yokota *et al.* 1991). A water-insoluble product was generated during the reaction of NdIS with 1,600 mM sucrose. The precipitated product of IS from *L. reuteri* 121, forms inulin nanoparticles and encapsulates flavonoids, such as quercetin and fisetin, to improve stability and water solubility (Charoenwongpaiboon *et al.* 2019b). Inulin produced by NdIS presumably have a different structure from those of *L. reuteri* 121, in terms of their molecular mass and branch structure. Therefore, the water-insoluble fructan produced by NdIS may have novel functions, for example, inclusion capability that is different from the inulin nanoparticles described above. In addition, long chain linear inulins have higher viscosity than short chain inulins (Wada *et al.* 2005) and may be superior to existing inulins for texture improvement applications.

Evaluation of substrate specificity suggested that the +1 subsite of NdIS prefers the D-glucosyl structure and not the D-fructosyl structure, while the +2 subsite prefers the D-fructosyl structure and not the D-glucosyl structure. Therefore, sucrose is used as the donor and FOS as the acceptor, which is important for the synthesis of long-chain inulin. Using this property, control of average DP of products was demonstrated to some extent in this work by using sucrose and FOS such as 1-kestose or nystose at appropriate ratios. It is known that the prebiotic effect of inulin depends on the chain length: for example, short chain inulin has higher effects on *B. longum* and *B. animalis* growth than long chain inulin (Biedrzycka and Bielecka 2004). Changes in short chain fatty acid production in the gut due to differences in DP distribution have also been noted (van de Wiele *et al.* 2007). The application of this study will enable tailor-made synthesis of inulin with the desired average DP, which will be beneficial for industrial use.

As mentioned above, linear inulin synthesized at high sucrose concentrations by NdIS formed precipitates, but branched inulin synthesized in the presence of NdFosA did not. Here again water solubility of inulin is discussed: as mentioned in Chapter 4, inulin forms a single helical structure, which reduces its compatibility with water (Mensink *et al.* 2015). The introduction of a branched structure into linear inulin may inhibit the uniform molecular alignment and weaken intermolecular interactions, thereby preventing precipitation due to aggregation. This suggests that branched inulin is more water soluble than linear inulin. The introduction of a branched structure to inulin is expected to expand the range of applications, such as enabling an increase in the amount of inulin in beverages and the use in products requiring immediate solubility. In addition, branched inulin may have a different prebiotic effect than linear inulin by suppressing the growth of bacteria that dislike the branched structure and by selectively growing bacteria that prefer it. On the other hand, in the case of material production from inulin, branching structure is not desirable. Because when functional carbohydrate, such as DFA III and

cycloinulooligosaccharide, are synthesized from the inulin, the branched structure reduces the yield of the target product.

The results of this study will contribute to the enzymatic synthesis of inulin and related oligosaccharides and their diversification, such as the regulation of average DP during inulin synthesis by IS and the introduction of branches into inulin by NdFosA. Industrial applications of this research are expected. I hope that the study based on the enzyme functions and structures will contribute to more detailed understanding of GH68 enzymes.

Table 5-1. List of microorganisms which have the NdIS homologous gene.

Origin	Similarity (%)		GenBank Accession No.	
	NdIS-like	NdFosA-like	NdIS-like	NdFosA-like
Bacillus sp. AFS031507	99	99	WP_098930566.1	WP_098930308.1
Priestia megaterium	98	99	WP_168242084.1	WP_168242085.1
Bacillus sp. MM2020_1	98	99	WP_166256437.1	WP_166256440.1
Bacillus sp. ISL-46	97	97	WP_214731329.1	WP_251026627.1
Bacillus sp. X1(2014)	96	94	WP_144554313.1	WP_144554311.1
Neobacillus bataviensis	97	93	WP_223589390.1	WP_223589392.1
Fredinandcohnia onubensis	85	90	WP_099354678.1	WP_099354679.1
Metabacillus bambusae	86	89	WP_243459527.1	WP_207980430.1
Alkalihalobacillus krulwichiae	68	86	WP_066151831.1	WP_066151830.1
Litchfieldia salsa	83	86	WP_090856257.1	WP_090856254.1
Mycobacteroides abscessus subsp. *Abscessus*	81	85	SHR63461.1	SHR63422.1
Bacillus sp. Y1	82	85	WP_119706532.1	WP_119706533.1
Robertmurraya korlensis	80	85	WP_066052162.1	WP_066052166.1
Brevibacillus formosus	81	81	KLH99469.1	KLH99468.1
Brevibacillus formosus	81	81	MBG9945612.1	MBG9945611.1
Brevibacillus sp. RS1.1	79	79	WP_173627227.1	WP_173627228.1
Brevibacillus brevis	79	79	WP_064202058.1	WP_064202059.1
Ammoniphilus sp. YIM 78166	80	79	WP_134704861.1	WP_134704859.1
Brevibacillus sp. HB2.2	79	79	WP_173604212.1	WP_173604213.1
Brevibacillus formosus	79	79	WP_088909524.1	WP_088909523.1
Brevibacillus sp. M2.1A	79	79	WP_173611150.1	WP_173611151.1
Brevibacillus dissolubilis	82	79	WP_139492529.1	WP_139492467.1
Brevibacillus formosus	79	79	WP_052773388.1	WP_083995063.1
Brevibacillus migulae	77	78	WP_134686958.1	WP_134686959.1
Paenibacillus sp. A3	73	77	WP_054972565.1	WP_054972566.1
Paenibacillus sp. WST5	72	77	WP_188172560.1	WP_188172561.1
Paenibacillus elgii	73	77	WP_108533519.1	WP_108533520.1
Paenibacillus tyrfis	73	77	GLI10888.1	GLI10887.1
Paenibacillus elgii	73	77	WP_163855093.1	WP_163855095.1
Paenibacillus prosopidis	68	75	WP_245975758.1	WP_245975758.1
Paenibacillus sp. YIM B00362	71	72	WP_199616134.1	WP_199616132.1
Paenibacillus sp. LMG 31458	70	72	WP_171649234.1	WP_171649235.1
Bacillus sp. LL01	69	68	WP_053073957.1	WP_047973383.1
Salipaludibacillus agaradhaerens WDG185	68	66	ATN45518.1 (InuO)	ATN45517.1 (SaFosA)

Similarity indicates the homology of the NdIS-like/NdFosA-like protein sequence of each microorganism to NdIS/NdFosA.

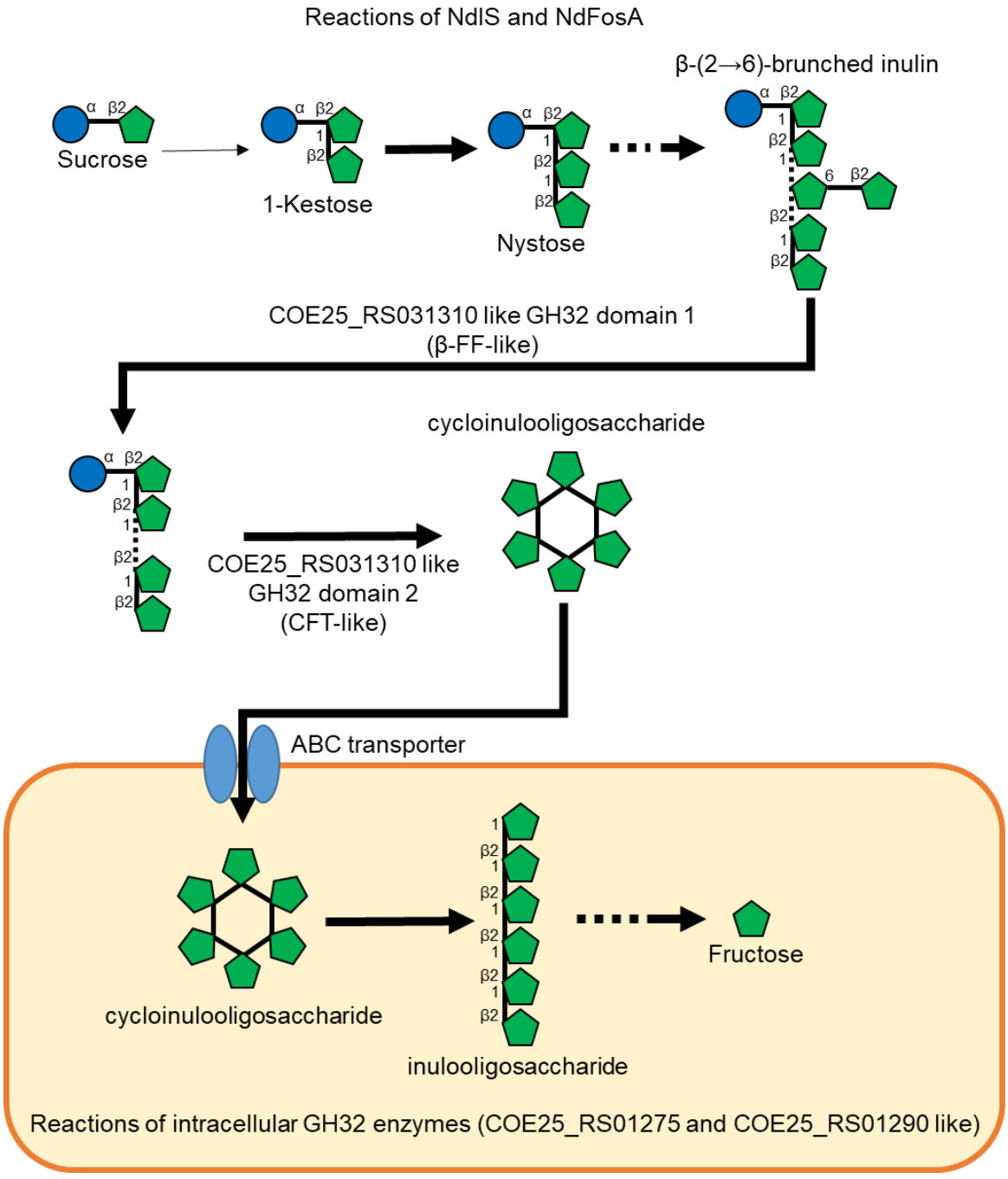

Fig. 5-1. Predicted mechanism of sucrose metabolism of *N. drentensis* 57N.

References

Agrawal PK. NMR Spectroscopy in the structural elucidation of oligosaccharides and glycosides. *Phytochemistry* 1992;**31**:3307–3330.

Altschul SF, Gish W, Miller W, Myers EW, Lipman DJ. Basic local alignment search tool. *J Mol Biol* 1990;**215**:403–410.

Anwar MA, Kralj S, Pique AV, Leemhuis H, van der Maarel MJ, Dijkhuizen L. Inulin and levan synthesis by probiotic *Lactobacillus gasseri* strains: characterization of three novel fructansucrase enzymes and their fructan products. *Microbiology* 2010;**156**:1264–1274.

Anwar MA, Kralj S, van der Maarel MJ, Dijkhuizen L. The probiotic *Lactobacillus johnsonii* NCC 533 produces high-molecular-mass inulin from sucrose by using an inulosucrase enzyme. *Appl Environ Microbiol* 2008;**74**:3426–3433.

Apolinário AC, de Lima Damasceno BPG, de Macêdo Beltrão NE, Pessoa A, Converti A, da Silva JA. Inulin-type fructans: a review on different aspects of biochemical and pharmaceutical technology. *Carbohydr Polym* 2014;**101**:368–378.

Armenteros JJA, Tsirigos KD, Sønderby CK, Petersen TN, Winther O, Brunak S, von Heijne G, Nielsen H. SignalP 5.0 improves signal peptide predictions using deep neural networks. *Nat Biotechnol* 2019;**37**:420–423.

Barrow GI, Feltham RKA. Cowan and Steel's manual for the identification of medical bacteria. 3rd edition. Cambridge University Press; 1993.

Batista FR, Hernández L, Fernández JR, Arrieta J, Menéndez C, Gómez R, Támbara Y, Pons T. Substitution of Asp-309 by Asn in the Arg-Asp-Pro (RDP) motif of *Acetobacter diazotrophicus* levansucrase affects sucrose hydrolysis, but not enzyme specificity. *Biochem J* 1999;**337**:503–506.

Biedrzycka E, Bielecka M. Prebiotic effectiveness of fructans of different degrees of polymerization.

Trends Food Sci Technol 2004;**15**:170–175.

Birkhed D, Rosell KG, Granath K. Structure of extracellular water-soluble polysaccharides synthesized from sucrose by oral strains of *Streptococcus mutans*, *Streptococcus salivarius*, *Streptococcus sanguis* and *Actinomyces viscosus*. *Arch Oral Biol* 1979;**24**:53–61.

Bruker H III, Sims PF, Sinnott ML. Lignocellulose degradation by *Phanerochaete chrysosporium*: purification and characterization of the main α-galactosidase. *Biochem J* 1999;**339**:43–53.

Chambert R, Gonzy-Treboul G. Levansucrase of *Bacillus subtilis*. Characterization of a stabilized fructosyl-enzyme complex and identification of an aspartyl residue as the binding site of the fructosyl group. *Eur J Biochem* 1976;**71**:493–508.

Chambert R, Treboul G, Dedonder R. Kinetic studies of *Bacillus subtilis* levansucrase. *Eur J Biochem* 1974;**41**:285–300.

Charoenwongpaiboon T, Sitthiyotha T, Ayutthaya PPN, Wangpaiboon K, Chunsrivirot S, Prousoontorn MH, Pichyangkura R. Modulation of fructooligosaccharide chain length and insight into the product binding motif of *Lactobacillus reuteri* 121 inulosucrase. *Carbohydr Polym* 2019a;**209**:111–121.

Charoenwongpaiboon T, Wangpaiboon K, Panpetch P, Field RA, Barclay JE, Pichyangkura R, Kuttiyawong K. Temperature-dependent inulin nanoparticles synthesized by *Lactobacillus reuteri* 121 inulosucrase and complex formation with flavonoids. *Carbohydr Polym* 2019b;**223**:115044.

Crittenden RG, Doelle HW. Structural identification of oligosaccharides produced by *Zymomonas mobilis* levansucrase. *Biotechnol Lett* 1993;**15**:1055–1060.

del Moral S, Olivera C, Rodriguez ME, Munguia AL. Functional role of the additional domains in inulosucrase (IslA) from *Leuconostoc citreum* CW28. *BMC Biochem* 2008;**9**:1–10.

Demel RA, Dorrepaal E, Ebskamp MJM, Smeekens JCM, De Kruijff B. Fructans interact strongly with

model membranes. *Biochim Biophys Acta Biomembr* 1998;**1375**:36–42.

Drula E, Garron ML, Dogan S, Lombard V, Henrissat B, Terrapon N. The carbohydrate-active enzyme database: functions and literature. *Nucleic Acids Res* 2022;**50**:571–577.

Duchateau N, Bortlik K, Simmen U, Wiemken A, Bancal P. Sucrose:fructan 6-fructosyltransferase, a key enzyme for diverting carbon from sucrose to fructan in barley leaves. *Plant Physiol* 1995;**107**:1249–1255.

Edelman J, Jefford TG. The mechanism of fructosan metabolism in higher plants as exemplified in *Helianthus tuberosus*. *New Phytol* 1968;**67**:517–531.

Euzenat O, Guibert A, Combes D. Production of fructo-oligosaccharides by levansucrase from *Bacillus subtilis* C4. *Process Biochem* 1997;**32**:237–243.

Fersht AR, Shi JP, Knill-Jones J, Lowe DM, Wilkinson AJ, Blow DM, Brick P, Waye MMY, Winter G. Hydrogen bonding and biological specificity analysed by protein engineering. *Nature* 1985;**314**:235–238.

Flores AC, Morlett JA, Rodríguez R. Inulin potential for enzymatic obtaining of prebiotic oligosaccharides. *Crit Rev Food Sci Nutr* 2016;**56**:1893–1902.

Fransen F, Sahasrabudhe NM, Elderman M, Bosveld M, Aidy SE, Hugenholtz F, Borghuis T, Kousemaker B, Winkel S, van der Gaast-de Jongh C, de Jonge MI, Boekschoten MV, Smidt H, Schols HA, de Vos P. β2→1-Fructans modulate the immune system *in vivo* in a microbiota-dependent and -independent fashion. *Front Immunol* 2017;**8**:154.

Frasch HJ, van Leeuwen SS, Dijkhuizen L. Molecular and biochemical characteristics of the inulosucrase HugO from *Streptomyces viridochromogenes* DSM40736 (Tü494). *Microbiology* 2017;**163**:1030–1041.

Fujita K, Hara K, Hashimoto H, Kitahata S. Purification and some properties of β-fructofuranosidase I from *Arthrobacter* sp. K-1. *Agric Biol Chem* 1990;**54**:913–919.

Gay P, Le Coq D, Steinmentz M, Ferrari E, Hoch JA. Cloning structural gene *sacB*, which codes for exoenzyme levansucrase of *Bacillus subtilis*: expression of the gene in *Escherichia coli*. *J Bacteriol* 1983;**153**:1424–1431.

Ghauri K, Ali H, Munawar N, Ghauri MA, Anwar MA. Glycoside hydrolase family 68 gene of halophilic archaeon *Halalkalicoccus jeotgali* B3T codes for an inulosucrase enzyme. *Biocatal Biotransformation* 2021a;**39**:206–213.

Ghauri K, Pijning T, Munawar N, Ali H, Ghauri MA, Anwar MA, Wallis R. Crystal structure of an inulosucrase from *Halalkalicoccus jeotgali* B3T-a halophilic archaeal strain. *FEBS J* 2021b;**288**:5723–5736.

Gibson GR, Beatty ER, Wang XIN, Cummings JH. Selective stimulation of bifidobacteria in the human colon by oligofructose and inulin. *Gastroenterology* 1995;**108**:975–982.

Hernandez L, Arrieta J, Menendez C, Vazquez R, Coego A, Suarez V, Selman G, Petit-Glatron MF, Chambert R. Isolation and enzymic properties of levansucrase secreted by *Acetobacter diazotrophicus* SRT4, a bacterium associated with sugar cane. *Biochem J* 1995;**309**:113–118.

Heyrman J, Vanparys B, Logan NA, Balcaen A, Rodríguez-Díaz M, Felske A, De Vos P. *Bacillus novalis* sp. nov., *Bacillus vireti* sp. nov., *Bacillus soli* sp. nov., *Bacillus bataviensis* sp. nov. and *Bacillus drentensis* sp. nov., from the Drentse A grasslands. *Int J Syst Evol Microbiol* 2004;**54**:47–57.

Homann A, Biedendieck R, Götze S, Jahn D, Seibel J. Insights into polymer versus oligosaccharide synthesis: mutagenesis and mechanistic studies of a novel levansucrase from *Bacillus megaterium*. *Biochem J* 2007;**407**:189–198.

Kanai T, Ueki N, Kawaguchi T, Teranishi Y, Atomi H. Recombinant thermostable cycloinulo-oligosaccharide fructanotransferase produced by *Saccharomyces cerevisiae*. *Appl Environ Microbiol* 1997;**63**:4956–4960.

Kawai R, Igarashi K, Kitaoka M, Ishii T, Samejima M. Kinetics of substrate transglycosylation by glycoside hydrolase family 3 glucan (1→3)-β-glucosidase from the white-rot fungus *Phanerochaete chrysosporium*. *Carbohydr Res* 2004;**339**:2851–2857.

Kawamura M, Uchiyama T. Reactions catalyzed by cycloinulo-oligosaccharide fructanotransferase. *Biosci Biotechnol Biochem* 1993;**57**:343.

Kawamura M, Uchiyama T, Kuramoto T, Tamura Y, Mizutani K. Formation of a cycloinulo-oligosaccharide from inulin by an extracellular enzyme of *Bacillus circulans* OKUMZ 31B. *Carbohydr Res* 1989;**192**:83–90.

Kawasaki A, Yoshida M. Fructan:fructan 1-fructosyltransferase, a key enzyme for biosynthesis of graminan oligomers in hardened wheat. *Planta* 2005;**223**:90–104.

Keto K, Araki T, Kitamura T, Morita N, Moori M, Suzuki Y. Purification and properties of a thermostable inulinase (β-D-fructan fructohydrolase) from *Bacillus stearothermophilus* KP1289. *Starke* 1999;**51**:253–258.

Kim HY, Choi YJ. Molecular characterization of cycloinulooligosaccharide fructanotransferase from *Bacillus macerans*. *Appl Environ Microbiol* 2001;**67**:995–1000.

Kirtel O, Lescrinier E, van den Ende W, Toksoy Öner E. Discovery of fructans in Archaea. *Carbohydr Polym* 2019;**220**:149–156.

Knudsen BK, Hessov I. Recovery of inulin from Jerusalem artichoke (*Helianthus tuberosus* L.) in the small intestine of man. *Br J Nutr* 1995;**74**:101–113.

Kobayashi M, Hondoh H, Mori H, Saburi W, Okuyama M, Kimura A. Calcium ion-dependent increase in thermostability of dextran glucosidase from *Streptococcus mutans*. *Biosci Biotechnol Biochem* 2011;**75**:1557–1563.

Kralj S, Leeflang C, Sierra EI, Kempiński B, Alkan V, Kolkman M. Synthesis of fructooligosaccharides (FosA) and inulin (InuO) by GH68 fructosyltransferases from *Bacillus agaradhaerens* strain WDG185. *Carbohydr Polym* 2018;**179**:350–359.

Laemmli UK. Cleavage of structural proteins during the assembly of the head of bacteriophage T4. *Nature* 1970;**227**:680–685.

Lammens W, Le Roy K, Schroeven L, van Laere A, Rabijns A, van den Ende W. Structural insights into glycoside hydrolase family 32 and 68 enzymes: functional implications. *J Exp Bot* 2009;**60**:727–740.

Livingston DP, Hincha DK, Heyer AG. Fructan and its relationship to abiotic stress tolerance in plants. *Cell Mol Life Sci* 2009;**66**:2007–2023.

Mach H, Volkin DB, Burke CJ, Middaugh CR. Ultraviolet absorption spectroscopy. *Methods Mol Biol* 1995;**40**:91–114.

Malik A. Molecular cloning and in silico characterization of fructansucrase gene from *Weissella confusa* MBFCNC-2 (1) isolated from local beverage. *Asia Pac J Mol Biol Biotechnol* 2012;**20**:33–42.

Mancilla-Margalli NA, Lopez MG. Water soluble carbohydrates and fructan structure patterns from *Agave* and *Dasylirion* species. *J Agric Food Chem* 2006;**54**:7832–7839.

Martinez-Fleites C, Ortiz-Lombardia M, Pons T, Tarbouriech N, Taylor EJ, Arrieta JG, Hernández L, Davies GJ. Crystal structure of levansucrase from the Gram-negative bacterium *Gluconacetobacter diazotrophicus*. *Biochem J* 2005;**390**:19–27.

Meng G, Fütterer K. Structural framework of fructosyl transfer in *Bacillus subtilis* levansucrase. *Nat Struct Mol Biol* 2003;**10**:935–941.

Mensink MA, Frijlink HW, van der Voort Maarschalk K, Hinrichs WL. Inulin, a flexible oligosaccharide I: Review of its physicochemical characteristics. *Carbohydr Polym* 2015;**130**:405–419.

Miller GL. Use of dinitrosalicylic acid reagent for determination of reducing sugar. Anal Chem 1959;**31**: 426–428.

Milward CP, Jacques NA. Secretion of fructosyltransferase by *Streptococcus salivarius* involves the sucrose-dependent release of the cell-bound form. *J Gen Microbiol* 1990;**136**:165–169.

Minamida K, Asakawa C, Sujaya IN, Kaneko M, Abe A, Sone T, Hara H, Asano K, Tomita F. Effects of long-term ingestion of difructose anhydride III (DFA III) on intestinal bacteria and bile acid metabolism in humans. *J Biosci Bioeng* 2006;**101**:149–156.

Mirdita M, Schütze K, Moriwaki Y, Heo L, Ovchinnikov S, Steinegger M. ColabFold: making protein folding accessible to all. *Nat Methods* 2022;**19**:679–682.

Mo X, Pei J, Guo Y, Lin L, Peng L, Kou C, Fan D, Pang H. Genome Sequence of *Clostridium acetobutylicum* GXAS18-1, a Novel Biobutanol Production Strain. *Genome Announc* 2015;**3**:10–1128.

Moore S, Stein WH. Photometric ninhydrin method for use in the chromatography of amino acids. *J Biol Chem* 1948;**176**:367–388.

Morris C, Morris GA. The effect of inulin and fructo-oligosaccharide supplementation on the textural, rheological and sensory properties of bread and their role in weight management: A review. *Food Chem* 2012;**133**:237–248.

Muramatsu K, Onodera S, Kikuchi M, Shiomi N. Purification and some properties of β-fructofuranosidase from *Bifidobacterium adolescentis* G1. *Biosci Biotechnol Biochem* 1993;**57**:1681–1685.

Nakagawa K, Kawasaki H. DNA sequence analysis. In Society for Actinomycetes Japan (ed), Identification manual of Actinomycetes. Business Center for Academic Societies Japan, Tokyo, Japan 2001;83–117.

Nanjo F, Goto K, Oka H, Muramatsu H, Kato S, Nagata S. Purification and properties of cycloinulooligosaccharide fructanotransferase from *Paenibacillus polymyxa* MG-CF6. *J Appl Glycosci* 2008;**55**:217–224.

Niness KR. Inulin and oligofructose. *J Nutr* 1999;**129**:1402–1406.

Okuyama M, Serizawa R, Tanuma M, Kikuchi A, Sadahiro J, Tagami T, Lang W, Kimura, A. Molecular insight into regioselectivity of transfructosylation catalyzed by GH68 levansucrase and β-fructofuranosidase. *J Biol Chem* 2021;**296**:100398.

Olivares-Illana V, Wacher-Rodarte C, Borgne SL, López-Munguía A. Characterization of a cell-associated inulosucrase from a novel source: A *Leuconostoc citreum* strain isolated from Pozol, a fermented corn beverage of Mayan origin. *J Ind Microbiol Biotechnol* 2002;**28**:112–117.

Ozimek LK, Euverink GJW, van der Maarel MJEC, Dijkhuizen L. Mutational analysis of the role of calcium ions in the *Lactobacillus reuteri* strain 121 fructosyltransferase (levansucrase and inulosucrase) enzymes. *FEBS Lett* 2005;**579**:1124–1128.

Ozimek LK, Kralj S, van der Maarel MJ, Dijkhuizen L. The levansucrase and inulosucrase enzymes of *Lactobacillus reuteri* 121 catalyse processive and non-processive transglycosylation reactions. *Microbiology* 2006;**152**:1187–1196.

Pettolino FA, Walsh C, Fincher GB, Bacic A. Determining the polysaccharide composition of plant cell walls. *Nat Protoc* 2012;**7**:1590–1607.

Pijning T, Anwar MA, Böger M, Dobruchowska JM, Leemhuis H, Kralj S, Dijkhuizen L, Dijkstra BW. Crystal structure of inulosucrase from *Lactobacillus*: insights into the substrate specificity and product specificity of GH68 fructansucrases. *J Mol Biol* 2011;**412**:80–93.

Polsinelli I, Caliandro R, Demitri N, Benini S. The structure of sucrose-soaked levansucrase crystals from *Erwinia tasmaniensis* reveals a binding pocket for levanbiose. *Int J Mol Sci* 2020;**21**:83.

Ponstein AS, van Leeuwen MB. *In vitro* synthesis of inulin by the inulosucrase from *Streptococcus mutans*. *Studies in Plant Science* 1993;**3**:281–287.

Pranznik W, Beck RHF. Application of gel permeation chromatographic systems to the determination of the molecular weight of inulin. *J Chromatogr A* 1985;**348**:187–197.

Pudjono, Barwald G, Amanu S. Activity of inulinase of some strains of *Bifidobacterium* and their effects on the consumption of foods containing inulin or other fructans. *Studies in Plant Science* 1993;**3**:373–379.

Raga-Carbajal E, Díaz-Vilchis A, Rojas-Trejo SP, Rudiño-Piñera E, Olvera C. The molecular basis of the nonprocessive elongation mechanism in levansucrases. *J Biol Chem* 2021;**296**:100178.

Rathsam C, Giffard PM, Jacques NA. The cell-bound fructosyltransferase of *Streptococcus salivarius*: the carboxyl terminus specifies attachment in a *Streptococcus gordonii* model system. *J Bacteriol* 1993;**175**:4520–4527.

Ritsema T, Smeekens S. Fructans: beneficial for plants and humans. *Curr Opin Plant Biol* 2003;**6**:223–230.

Roberfroid MB. Introducing inulin-type fructans. *Br J Nutr* 2005;**93**:13–25.

Robert X, Gouet P. Deciphering key features in protein structures with the new ENDscript server. *Nucleic Acids Res* 2014;**42**:320–324.

Rosell KG, Birkhed D. An inulin-like fructan produced by *Streptococcus mutans*, strain JC2. *Acta Chem Scand B* 1974;**28**:589.

Rozen R, Steinberg D, Bachrach G. *Streptococcus mutans* fructosyltransferase interactions with glucans. *FEMS Microbiol Lett* 2004;**232**:39–43.

Sakurai H, Yokota A, Sumita Y, Mori Y, Matsui H, Tomita F. Metabolism of DFA III by *Arthrobacter* sp. H65-7: purification and properties of a DFA III hydrolysis enzyme (DFA IIIase). *Biosci Biotechnol Biochem* 1997;**61**:989–993.

Schägger H, Cramer WA, von Jagow G. Analysis of molecular masses and oligomeric states of protein complexes by blue native electrophoresis and isolation of membrane protein complexes by two-dimensional native electrophoresis. *Anal Biochem* 1994;**217**:220–230.

Sebaihia M, Bocsanczy AM, Biehl BS, Quail MA, Perna NT, Glasner JD, DeClerck GA, Cartinhour S, Schneider DJ, Bentley SD, Parkhill J, Beer SV. Complete genome sequence of the plant pathogen *Erwinia amylovora* strain ATCC 49946. *J Bacteriol* 2010;**192**:2020–2021.

Seibel J, Moraru R, Götze S, Buchholz K, Na'amnieh S, Pawlowski A, Hecht HJ. Synthesis of sucrose analogues and the mechanism of action of *Bacillus subtilis* fructosyltransferase (levansucrase). *Carbohydr Res* 2006;**341**:2335–2349.

Shoaib M, Shehzad A, Omar M, Rakha A, Raza H, Sharif HR, Shakeel A, Ansari A, Niazi S. Inulin: Properties, health benefits and food applications. *Carbohydr Polym* 2016;**147**:444–454.

Singh RS, Singh RP. Production of fructooligosaccharides from inulin by endoinulinases and their prebiotic potential. *Food Technol Biotechnol* 2010;**48**:435–450.

Song DD, Jacques NA. Purification and enzymic properties of the fructosyltransferase of *Streptococcus salivarius* ATCC 25975. *Biochem J* 1999;**341**:285–291.

Sprenger N, Bortlik K, Brandt A, Boller T, Wiemken A. Purification, cloning, and functional expression of sucrose:fructan 6-fructosyltransferase, a key enzyme of fructan synthesis in barley. *Proc Natl Acad Sci U S A* 1995;**92**:11652–11656.

Strube CP, Homann A, Gamer M, Jahn D, Seibel J, Heinz DW. Polysaccharide synthesis of the

levansucrase SacB from *Bacillus megaterium* is controlled by distinct surface motifs. *J Biol Chem* 2011;**286**:17593–17600.

Suzuki T, Hara H. Difructose anhydride III and sodium caprate activate paracellular transport *via* different intracellular events in Caco-2 cells. *Life Sci* 2006;**79**:401–410.

Tamas I, Dedysh SN, Liesack W, Stott MB, Alam M, Murrell JC, Dunfield PF. Complete genome sequence of *Beijerinckia indica* subsp. *indica*. *J Bacteriol* 2010;**192**:4532–4533.

Thompson JD, Higgins DG, Gibson TJ. CLUSTAL W: improving the sensitivity of progressive multiple sequence alignment through sequence weighting, position-specific gap penalties and weight matrix choice. *Nucleic Acids Res* 1994;**22**:4673–4680.

Tonozuka T, Kitamura J, Nagaya M, Kawai R, Nishikawa A, Hirano K, Tamura K, Fujii T, Tochio T. Crystal structure of a glycoside hydrolase family 68 β-fructosyltransferase from *Beijerinckia indica* subsp. *indica* in complex with fructose. *Biosci Biotechnol Biochem* 2020;**84**:2508–2520.

Tonozuka T, Tamaki A, Yokoi G, Miyazaki T, Ichikawa M, Nishikawa A, Ohta Y, Hidaka Y, Katayama K, Hatada Y, Ito T, Fujita K. Crystal structure of a lactosucrose-producing enzyme, *Arthrobacter* sp. K-1 β-fructofuranosidase. *Enzyme Microb Technol* 2012;**51**:359–365.

Tsujimoto Y, Watanabe A, Nakano K, Watanabe K, Matsui H, Tsuji K, Tsukihara T, Suzuki Y. Gene cloning, expression, and crystallization of a thermostable exo-inulinase from *Geobacillus stearothermophilus* KP1289. *Appl Microbiol Biotechnol* 2003;**62**:180–185.

van de Wiele T, Boon N, Possemiers S, Jacobs H, Verstraete W. Inulin-type fructans of longer degree of polymerization exert more pronounced *in vitro* prebiotic effects. *J Appl Microbiol* 2007;**102**:452–460.

van den Ende W, Michiels A, van Wonterghem D, Vergauwen R, van Laere A. Cloning, developmental, and tissue-specific expression of sucrose:sucrose 1-fructosyl transferase from *Taraxacum officinale* fructan localization in roots. *Plant Physiol* 2000;**123**:71–80.

van Hijum SAFT, van Geel-Schutten GH, Rahaoui H, van der Maarel MJEC, Dijkhuizen L. Characterization of a novel fructosyltransferase from *Lactobacillus reuteri* that synthesizes high-molecular-weight inulin and inulin oligosaccharides. *Appl Environ Microbiol* 2002;**68**:4390–4398.

van Laere A, van den Ende W. Inulin metabolism in dicots: chicory as a model system. *Plant Cell Environ* 2002;**25**:803–813.

Vereyken IJ, Chupin V, Demel RA, Smeekens SC, De Kruijff B. Fructans insert between the headgroups of phospholipids. *Biochim Biophys Acta Biomembr* 2001;**1510**:307–320.

Vergauwen R, van Laere A, van den Ende W. Properties of fructan: fructan 1-fructosyltransferases from chicory and globe thistle, two Asteracean plants storing greatly different types of inulin. *Plant Physiol* 2003;**133**:391–401.

Wada T, Ohguchi M, Iwai Y. A novel enzyme of *Bacillus* sp. 217C-11 that produces inulin from sucrose. *Biosci Biotechnol Biochem* 2003;**67**:1327–1334.

Wada T, Sugatani J, Terada E, Ohguchi M, Miwa M. Physicochemical characterization and biological effects of inulin enzymatically synthesized from sucrose. *J Agric Food Chem* 2005;**53**:1246–1253.

Walter J, Schwab C, Loach DM, Gänzle MG, Tannock GW. Glucosyltransferase A (GtfA) and inulosucrase (Inu) of *Lactobacillus reuteri* TMW1.106 contribute to cell aggregation, in vitro biofilm formation, and colonization of the mouse gastrointestinal tract. *Microbiology* 2008;**154**:72–80.

Wuerges J, Caputi L, Cianci M, Boivin S, Meijers R, Benini S. The crystal structure of *Erwinia amylovora* levansucrase provides a snapshot of the products of sucrose hydrolysis trapped into the active site. *J Struct Biol* 2015;**191**:290–298.

Yanase H, Maeda M, Hagiwara E, Yagi H, Taniguchi K, Okamoto K. Identification of functionally important amino acid residues in *Zymomonas mobilis* levansucrase. *J Biochem* 2002;**132**:565–572.

Yokoi K, Tsutsui S, Arakawa GY, Takaba M, Fujii K, Kaneko S. Molecular and biochemical characteristics of inulosucrase InuBK from *Alkalihalobacillus krulwichiae* JCM 11691. *Biosci Biotechnol Biochem* 2021;**8**:1830–1838.

Yokota A, Hirayama S, Enomoto K, Miura Y, Takao S, Tomita F. Production of inulin fructotransferase (depolymerizing) by *Arthrobacter* sp. H65-7 and preparation of DFA III from inulin by the enzyme. *J Ferment Bioeng* 1991;**72**:258–261.

Zhu Z, He J, Liu G, Barba FJ, Koubaa M, Ding L, Bals O, Grimi N, Vorobiev E. Recent insights for the green recovery of inulin from plant food materials using non-conventional extraction technologies: a review. *Innov Food Sci Emerg Technol* 2016;**33**:1–9.

ACKNOWLEDGEMENTS

First of all, I would like to express my deepest gratitude to my first advisor Professor Haruhide Mori for his kindly suggestion throughout my project. Besides, I deeply appreciate Associate Professor Wataru Saburi for guidance and his help in progressing my research.

I would also thank Professor Haruhide Mori, Professor Satoru Fukiya, Professor Masayuki Okuyama, and Associate Professor Wataru Saburi for their guidance and encouragement in the preparation of this paper.

I would like to thank Dr. Eri Fukushi, GC-MS&NMR Room, Research Faculty of Agriculture, Hokkaido University for her cooperation in NMR measurements.

I would like to thank Mr. Tomohiro Hirose, Instrumental Analysis Division, Global Facility Center, Creative Research Institution, Hokkaido University for conducting the ESI-MS measurements using the Thermo Scientific Exactive.

I would like to thank Ms. Nozomi Takeda, Instrumental Analysis Division, Global Facility Center, Creative Research Institution, Hokkaido University for performing amino acid and protein analysis using JLC-500/V and Procise 492HT.

I would like to thank Dr. Masahiko Tamura, Senior Executive Officer of Nippon Sugar Beet Mfg. I would like to express my sincere gratitude to Dr. Hirokatsu Uchino, Director General of the Research Center of Nippon Sugar Beet Mfg., Dr. Taizo Nagura, Deputy Director General of the Research Center of Nippon Sugar Beet Mfg., and Dr. Dai Mikumo, Chief Researcher, and other members of the Food Development Group of the Research Center of Nippon Sugar Beet Mfg.

Last but not least, I would like to express my deepest gratitude to my family for warmly watching over me and supporting my health as I took on the challenge of the doctor course.

Yusuke Kido

謝辞

本研究を遂行するにあたり，学部学生時代から長きにわたり，厳しくも愛のあるご指導をいただきました北海道大学大学院農学研究院 森 春英 教授および佐分利 亘 准教授に深く感謝申し上げます.

また，本論文を作成するにあたり，ご指導，ご鞭撻をいただきました北海道大学大学院農学研究院 森 春英 教授，吹谷 智 教授，奥山 正幸 教授，および佐分利 亘 准教授に感謝いたします.

NMR の測定にご協力いただきました北海道大学大学院農学研究院 GC-MS＆NMR 室 福士 江里 博士に感謝いたします.

Thermo Scientific Exactive を使用した ESI-MS 測定を実施していただきました北海道大学 創成研究機構 グローバルファシリティセンター 機器分析受託部門 広瀬 知弘 氏に感謝いたします.

JLC-500/V および Procise 492HT を使用したアミノ酸組成分析および N 末端配列分析を実施していただきました北海道大学 創成研究機構 グローバルファシリティセンター 機器分析受託部門 武田 希美 氏に感謝いたします.

本研究を遂行する機会を与えて下さり，会社業務と博士課程の両立に多大なるご支援，ご指導，ご鞭撻を賜りました日本甜菜製糖株式会社 田村 雅彦 総合研究所担当、内野 浩克 総合研究所長，名倉 泰三 総合研究所副所長，そして三雲 大 主任研究員をはじめとする総合研究所 食品研究グループの皆様に厚く御礼申し上げます.

最後になりましたが，博士後期課程への挑戦を温かく見守り，健康面・精神面を支えてくださった家族に深く感謝いたします.

城戸 悠輔